SCOTT POLAR RESEARCH INSTITUTE
Lensfield Road
UK - Cambridge CB2 1ER

Relating surface and bed properties of Antarctic ice streams

JAN DE RYDT

Selwyn College

Supervisor:
Dr. Poul Christoffersen

Dissertation submitted
for the degree of
Master of Philosophy

June 2011

Declaration

This dissertation is the result of my own work and includes nothing which is the outcome of work done in collaboration except where specifically indicated in the text. The dissertation is no more than 20,000 words in length excluding the declaration, acknowledgements, equations, tables, captions and list of references.

Acknowledgements

The subject of this study was suggested by Dr. Hilmar Gudmundsson. I gratefully acknowledge his continuous support during all stages of this work. His encouragements and skillful advice have significantly improved the quality of this research, and his enthusiasm has made the transition from string theory to geophysics a particularly enjoyable one.

This study was made possible through the hospitality and help of various people at the British Antarctic Survey. I thank Hugh Corr for providing the data, and for showing interest in our work. Prof. David Vaughan provided useful remarks to earlier versions of chapter 4, and gave me the opportunity to share our findings with a broader audience at BAS.

I'm much indebted to Dr. Poul Christoffersen, who accepted me as his student at the University of Cambridge. He gave me the freedom to explore the field of glaciology according to my own taste, and provided crucial advice at numerous moments. It was a pleasure to collaborate on two exciting projects.

For creating a friendly and welcoming working atmosphere, I thank all the people at the Scott Polar Research Institute. A special word goes to my fellow MPhil students, with whom I had the pleasure to share many fine moments, both inside and outside the walls of SPRI.

Tot slot, en zoals altijd, vele dikke kussen voor moeke, paps, kleine broer en grote zus. Ook dit werkstukje was er niet gekomen zonder jullie steun. Ik hoop dat we als familie onze dromen kunnen blijven waarmaken!

Abstract

Theoretical models predict that fast-flowing ice streams transmit information about their bedrock topography most efficiently to the surface for two distinct windows of length-scales. Previous studies have shown a good transfer for basal undulations with wavelengths longer than 10^3 ice thicknesses. In addition, a local maximum in the theoretical transfer function appears for intermediate wavelengths between 1 and 20 ice thicknesses. So far, however, no experimental evidence for this important transfer at intermediate wavelengths has been obtained. In our work we use recently acquired radar data for the Rutford Ice Stream and Evans Ice Stream to provide the first experimental confirmation for this theoretical prediction, and show that fast-flowing ice is highly transparent to bedrock irregularities with wavelengths between 1 and 20 ice thicknesses. The amplitude of this local maximum depends on various flow parameters such as Glen's flow law exponent and the slip ratio, i.e., the ratio between mean basal sliding velocity and mean deformational velocity. We find that higher values of the slip ratio generally lead to a more efficient transfer. Our results underline the importance of bedrock topography for ice stream dynamics, and exclude basal slipperiness as the only determining factor for variations in the flow regime and surface topography.

In the second part of this work, we address the role of the basal sliding law in statistical inversion methods that use surface data (topography and velocity) to obtain information about the basal slipperiness distribution

and bed topography. We show that different sliding laws generally lead to the retrieval of different but equally realistic basal conditions. Since the correct form of the sliding law is still disputed, the use of inversion methods to obtain unambiguous information about the bed therefore remains problematic.

Nomenclature

A	rate factor
$b(x, y)$	bedrock topography
b_0	mean bedrock profile
$\Delta b(x, y)$	small bedrock perturbation
$c(x, y)$	basal slipperiness distribution
c_0	mean basal slipperiness
$\Delta c(x, y)$	small slipperiness perturbation
$C^{(0)}$	mean slip ratio
$C_{x\tilde{x}}$	covariance matrix of a priori errors
$C_{y\hat{y}}$	covariance matrix of measurement errors
$\boldsymbol{g}$	acceleration due to gravity
H	mean ice thickness
$(k_x,\, k_y)$	wavenumbers
l	radar profile length
L	window length in Welsh's periodogram method
m	sliding exponent
n	Nye-Glen's flow law exponent
$P(i\|j)$	conditional probability for an event i, given j
$s(t, x, y)$	surface topography
s_0	mean surface profile
$\Delta s(t, x, y)$	small surface perturbation
$\boldsymbol{T}_b$	basal shear stress
$T = (T_{sb} \quad T_{sc}\,;\, T_{v_ib} \quad T_{v_ic})$	theoretical transfer functions

$T^{(\mathrm{m})} = \begin{pmatrix} T_{sb}^{(\mathrm{m})} & T_{sc}^{(\mathrm{m})} \,;\, T_{v_i b}^{(\mathrm{m})} & T_{v_i c}^{(\mathrm{m})} \end{pmatrix}$	observed transfer functions
$T^{(\mathrm{sa})} = \begin{pmatrix} T_{sb}^{(\mathrm{sa})} & T_{sc}^{(\mathrm{sa})} \,;\, T_{v_i b}^{(\mathrm{sa})} & T_{v_i c}^{(\mathrm{sa})} \end{pmatrix}$	semi-analytical transfer functions
$\boldsymbol{v} = (v_x, v_y, v_z)$	ice flow velocity vector
Δv_i	small velocity perturbations
$\boldsymbol{v}_b$	basal sliding velocity
$v_{d,x}^{(0)}$	mean deformation velocity at the surface
$\boldsymbol{x} = (b, c)$	true system state
$\tilde{\boldsymbol{x}} = (\tilde{b}, \tilde{c})$	a priori estimate of the system state
$\hat{\boldsymbol{x}} = (\hat{b}, \hat{c})$	a posteriori estimate of the system state
$\boldsymbol{y} = (s, v_i)$	true surface properties
$\hat{\boldsymbol{y}} = (\hat{s}, \hat{v}_i)$	surface measurements
α	mean surface slope
$\dot{\boldsymbol{\epsilon}}$	strain rate tensor
$\boldsymbol{\epsilon}_{\tilde{\boldsymbol{x}}} = (\epsilon_{\tilde{b}}, \epsilon_{\tilde{c}})$	a priori errors
$\boldsymbol{\epsilon}_{\boldsymbol{y}} = (\epsilon_s, \epsilon_{v_i})$	measurement errors
η	ice viscosity
$(\lambda_x,\, \lambda_y)$	wavelengths along and transverse to the flow
$\lambda_{\tilde{b}}$	decay length scale
ρ	ice density
$\boldsymbol{\sigma}$	stress tensor
$\boldsymbol{\tau}$	deviatoric stress tensor
$\tau_{(\mathrm{II})}$	effective stress
$\phi_{\tilde{b}}$	regression coefficient

List of Figures

Contents

Chapter 1

Introduction

The flow regime of the Antarctic Ice Sheet (AIS) is dominated by an extensive network of fast-flowing ice streams and outlet glaciers. This is illustrated in Figure 1.1, which shows modeled balance velocities obtained from surface slopes, ice thickness and mean net surface mass balance. Ice streams with speeds up to several hundred meters per year are clearly visible, primarily along the margins of the AIS, and with tributaries extending deep into the interior. Calculations using balance velocities have shown that these fast-flowing features are responsible for as much as 90% of the AIS discharge [Bamber et al., 2000].

However, a stable flow-configuration as shown in Figure 1.1, cannot be used to accurately estimate the total mass balance of the past, present or future AIS. Over the last two decades, numerous studies have indicated that the stable configuration is easily disturbed by dynamic changes in flow velocity and/or geometrical configuration at timescales that are much shorter than the expected response time of the ice sheet. As a result, rapid spatial and temporal changes in discharge are to be expected. During recent years, such dynamic changes have been observed for most coastal regions of Antarctica, with increased flow speeds [Rignot et al., 2008] and dynamic thinning [Pritchard et al., 2009]. A prime example are the glaciers draining into the Amundsen Sea Embayment, in particular Pine Island Glacier which is now flowing at a speed that is almost double that needed to balance snowfall in its catchment basin [Joughin et al.,

2010, Thomas et al., 2011]. On the other hand, Kamb Ice Stream (Siple Coast) switched from fast to slow flow about 150 years ago [Retzlaff and Bentley, 1993] and Whillans Ice Stream is currently slowing down by about 5 m/yr [Joughin et al., 2005]. These changes caused the region to switch from a negative to a positive mass balance regime [Joughin and Tulaczyk, 2002], and the local ice sheet thickened by 0.25-0.65 m/yr between 2003 and 2007 [Pritchard et al., 2009]. Clearly, accurate predictions about the mass balance of the AIS rely on a good understanding of the dynamical mechanisms that control the flow of its ice streams and glaciers.

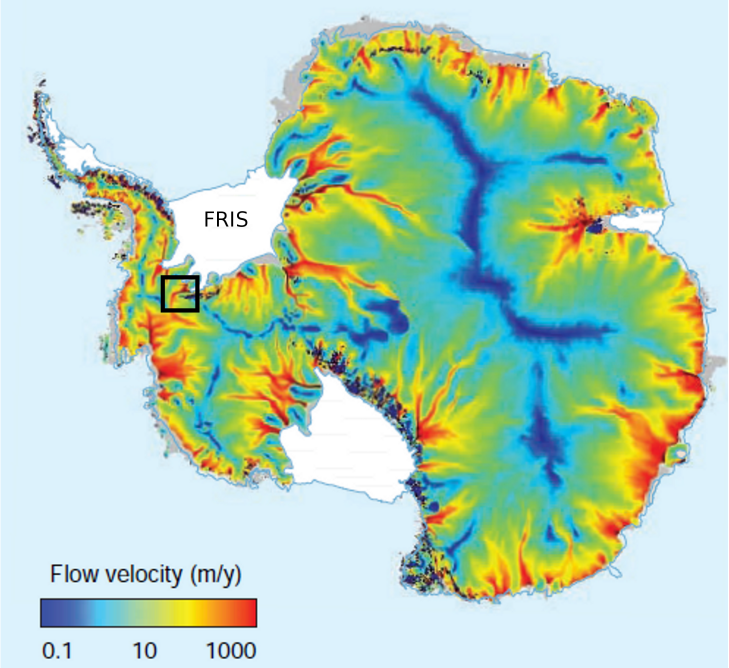

Figure 1.1: Map showing balance velocities for the Antarctic Ice Sheet, obtained from computer model simulations. This picture is reproduced from Hamblin and Christiansen [2003]. Fast-flowing ice steams (with typical speeds > 100 m/yr) are clearly visible along the margins of the ice sheet, and are bounded by slower moving ice. The region of interest for our work in chapter 4 is outlined by the black square. It contains the Rutford and Evans Ice Streams, flowing into the Filchner-Ronne Ice Shelf (FRIS). The lower part of the square roughly corresponds to the coverage of Figure 1.2.

An important role in the regulation of ice stream flow is played by their basal conditions, i.e., bedrock topography and variations in basal slipperiness.[1] For example,

[1]We use the term "slipperiness" as a measure for the amount of sliding over a hard bed, or the

active ice streams of the Siple Coast exhibit high flow velocities (~ 500 m/yr) despite low gravitational driving stresses ($\sim 10-20$ kPa) due to a weak subglacial till layer and high effective basal lubrication [Tulaczyk et al., 2001]. The main constraints on their motion come from shear resistance at the margins and the presence of localized "sticky spots", i.e., places where the resistance to basal sliding is significantly higher than in the surrounding areas [Alley, 1993, Joughin et al., 2004, 2006]. The physical character of these pinning points can be local bedrock undulations or small-scale variations in basal slipperiness. Since basal friction has the potential to change more dynamically than other resistive stresses (such as marginal shear), the effect of small basal perturbations on flow characteristics is of particular importance.

The best way to obtain information about the conditions at the base of ice streams is by direct access via boreholes [Kamb, 2001]. However, such experiments are challenging and provide only information about a very limited section of the bed. Moreover, this method cannot be used to address the role of the bedrock topography on ice flow dynamics. Alternatively, remote sensing techniques such as seismic [Blankenship et al., 1986, 1987, Anandakrishnan et al., 1998, Smith et al., 2007, Smith and Murray, 2009] and radar [Bentley et al., 1998, Gades et al., 2000, Rippin et al., 2006, King et al., 2009] measurements provide detailed maps of till conditions and basal topography along flightlines or for gridded areas. A third line of attack involves the inversion of irregularities at the surface arising from bedrock bumps or variations in slipperiness. Control method inversion uses accurate remote sensing data about the surface velocity field in combination with theoretical ice flow models to obtain information about the basal shear stress distribution of ice streams [MacAyeal et al., 1995, Vieli and Payne, 2003, Joughin et al., 2004, 2006]. Statistical inversion methods have been developed to study the simultaneous retrieval (or update) of bed topography and basal slipperiness from surface topography and velocity measurements [Gudmundsson, 2004, Raymond

combination of sliding and till-deformation for a weak bed. In the literature one often refers to "basal lubrication" or "basal drag". In general, the slipperiness is a complicated (and often unknown) function of many physical parameters such as temperature, basal water pressure, till strength, and so on.

and Gudmundsson, 2009, Raymond-Pralong and Gudmundsson, 2011].

All inversion methods obtain information about the bed in an indirect way, and rely on a good theoretical understanding of how surface properties connect to conditions at the bed. Such a connection between bed and surface properties has been a topic of major interest to glaciologist for many decades, and is still only partially understood.[2] Evidence for the complexity of such a relation is provided by observations of the surface topography of Antarctic ice streams. In Figure 1.2 we present a section of the AIS corresponding to the lower part of the black square in Figure 1.1. Several flow-features are clearly visible: the Rutford Ice Stream, Carlson Inlet, and Talutis Ice Stream. The Rutford Ice Stream is fast-flowing, with an average speed of 400 m/yr [Gudmundsson and Jenkins, 2009], whereas the Carlson Inlet is a slow-moving part of the ice sheet, and its categorization as an ice stream has recently been questioned by King [2011]. However, what's important for us are the apparent differences in surface topography between these two features. For the fast-flowing Rutford Ice Stream, surface undulations of many different length scales are clearly visible. These can only be explained by varying conditions at the bed, i.e., either bedrock bumps or variations in basal slipperiness. On the other hand, for the slow-moving Carlson Inlet, such features are largely absent, even though radar investigations show that its bedrock topography is very similar to the one of Rutford Ice Stream (with bumps of comparable amplitudes). Similar findings about the presence or absence of surface undulations with typical lengths scales have been presented for several other places on the Greenland and Antarctic Ice Sheets. In particular, it was repeatedly reported that undulations with length scales of approximately 2-5 ice thicknesses are very pronounced [Robinson, 1966, Zwally et al., 1979, 1983, Whillans et al., 1984, Overgaard and Gundestrup, 1985].

It is hard to believe that this observation is a coincidence. Instead, one might wonder whether it tells us something about the general relation between surface undulations and basal conditions, in particular about the dependence of such a relation on the ice

[2] A detailed account of the literature on this subject will be given in section 3.1.

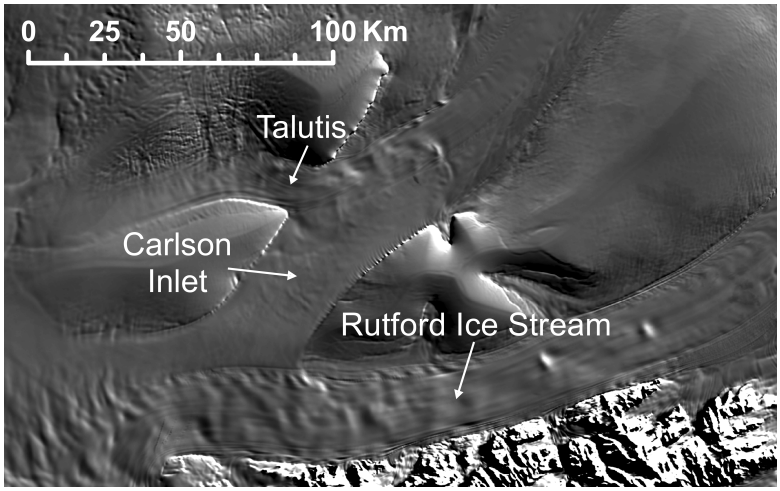

Figure 1.2: Surface topography of the Rutford Ice Stream, Carlson Inlet and Talutis Ice Stream, Antarctica. The image is a subset of the MODIS mosaic for Antarctica.

flow velocity. Indeed, theoretical models predict [Gudmundsson, 2003, Raymond and Gudmundsson, 2005] that bedrock undulations with length scales between 2 and 20 ice thicknesses (i.e., typically between 4 and 40 km) are transmitted to the surface much more efficiently than perturbations at other wavelengths. In addition, this is only true for ice streams that attain a substantial part (typically 95% or more) of their surface velocity by basal sliding. These theoretical results give a first indication as to why we only observe surface undulations in Figure 3 that have length scales on the order of a few kilometers, and why they only appear at the surface of the fast-flowing Rutford Ice Stream. This explanation is obviously not restricted to the part of the AIS presented in Figure 1.2, but is expected to hold generally for any ice stream.

Although the qualitative argument above might be appealing, direct evidence is needed to fully confirm the link between theory and observation. Because accurate and extensive measurements of the bed topography of Antarctic ice streams have been very limited so far, direct experimental evidence has not been obtained to date. However, in this dissertation we are able to provide such evidence for the first time, using recently acquired radar data for the ice streams in Figure 1.2 and Evans Ice Stream, which is situated to the east of this region. We provide convincing experimental support

for the theoretical models that describe the bed-to-surface transfer characteristics of fast-flowing ice. Moreover, our study is an important validation for the use of these theoretical results in inversion models. Such inversion models, and their sensitivity to the specific transfer characteristics of ice, will be studied in the second part of this report.

1.1 Goals of this work

The broad aim of our work is to contribute to the understanding of ice stream dynamics, using both observational data and modeling techniques. Hence, this dissertation covers two broad aspects of glaciology: a theoretical element and an experimental element. Combining the two is often challenging, and not every reader is familiar with the detailed aspects of theoretical glaciology. Our first challenge is therefore to provide a comprehensive introduction to the theoretical background needed for the bulk of our research. We subsequently present results from new investigations, which fall into 2 categories.

In the *first part* of our research, we focus on the empirical validation of theoretical models that describe the transfer of information about basal undulations to the surface of fast-flowing ice streams. We use appropriate datasets of surface and bed topography measured along the flow of various ice streams in Antarctica. This research is carried out in collaboration with Hilmar Gudmundsson[3] at the British Antarctica Survey, where many excellent datasets have recently become available, e.g. for the Rutford Ice Stream and Evans Ice Stream. We primarily test the dependence of the bed-to-surface transfer amplitude on the length scale of the basal undulations, and on several physical parameters such as the slip ratio (i.e., the ratio between the mean basal sliding velocity and mean forward deformational velocity). In the first place, we seek to validate theoretical results, but a careful comparison between observed and modeled behavior also leads to new insights into the flow dynamics of these ice streams.

[3]British Antarctic Survey, High Cross Madingley Road, Cambridge CB3 0ET, UK. (ghg@bas.ac.uk)

In the *second part* of our research, we turn our attention to inverse modeling techniques that use surface measurements to deduce information about the basal conditions (topography and slipperiness) of ice flows. Given the difficulty of obtaining direct experimental information about the base of an ice stream, such techniques are very valuable. However, quantitative tests of their accuracy haven been limited so far. In our work, we question the reliability of a particular inversion method (the so-called Bayesian statistical inversion) in the absence of a well-constrained form of the sliding law. Through various numerical sensitivity tests on synthetic data, we aim to apprehend the dependence of the retrieved basal conditions on the form of the sliding law. A better understanding of the successes and limitations of the inversion procedure provides a measure for the accuracy of the results obtained from the inversion of real data. Again this research is carried out in collaboration with Hilmar Gudmundsson, who first introduced the Bayesian approach as an inverse modeling technique in glaciology.

1.2 Outline

We report about our results on two separate studies that relate to the same theoretical framework. This framework is introduced in chapters 2 and 3. Chapter 2 provides the necessary background on ice flow mechanics, with emphasis on topics that are needed for further developments in this text. Chapter 3 provides an introduction to the theory of transfer functions, which describe the transient response of the surface of an ice stream to spatial and temporal changes at its base. The actual results of our research are presented in chapters 4 and 5. These chapters can be read independently, although they both rely on chapters 2 and 3 for the theoretical context and the introduction of notations and conventions. Chapters 4 and 5 each have the structure of a research paper; they start with a short introduction, followed by an overview of the used methods, presentation of the results, a discussion of the results and conclusions.

Here follows a more detailed account of the content of each chapter:

Chapter 2: Introduction to ice flow mechanics. All models of large-scale ice flow incorporate a convenient description of the ice rheology and of the dynamics at the ice-bed interface. The ice rheology is commonly described by Glen's empirical flow law, whereas the ice-bed interaction is simulated by a basal sliding law of some sort. Empirical constraints on both laws are still limited though, and their general validity should not be taken for granted. Although most readers are familiar to some extend with ice rheology and basal sliding laws, we find it appropriate to review the basic argumentation behind their form, and to outline potential pitfalls that could limit their applicability for ice flow modeling. Subsequently, the basic dynamical equations of ice flow are reviewed, and special attention is given to the approximations used to solve these equations in chapter 3.

Chapter 3: Theory of transfer functions. The flow law and sliding law are used as input to calculate the transfer functions that describe the surface response of a flowing ice mass to basal perturbations (bedrock undulations and variations in slipperiness). We discuss the analytical solutions for the transfer problem in two distinctive frameworks: (i) a full-Stokes flow with a linear ice rheology and linear sliding law, and (ii) the shallow-ice-stream approximation with a linear rheology and non-linear sliding law. The former is used as a benchmark for experimental results in chapter 4. The latter is used to investigate the dependence of inversion methods on the value of the sliding exponent in chapter 5. The reasons why these chapters rely on a different theoretical treatment are discussed.

Chapter 4: Observational evidence for bed-to-surface transfer. This chapter reports on our study of an extensive set of radar measurements of the bed and surface topography of several Antarctic ice streams. In total, 22 radar profiles along 3 separate ice streams (Rutford Ice Stream, Evans Ice Stream and the Carlson Inlet) are studied. Our aim is to obtain experimental evidence for the theoretical predictions about the bed-to-surface transfer characteristics described in chapter 3. First we provide a

detailed description of the data, together with an overview of the used analysis methods. The results are subsequently presented. We emphasize the unifying aspects of the study, i.e., the similarities and differences seen in the various radar profiles. Also the agreements and conflicts between theory and observation are described. A detailed explanation for each of the observed discrepancies is given, providing insight into the potential weaknesses of the theory.

Chapter 5: Inversion of surface properties and the form of the basal sliding law. The form of the basal sliding law has a decisive impact on the results of large-scale ice flow modeling. Understanding the form of the ice-bed interaction remains an important challenge in glaciology today. Therefore, in inverse modeling techniques we rely on an ad hoc choice of the sliding law, and this choice might strongly influence the form of the retrieved basal properties. In this chapter we first give a detailed introduction to the Bayesian inversion method, which provides the framework for our study. Next, the results of various numerical experiments are presented, whereby we test the sensitivity of the retrieved basal properties on the form of the basal sliding law. These results are supplemented by additional analytical arguments. Although our results are preliminary, a clear picture emerges that raises questions about the accuracy of Bayes' inversion to obtain information about the basal slipperiness. The implications of this discovery are discussed in detail.

Chapter 2

Introduction to ice flow dynamics

All physical models are approximations to reality, all make compromises between accuracy, the scope of applicability and efficiency. Models for ice flow are no different in this respect. Any attempt to compare these models to experimental results therefore requires a good understanding of their potential successes and shortcomings. In this chapter we present a critical introduction to the different model constituents and approximations that will be used in the theoretical study of ice flow transfer characteristics in chapter 3.

2.1 Ice rheology

The key input to any flow model is a description of how the ice deforms in response to an external stress regime. Such a description is given by a constitutive relation or *flow law*. The form of this law depends on several factors.

- At the microscopic scale, ice is a hexagonal crystal. In glaciers, individual crystals cluster in grains which have no preferred orientation. When grain sizes are small with respect to characteristic length scales at which deformation occurs, glacier ice can be treated as an isotropic polycrystalline material. It should be noted that such an assumption can break down under very extreme stress regimes, for

example near the base of the Greenland and Antarctic Ice Sheets. In these places, recrystallization can occur, which forces the ice to be in an anisotropic state. In this work we will only consider the flow law for *isotropic ice*, which is also the case most commonly encountered in the literature. Work on anisotropic constitutive relations or enhancement factors is limited, see e.g. Gagliardini et al. [2009] for a recent review.

- A distinction should be made between regimes of primary (or transient) and steady deformation, depending on the characteristic timescales and stresses involved in the creep process. In glaciers and ice sheets, deformation takes place under conditions that apply to *steady creep*, since the ice is subjected to a certain stress regime for very long times ($\gg$ hours). For a fixed stress, the steady state can be further subdivided into two phases, depending on the cumulative strain. For high enough values of the cumulative strain (usually at values of about 0.01), the strain rate obtains a minimum which is called the secondary creep rate. For very high stresses ($> 10^6$ Pa) and long enough timescales, the strain rate obtains a steady value as a function of the total strain, called the tertiary creep rate. During tertiary creep, recrystallization often occurs due to the high stresses, and the polycrystalline ice is, in general, no longer isotropic.

- Other factors that influence the relation between stress and deformation of ice include the presence of impurities such as air or water bubbles, internal cracks, and so on. These aspects will not be considered.

For isotropic polycrystalline ice in the steady secondary or tertiary creep state, the deformation due to external stresses can be described by a power-law. Such a law was first suggested by Glen as an empirical fit to his laboratory experiments on uniaxial compression [Glen, 1955], and is hence called *Glen's flow law*.[1] It states that the strain rate at a given strain is proportional to the stress raised to some power n. If the strain

[1] Steinemann [1954, 1958a,b] presented independent results that were similar to those obtained by Glen and therefore he also deserves credit for his work.

rate is denoted by $\dot{\epsilon} \equiv \frac{\partial \epsilon}{\partial t}$ and the stress by σ, Glen's law has the form

$$\dot{\epsilon} = A\sigma^n \,, \tag{2.1.1}$$

where A and n are parameters determined by measurements. The first parameter is called the *rate factor* and is related to the effective ice viscosity, η, defined as

$$\eta \equiv \left(\frac{1}{A}\right)^{1/n} . \tag{2.1.2}$$

The viscosity strongly depends on parameters that influence the softness (or stiffness) of the ice, such as the temperature and the fabric of the ice. In our work, the precise dependency of η on these quantities will be neglected, and we refer to Cuffey and Paterson [2010] for more details. In particular, we assume that η is constant with depth. Such an assumption is not necessary valid for Antarctic ice streams since the ice viscosity generally evolves from lower values at their base (temperate ice) to higher values at the surface (colder and hence stiffer ice). We will come back to this issue in section 4.4.

The second parameter, n, in equation (2.1.1) is *Glen's flow law coefficient* or creep coefficient. The value of n depends on the creep mechanism operating, and experiments have shown a plausible range of values between $n = 2$ and $n = 4$ with a most likely value of $n \approx 3$. Although physically less interesting, it is also worth considering the limiting case for which $n = 1$. In this case, ice is described as a linear viscous (or Newtonian) material. A linear ice rheology is only accurate for moderately low stresses below 10^5Pa and slowly applied forces. On the other hand – and more importantly in the context of this work – the use of a linear flow law in theoretical glaciology often simplifies the calculations, and gives valuable insights in the qualitative behavior of processes for which a non-linear flow law is more appropriate. We will see in section 3 that an analytical solution to the full-Stokes transfer problem is only known for $n = 1$. Nevertheless, this simplified model exhibits the same qualitative transfer characteristics

as its non-linear counterpart.

Glen's original flow law (equation (2.1.1)) only applies to cases where one component of the full stress tensor dominates. For most realistic ice masses, such as the ones encountered in our work, this condition is not satisfied and a generalization to 3 dimensions is required. Both Nye [1951] and Glen [1958] have proposed such a generalization, based on the following principles.

- Rigsby [1958] demonstrated that hydrostatic pressure does not influence the flow law and ice can therefore be treated as an incompressible material. In terms of the strain rates, this condition can be formulated as follows:

$$\dot{\epsilon}_{xx} + \dot{\epsilon}_{yy} + \dot{\epsilon}_{zz} = 0\,, \quad \text{with} \quad \dot{\epsilon}_{xx} = \frac{\partial v_x}{\partial x},\, \dot{\epsilon}_{yy} = \frac{\partial v_y}{\partial y}\,, \dot{\epsilon}_{zz} = \frac{\partial v_z}{\partial z}\,, \tag{2.1.3}$$

  and v_x, v_y and v_z are the x-, y- and z-components of the flow velocity. This equation states that the first invariant of the strain rate tensor $\dot{\boldsymbol{\epsilon}}$ vanishes, and the relation is therefore independent on our choice of coordinate system.

  The condition of incompressibility can be implemented in the flow law by assuming that the strain rate tensor only depends on the *deviatoric stresses*. The latter are defined as

$$\tau_{ij} = \sigma_{ij} - \frac{1}{3}\delta_{ij}\sigma_{kk}\,, \tag{2.1.4}$$

  where the Roman indices $i, j, \ldots$ take values in the set $\{x, y, z\}$, σ_{ij} are the components of the full stress tensor, δ_{ij} is the Kronecker delta, and we adopted the convention that repeated indices are summed.

- In general, the flow law can be written as

$$\dot{\epsilon}_{ij} = f_{ij}(\boldsymbol{\tau}, T)\,, \tag{2.1.5}$$

  where f_{ij} is some function of the deviatoric stresses $\boldsymbol{\tau}$ and the temperature T, such that equation (2.1.3) is satisfied. Moreover, the constitutive function f_{ij} must

be a tensor-valued function of its arguments, and because (2.1.5) is a physical property of ice, its form cannot depend on the choice of a coordinate system. If we take these restrictions into account, the general form of the flow law reduces to

$$\dot{\epsilon}_{ij} = -\frac{2}{3}\tau_{(\mathrm{II})}\mathcal{C}_1\,\delta_{ij} + \mathcal{C}_2\tau_{ij} + \mathcal{C}_1\tau_{ik}\tau_{kj}\,, \tag{2.1.6}$$

where $\mathcal{C}_1$ and $\mathcal{C}_2$ are scalar valued functions of the second and third invariants of the deviatoric stress tensor[2] and the temperature:

$$\mathcal{C}_1 = \mathcal{C}_1(\tau_{(\mathrm{II})}, \tau_{(\mathrm{III})}, T)\,, \quad \text{and} \quad \mathcal{C}_2 = \mathcal{C}_2(\tau_{(\mathrm{II})}, \tau_{(\mathrm{III})}, T)\,, \tag{2.1.7}$$

with

$$\tau^2_{(\mathrm{II})} = \frac{1}{2}\tau_{ij}\tau_{ij}\,, \tag{2.1.8}$$

$$\tau_{(\mathrm{III})} = \det(\boldsymbol{\tau})\,. \tag{2.1.9}$$

The second invariant $\tau_{(\mathrm{II})}$ is often referred to as the *effective stress*.

- Nye [1951] in his treatment furthermore added the assumptions that (i) the third invariant $\tau_{(\mathrm{III})}$ has no effect on the deformation of ice and (ii) the components of the strain rate and stress tensor are proportional. This implies that $\mathcal{C}_1 = 0$ and

$$\dot{\epsilon}_{ij} = \mathcal{C}_2(\tau_{(\mathrm{II})}, T)\tau_{ij}\,. \tag{2.1.10}$$

So far, no experimental results have contradicted Nye's assumptions, and (2.1.10) remains valid until the contrary is proved.

If we finally require that the generalized relation (2.1.10) reduces to the simple one (2.1.1) for the cases where only one component pair $\dot{\epsilon}_{ij}$ and τ_{ij} is nonzero, then we find

[2] It is straightforward to show that the first invariant of the deviatoric stress tensor vanishes automatically.

the *Nye-Glen isotropic flow law* for ice:

$$\dot{\epsilon}_{ij} = A\tau_{(\mathrm{II})}^{n-1}\tau_{ij}\,, \tag{2.1.11}$$

with A and n the same physical constants as in (2.1.1). This generalized flow law forms the basis for all further developments in this text.[3] The parameters A and n are kept arbitrary at the moment.

2.2 The basal sliding law

In the previous section we have presented a theoretical description for the deformation of ice in response to external stresses. In order to describe the flow of finite ice masses such as glaciers and ice sheets, our knowledge about the ice rheology needs to be supplemented by boundary conditions at the upper free surface and the base, or bed, of the glacier or ice sheet. In this section the mechanical boundary conditions at the ice-bed interface will be discussed. Since the motion of many fast-flowing glaciers (including the Antarctic ice streams we will study) is dominated by basal motion, while deformation within the bulk of the ice is limited, a good understanding of the mechanics at the bed is central to our ability to predict the behavior of these glaciers.

The basal component of glacier flow consists of two parts in general: (i) basal sliding and (ii) deformation of the underlying sediment. The relative contributions of both effects vary greatly depending on the thermal regime of the basal ice (cold versus temperate) and the morphology of the bed (hard versus soft). For example, temperate Alpine glaciers flowing over hard bedrock can attain a substantial part of their surface speed by sliding, a mechanism that crucially depends on the effective hydrological pressure at the bed. On the other hand, fast-flowing Antarctic ice streams are often supported by a soft bed with a rapidly deforming layer of pressurized subglacial till. Given the complexity of the basal motion and the sparsity of observational data, no

[3] An alternative description for ice rheology can be found, for example, in Goldsby and Kohlstedt [2001].

concise and firm theoretical framework has been developed that describes the various mechanisms. In particular, the relation between the sliding velocity or till deformation and the relevant physical parameters is still an open question, as is the exact form of the sliding law.

We will not attempt to give an exhaustive overview of the current state of affairs, but rather concentrate on the aspects that are relevant for further developments in this text. In particular, we will motivate the use of a Weertman-type sliding law of the form

$$v_b = c\tau_b^m \,, \tag{2.2.12}$$

where v_b and τ_b are the basal velocity and basal shear stress respectively, and c and m are positive adjustable parameters. The *sliding exponent* m should not be confused with Glen's exponent n, although they are related for certain oversimplified geometries of the bed. The *basal slipperiness* $c = c(x, y)$ is allowed to vary along the bed, and is therefore a function of x and y – the coordinates in the direction of the flow and transverse to the flow. In general, $c(x, y)$ describes variations in subglacial conditions such as the bed roughness, thermodynamic properties of the ice and bed, effective basal water pressure, and so on. As such, the flow around "slippery" or "sticky" spots may be analyzed. Both the sliding exponent and the slipperiness distribution are poorly constrained by direct observations. One of the aims of our work is to obtain a better understanding of their influence on flow dynamics, and to investigate indirect methods that confine their value.

Let us now provide some motivation for the form of the proposed sliding law (2.2.12). The traditional sliding problem as studied by Weertman [1957, 1964, 1979], assumes the movement of temperate clean ice over an irregular hard bed (the so-called tombstone bed) without bed separation. Weertman proposed two physically different processes, the validity of which has now been confirmed by observations. The first process is *regelation*, which involves the melting of ice on the up-stream side of an obstacle, and the refreezing of that water on the down-stream side of the obstacle. The second mech-

anism is *viscous creep*, whereby the ice deforms and flows around obstacles. Weertman found that for a given driving stress τ_b, the components of the sliding velocity due to regelation and creep are proportional to τ_b and τ_b^n respectively, where n is Glen's exponent. This result is consistent with equation (2.2.12) for values of $m = 1$ and $m = n$ respectively.

Subsequently, several improvements to Weertman's analysis have been proposed. Nye [1969, 1970] and Kamb [1970] studied the flow of linear viscous ice over a more realistic bed geometry consisting of superimposed sine waves. In the limit of small roughness, i.e., for undulations with an amplitude that is small compared to the wavelength, both authors found a linear relationship between the basal sliding velocity and basal shear stress – in agreement with (2.2.12) for $m = 1$. Kamb [1970] also extended his linear analysis to a non-linear rheology, and obtained an approximate solution for the sliding law which is of the Weertman-type.

Lliboutry [1958, 1959, 1968], on the other hand, has challenged Weertman's approach to sliding without bed separation, and argued that the formation of water-filled cavities in the lee of bed obstacles is an important additional mechanism that leads to faster sliding velocities. However, when the ice is allowed to separate from the bed, a simple power-law relation as in (2.2.12) may cease to exist. Indeed, it has been argued that because of cavity formation, the basal drag cannot rise above a limiting value [Iken, 1981, Schoof, 2005, Gagliardini et al., 2007]. For high basal speeds, longitudinal and/or lateral stresses become more important in ensuring force balance on the glacier, leading to an overall decrease of the basal shear stress. Hence, for increasing sliding velocities, the shear stress first increases, then reaches a maximum, and subsequently decreases again. Since the basal velocity is not a single valued function of the shear stress anymore, a simple relationship $v_b(\tau_b)$ does not exist. Instead, one should think of the sliding law as a function of the form $\tau_b(v_b)$.

To summarize, it is clear that a Weertman-type sliding law is only valid if the basal velocity can be described by a monotonic increasing function of the basal shear stress. Such a relation is not necessarily valid for high values of the sliding velocity and in the

presence of cavity formation. A multitude of sliding laws have been proposed in the literature, and no general consensus has been reached on their form. Most probably, a universal expression of the type $\tau_b(v_b)$ is hard to obtain, let alone to identify the physical quantities that enter such a relationship. More experimental work is needed to further constrain the form of $\tau_b(v_b)$. Given this uncertainty, progress in ice flow modeling relies on the choice of an *ad hoc* sliding law, which is sufficiently general to adequately describe diverse conditions at the ice-bed interface. At the same time, the form of the sliding law should be sufficiently constrained in order to give the models enough predictive power and to make analytical calculations possible.

The sliding law that is most commonly encountered in the literature on ice flow modeling is of the Weertman-type (recall equation (2.2.12)). In 3 dimensions, such a relation has the form

$$\boldsymbol{v}_b = c(x,y)|\boldsymbol{T}_b|^{m-1}\boldsymbol{T}_b\,, \tag{2.2.13}$$

where $\boldsymbol{T}_b$ is the basal stress vector given by $\boldsymbol{T}_b = \boldsymbol{\sigma}\boldsymbol{n} - (\boldsymbol{n}^T \cdot \boldsymbol{\sigma}\boldsymbol{n})\boldsymbol{n}$, with $\boldsymbol{n}$ a unit normal vector to the bed pointing into the ice, and $\boldsymbol{v}_b$ the basal sliding velocity given by $\boldsymbol{v} - (\boldsymbol{n}^T \cdot \boldsymbol{v})\boldsymbol{n}$, with $\boldsymbol{v}$ the flow velocity vector. This form of the sliding law will be used throughout the remainder of this text.

As a final remark, we point out that our focus so far has been on classical theories of sliding over a hard bed, whereas most of the recent work has focused on the effect of subglacial till deformation (see e.g. [Tulaczyk et al., 2000] or Clarke [2005] for an overview). Since our interest in chapters 4 and 5 will be mainly in fast-flowing West Antarctic ice streams – which obtain a large fraction of their speed by till deformation – it is important to point out that a relationship of the form (2.2.12) is also approximately valid for soft beds, particularly soft beds where the physical properties of the subglacial sediment are unknown. In general, the slipperiness of the bed, $c(x,y)$, will depend on the strength of the substrate. Weak beds (with low yield stresses $\tau_* \sim 1 - 50$ kPa) generally allow a rapid slip motion despite low basal shear stresses – a situation that was shown to be valid for Whillans Ice Stream [Kamb, 1991, 2001] and Bindschadler

Ice Stream [Kamb, 2001]. The value of m is often considered to be infinite, i.e., the constitutive response of the till is plastic. This is in agreement with experimental data [Tulaczyk et al., 2000], but should not be accepted as a general rule.

In the remainder of this and the next chapter, $c(x, y)$ and m will be treated as adjustable quantities. In this way we keep the sliding law sufficiently general, and avoid the introduction of physical parameters that are difficult to measure for individual ice streams. Moreover, part of our aim in section 5 will be to investigate how our knowledge about $c(x, y)$ and m can be improved using surface measurements and inverse modeling techniques.

2.3 Basic ingredients of ice flow dynamics

Our aim is to develop a better understanding of how basal properties (topography $b(x, y)$ and slipperiness $c(x, y)$) of a glacier or ice sheet transfer through the ice and leave their fingerprint at the surface. So far, we have discussed the mechanical properties of ice in section 2.1 and of the ice-bed interface in section 2.2. In this section we introduce the *dynamical equations* that allow us to model the time-dependent evolution of the flow. In particular, a time-dependent solution for the surface topography and surface velocities can be obtained. The relation between these surface quantities and the basal properties determines the transfer functions which will be discussed in chapter 3.

Any ice flow must obey the fundamental conservation laws of classical continuum physics for an isolated system. We state these laws in their local form, which is most useful for our purposes.

- *Conservation of mass* (continuity equation):

$$\partial_t \rho + \partial_i (\rho v_i) = 0 \,, \tag{2.3.14}$$

where the notations $\partial_t = \frac{\partial}{\partial t}$ and $\partial_i = \frac{\partial}{\partial x_i}$ are introduced with $x_i \in \{x, y, z\}$. If

the density of ice is taken constant, $\rho = 917\,\mathrm{kg/m^3}$, then (2.3.14) reduces to

$$\partial_i v_i = 0\,. \tag{2.3.15}$$

The conservation of mass is therefore equivalent to the incompressibility equation (2.1.3). Since ρ is constant, conservation of mass implies conservation of volume.

- *Conservation of linear momentum* (balance of forces):

$$\partial_j \sigma_{ij} + \rho g_i = \rho \frac{\mathrm{d}v_i}{\mathrm{d}t}\,, \tag{2.3.16}$$

where g_i are the x-, y- and z-components of acceleration due to gravity. If we assume the flow to be in static equilibrium, the acceleration terms on the right hand side of equation (2.3.16) can be neglected, i.e., $\frac{\mathrm{d}v_i}{\mathrm{d}t} \approx 0$.

- *Conservation of angular momentum*:

$$\sigma_{ij} = \sigma_{ji}\,. \tag{2.3.17}$$

This relation implies that there are only 6 independent local stress components: 3 normal stresses σ_{ii} and 3 shear stresses σ_{ij}, $i < j$.

The balance equations (2.3.15) and (2.3.16) provide 4 independent relations between 9 physical quantities (the 6 stress components σ_{ij} and the 3 velocity components v_i). The system is underconstrained and needs to be supplemented by the flow law (2.1.11) such that a unique solution exists. Glen's law provides 6 independent relations between the physical variables, and since it automatically incorporates the conservation of mass (2.3.15), we are left with 9 independent equations which can be solved for the 3 normal stresses, 3 shear stresses, and 3 velocities.[4]

[4]It should be noted that for any realistic glacier or ice sheet, an additional set of equations needs to be solved that determines the thermodynamic properties of the flow. These equations correspond to the conservation of energy and the conservation of entropy. In our work the thermodynamic equations of state will not be considered though.

The relevant boundary conditions are given by the sliding law – which we discussed at length in section 2.2 – and the *kinematic boundary conditions* at the bed $z = b(t, x, y)$ and surface $z = s(t, x, y)$:

$$\text{bed:} \qquad \boldsymbol{v} \cdot \boldsymbol{n} = 0 \quad \text{at} \quad z = b(t, x, y)\,, \tag{2.3.18}$$

$$\text{surface:} \qquad \partial_t s + v_x \partial_x s + v_y \partial_y s - v_z = 0 \quad \text{at} \quad z = s(t, x, y)\,. \tag{2.3.19}$$

Since (2.3.15) and (2.3.16) both describe a steady state, the only explicit time dependence of the flow is introduced via the surface boundary condition (2.3.19). Basal elevation changes are assumed to be negligible, i.e., $b = b(x, y)$, and surface accumulation and ablation as well as basal melting and refreezing are ignored. These assumptions are only approximately valid for some interior parts of the East Antarctic Ice Sheet and a direct comparison between our theoretical results and observational data therefore needs careful consideration.

In principle, the set of relations (2.1.5) and (2.3.15)-(2.3.19) can be solved assuming sufficient knowledge about the initial conditions. In practice, though, a full solution of this complicated set of differential equations is very hard to obtain, and one often relies on numerical analysis. To make the analytical/numerical problem more tractable, (physically motivated) assumptions have to be imposed on the quantities that are involved. We now discuss several of these approximations that will be relevant later on.

2.3.1 Linearizations

The ice flow problem can be linearized at different levels.

(i) One sometimes assumes a linear ice rheology (i.e., $n = 1$) and/or a linear sliding law (i.e., $m = 1$). Although physically less sound, these are often the only cases for which an exact analytical solution can be obtained.[5] As we pointed out before,

[5]The reasons why we insist on having an analytical solution are twofold. Analytical solutions are computationally much more efficient to use, and they provide better insight into the structure of the

the full-Stokes transfer problem has only been solved analytically for this linear case [Gudmundsson, 2003]. However, numerical analysis have shown that non-linear effects do not drastically change the behavior of the solution [Raymond and Gudmundsson, 2005]. We will come back to this in chapter 3.

(ii) The boundary conditions can be linearized. One assumes that the bed topography, basal slipperiness, surface topography and surface speeds can be expanded around a constant mean value, indicated by a superscript $.^{(0)}$:

$$\begin{aligned} b(x,y) &= b^{(0)} + \Delta b(x,y)\,, \\ c(x,y) &= c^{(0)} + \Delta c(x,y)\,, \\ s(t,x,y) &= s^{(0)} + \Delta s(t,x,y)\,, \\ v_i(t,x,y,z=s) &= [v_i^{(0)}(z) + \Delta b(x,y)\,\partial_z v_i^{(0)} + \Delta v_i(t,x,y,z)](z=s^{(0)})\,. \end{aligned} \tag{2.3.20}$$

The deviations from the mean values are assumed to be "small". For the bed and surface topography this means that $\Delta b/H \ll 1$ and $\Delta s/H \ll 1$ with H the mean ice thickness of the glacier or ice sheet (Figure 2.1). For the slipperiness perturbation and speeds we must have $\Delta c/c^{(0)} \ll 1$ and $\Delta v_i/v_i \ll 1$. The Ansatz (2.3.20) can be substituted into the equations (2.1.5), (2.3.15)-(2.3.19) and after a Taylor expansion only the terms up to first order in Δb, Δc, Δs and Δv_i are retained. The resulting equations are linear in the deviations and substantially easier to solve.

It is common to choose the mean values $b^{(0)}$, $c^{(0)}$, $s^{(0)}$ and $v_i^{(0)}$ as the solutions for the undisturbed flow (i.e., the zeroth order solution) along an infinite-plane-slab geometry. Such a configuration is shown in Figure 2.1 (red dashed lines). The x-axis is taken along the upper surface in the direction of the flow, the y-axis transverse to the flow, and the z-axis normal to the surface. The slab has mean

problem.

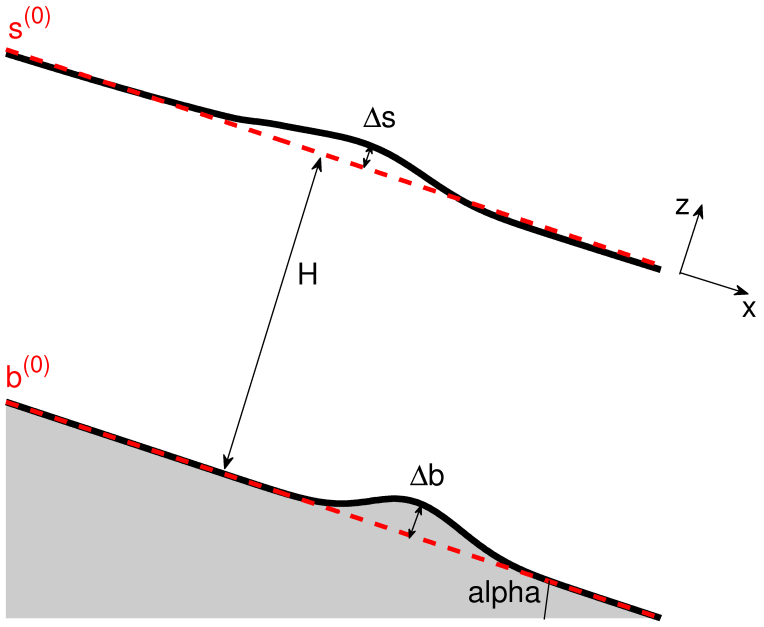

Figure 2.1: Cartoon representation of ice flow in the perturbed plane-slab approximation. The ice thickness and uniform inclination of the slab are denoted by H and α respectively. The undisturbed bed ($b^{(0)}$) and surface ($s^{(0)}$) are represented by the red dashed lines. The small disturbances are denoted by Δb and Δs. A convenient coordinate system is chosen with the x-axes along $s^{(0)}$ and the z-axes perpendicular to the surface.

thickness H and a mean slope α. For our choice of the coordinate system, the zeroth-order solution takes the form (for $n = 1$ and $m = 1$)

$$
\begin{aligned}
& b^{(0)} = -H\,, \qquad s^{(0)} = 0\,, \\
& c^{(0)} = v_{b,x}^{(0)} / \sigma_{xz}^{(0)}(-H)\,, \qquad \sigma_{xz}^{(0)}(z) = -\sin(\alpha)\rho g z\,, \\
& v_x^{(0)}(z) = -\sin(\alpha)\rho g \left[A(z^2 - H^2) - c^{(0)} H\right]\,, \qquad v_y^{(0)} = v_z^{(0)} = 0\,,
\end{aligned}
\tag{2.3.21}
$$

where $g = 9.81\,\mathrm{m/s^2}$ is the acceleration due to gravity. This solution is also known as a plug flow. We find that the mean value of the basal sliperiness, $c^{(0)}$, corresponds to the ratio of the mean basal sliding velocity and the driving stress. This quantity, which is generally small (< 10) for Alpine glaciers but large

(> 100) for fast-flowing ice streams, will play an important role in our analysis later on.

A linear ice rheology and sliding law will be encountered in chapter 3, but non-linearities will briefly be discussed as well. The perturbation approach up to first order in the bed- and surface variations along a plane-slab will be used throughout the remainder of this text.

2.3.2 Shallow-ice approximation

This approximation, which was first studied by Fowler and Larson [1978] and Hutter [1983], assumes that the ice thickness is small with respect to the horizontal extend of the ice sheet. If $[x] \approx [y]$ and $[z]$ denote the typical horizontal and vertical length scales, and $[z] \approx H$, then

$$\delta = [z]/[x] \ll 1\,. \tag{2.3.22}$$

In particular, this means that longitudinal derivatives of the stress and velocity are small compared to vertical derivatives. Models that have this property are sometimes referred to as long-wavelength models, for obvious reasons. Often the limit $\delta \to 0$ is taken, which corresponds to a zeroth-order approximation.

2.3.3 Shallow-ice-stream approximation

This approximation is based on the assumption that the vertical shear stresses are small compared to all other stress components, i.e.,

$$(\sigma_{xx}, \sigma_{yy}, \sigma_{zz}, \tau_{xy}, \tau_{xz}, \tau_{yz}) = [\sigma](\sigma^*_{xx}, \sigma^*_{yy}, \sigma^*_{zz}, \tau^*_{xy}, \delta\tau^*_{xz}, \delta\tau^*_{yz})\,, \tag{2.3.23}$$

with $[\sigma] = \rho g[z]$ a typical scale for the normal stresses and (2.3.22) is imposed. The shallow-ice-stream approximation is often used in current-day studies of ice stream dynamics and its equations have been derived several times in the literature, see e.g. MacAyeal [1989], Baral and Hutter [1999] or Schoof [2006]. In a nutshell, the conditions

(2.3.22) and (2.3.23) are substituted in (2.1.5) and (2.3.15)-(2.3.19), and only terms of zeroth order in δ are collected (this effectively corresponds to taking the limit $\delta \to 0$).

We have now gathered enough background material to initiate our discussion about the transfer of basal perturbances to the surface of glaciers and ice sheets. This flow mechanism is described by the so-called transfer functions, which will be introduced at length in the next chapter. But before we do that, let us briefly summarize the main lessons learned so far.

2.4 Summary

- Nye-Glen's flow law is the most commonly used description of ice rheology in large-scale ice-flow modeling. Its 3-dimensional form is inspired by experimental data and based on general theoretical arguments. Often the stress perturbations are assumed to be small enough such that the flow law can be linearized around a mean stress field. This corresponds to the case $n = 1$, which will be exploited in section 3.2. Experiments have shown that a nonlinear rheology ($n \approx 3$) is more appropriate, and extra care is needed when comparing linear models to real data.

- Despite numerous efforts to put some constraints on the form of the sliding law, no consensus has yet emerged on the general applicability of Weertman's law in the context of ice-flow modeling. In particular, no agreement has emerged on realistic values for m and values ranging from 1 to infinity are commonly encountered. Until a better understanding of basal sliding is obtained, Weertman's general law will be used. In our analysis it has two adjustable parameters, the basal slipperiness $c(x, y)$ and the stress exponent m.

- In the remainder of this text, the bed and surface profiles as well as the basal slipperiness will be split into a mean and a deviatoric part. All dynamic equations are studied up to first order in the small deviations. An important concept

is the plane-slab flow, which is the zeroth-order unperturbed solution to the flow equations. Further assumptions about the stress field can be imposed – we discussed the shallow-ice-stream approximation which will be used in chapter 5.

Chapter 3

Theory of transfer functions

This chapter is organized as follows: in section 3.1 we present a *brief overview of the literature* on bed-to-surface transfer characteristics. This will help the reader who is less familiar with this topic to assess the current state of research, and it allows us to provide the relevant references for those who seek a more in-debt understanding of the subject. Subsequently, in section 3.2 the *analytical transfer functions* are introduced for two particular forms of the momentum equations. First we present the solution to the full-Stokes problem with a linear ice rheology and linear sliding law, as obtained by [Gudmundsson, 2003]. This solution will be used as a benchmark for experimental data in chapter 4. In order to validate the use of this analytical result, we compare it to numerical experiments for arbitrary values of n and m [Raymond and Gudmundsson, 2005]. Secondly, the transfer functions for the shallow-ice-stream approximation with a linear ice rheology and arbitrary sliding exponent are reviewed [Gudmundsson, 2008]. This solution will be used in chapter 5 to investigate the sensitivity of inverse modeling results (i.e., the retrieved basal topography and slipperiness) to the form of the sliding law, and in particular to the value of m.

3.1 Previous work on the relation between bed and surface properties

The theoretical study of ice-flow equations subjected to varying boundary conditions has been a long-standing topic of interest to geophysicists. One of the earliest theoretical attempts to understand the effect of bedrock undulations on the surface topography of a flowing ice mass was made by Nye [1959]. Nye estimated the steady-state and transient transfer for a 2-dimensional flow with a simplified sliding law and for length scales that are long compared to the ice thickness. Subsequent analysis for the steady-state flow over a harmonic bed were done by Yosida [1964] for a Newtonian viscous medium with no slip, and by Budd [1970, 1971] for a non-linear medium. Budd [1970] obtained an approximate expression for the "damping factor" which governs the relation between the surface and bedrock shapes (similar to the transfer function). He found that bedrock undulations with wavelengths on the order of a few ice thicknesses are least dampened and therefore are most prominent at the surface. As we pointed out in the introduction (chapter 1), this is an effect that has been observed many times on the Greenland and Antarctic Ice Sheets [Robinson, 1966, Zwally et al., 1979, 1983, Whillans et al., 1984, Overgaard and Gundestrup, 1985].

The time-dependent changes in surface geometry due to changes in mass-balance were first analyzed by Nye [1963a,b, 1965], Lliboutry [1971] and Landon and Raymond [1978] for simplified 2-dimensional models. The propagation and decay of small surface disturbances was calculated by Lick [1970], both in the short and long wavelenth limit. Subsequently, Thompson [1979] and van de Wal and Oerlemans [1995] studied the phase velocity of surface waves in more detail, assuming a non-linear flow law. More recent theoretical and numerical results on glacier response to mass balance changes can be found in Bahr et al. [1998], Pfeffer et al. [1998], Harrison et al. [2001], Pattyn [2002], Leysinger Vieli and Gudmundsson [2004] and Lüthi [2009]. These results are less relevant in the context of our work, since we assume that ablation and accumulation

can be neglected or are uniform over the area of interest.

The effect of basal boundary conditions that vary spatially across or transverse to the flow direction have obtained less attention in the literature. An interesting early study was carried out by Raymond [1996], who found that a localized disturbance in slip resistance affects the basal stress and speed over distances that are many times the size of the disturbance. A nice example of such an effect are flow strips – depressions that often extend for hundreds of kilometers along the flow of fast moving ice streams. In Gudmundsson et al. [1998] their origin was related to local variations in either basal slipperiness or bedrock shape.

Finally, a systematic theoretical analysis of steady-state transfer amplitudes for basal undulations using *perturbation methods* (as discussed in section 2.3) was initiated by Hutter [1980, 1982, 1983] and Hutter et al. [1981]. This work, which was restricted to 2 dimensions, was later extended by Reeh [1987] to 3 dimensions for a linear rheology and sine-shaped basal undulations. Reeh [1987] found that 3-dimensional flow effects become substantial as the ratio between the longitudinal and the transverse wavelength increases. In particular, surface amplitudes are reduced significantly as compared to the 2-dimensional case. Basal velocity perturbations were incorporated by Balise and Raymond [1985] for a 2-dimensional flow of a linear medium, and Balise [1987] extended this analysis to a non-linear rheology. Johannesson [1992] significantly improved all previous analysis, and obtained the steady-state and transient response of a 2-dimensional ice flow subjected to bedrock and basal slipperiness perturbations. He also obtained a solution to the 3-dimensional steady-state problem.

Eventually, an analytical solution for the 3-dimensional full-Stokes transfer problem of bedrock and slipperiness perturbations with a linear ice rheology and linear sliding law was obtained by Gudmundsson [2003]. To date, this is still the most general analytical solution known. An exact solution for the transfer problem in the shallow-ice-stream approximation has been obtained by Gudmundsson [2008] for a linear rheology and arbitrary sliding exponent. Numerical experiments for a nonlinear flow and nonlinear sliding law were done by Raymond and Gudmundsson [2005].

Today, most of the work on transfer characteristics is related to the inverse problem. Instead of looking at the surface response of a known bedrock profile and basal slipperiness distribution, inverse modeling is used to obtain information about the bed from the measurement of surface data. Indirect information about the basal shear stress distribution of ice streams from surface measurements has been obtained, for example, by MacAyeal [1992, 1993], MacAyeal et al. [1995], Vieli and Payne [2003], Joughin et al. [2004, 2006]. The simultaneous retrieval of basal topography and basal slipperiness for a part of MacAyeal Ice Stream, West Antarctica, was done by Thorsteinsson et al. [2003]. A systematic approach to the retrieval of bed properties from surface data was developed by Gudmundsson [2004], Raymond [2007], Gudmundsson and Raymond [2008], Raymond and Gudmundsson [2009], based on the Bayesian statistical inversion method. This method has subsequently been applied to a flightline along Rutford Ice Stream Raymond-Pralong and Gudmundsson [2011]. For more information about the Bayesian inversion method we refer to chapter 5.

3.2 Transfer in the full-Stokes and shallow-ice-stream models

The *first order transient response* of a glacier's surface to small disturbances at its base is described by the *transfer functions*, T, which are defined as follows:

$$\Delta s = T_{sb}\,\Delta b + T_{sc}\,\Delta c\,, \tag{3.2.1}$$

$$\Delta v_i = T_{v_i b}\,\Delta b + T_{v_i c}\,\Delta c\,. \tag{3.2.2}$$

Each transfer function has two subindices, the first index relates to the effect and the second to the cause. For example, T_{sb} describes the effect on the surface topography (s) caused by perturbations in the bedrock topography (b), $T_{v_i c}$ describes the effect on the surface velocities (v_i) caused by variations in basal slipperiness (c), and so on.

The relations (3.2.1) and (3.2.2) form a perturbative solution to the conservation

equations and boundary conditions, up to first order in the small disturbances Δb, Δs, Δc and Δv_i. The transfer functions depend on the following parameters: (i) the spatial coordinates along the surface and time, (ii) the mean ice thickness and the inclination angle of the plane-slab, (iii) the mean slipperiness, (iv) Glen's flow law exponent and the sliding exponent, and (v) the ice viscosity.

It is often convenient to formulate the transfer problem in Fourier space, which makes it easier to solve the boundary and momentum equations. A forward Fourier transform relates spatial coordinates to wavenumbers as follows:

$$\hat{f}(k_x) = \int \mathrm{d}x \, f(x) \, \mathrm{e}^{2\pi \mathrm{i}(k_x x)} \,, \tag{3.2.3}$$

for any integrable function $f(x)$, and wavenumbers k_x. The latter are related to wavelengths via $\lambda_x = 2\pi/k_x$. In the following, we will only consider Fourier-transformed functions, and the hat-notation will be omitted for convenience. In particular, the transfer functions are

$$T = T(t, k_x, k_y, p) \quad \text{with} \quad p = \{H, \alpha, c^{(0)}, n, m, \eta\} \,. \tag{3.2.4}$$

The exact form of these functions depends on the chosen approximations scheme for the momentum equations and boundary conditions. For example, the transfer functions in the shallow-ice-stream approximation (i.e., $\delta \to 0$) deviate from the transfer functions for the full-Stokes flow (i.e., up to all orders in δ) for wavelengths shorter than a few ice thicknesses. In the remainder of this section, the transfer functions for both schemes will be presented, and their differences will be described in more detail.

3.2.1 The full-Stokes solution

Our discussion in this paragraph is based on the results obtained by Gudmundsson [2003] for a full-Stokes model with a linear ice rheology ($n = 1$) and a linear sliding law ($m = 1$). The results presented here will form the basis for our comparison with

experimental data in chapter 4. Since only the response of the surface topography to bedrock undulations will be studied, we restrict our attention to the transfer function T_{sb}. Similar expressions for the other transfer functions can be found in Gudmundsson [2003].

$$T_{sb}(t, k_x, k_y, H, \alpha, c^{(0)}, \eta) = \frac{\mathrm{i}\,\tilde{a}/\tilde{c}}{\mathrm{i}t_p^{-1} - t_d^{-1}} \left(1 - e^{\mathrm{i}t/t_p} e^{-t/t_d}\right) , \tag{3.2.5}$$

with the phase timescale t_p and decay timescale t_d given by

$$t_p = \tilde{c}/\tilde{d}\,, \qquad\qquad t_d = \tilde{c}/\tilde{b}\,, \tag{3.2.6}$$

and

$$\begin{aligned}
\tilde{a} &= \left[V_{s,x}^{(0)}\tilde{f} + \left(V_{s,x}^{(0)} + k^2 {C^{(0)}}^2\right)\cosh(\mathrm{k})\right] k\,k_x\,, \\
\tilde{b} &= \left[\tilde{f}\sinh(k) - k\right]\cot(\alpha)\,, \\
\tilde{c} &= k^3 V_{s,x}^{(0)} + \tilde{f} k \cosh(k)\,, \qquad \tilde{d} = k_x V_{s,x}^{(0)}\left(\tilde{c} + k\right)\,, \\
\tilde{f} &= \cosh(k) + k C^{(0)} \sinh(k)\,.
\end{aligned}$$

Furthermore we have used the following notations:

$$k = \sqrt{k_x^2 + k_y^2}\,, \qquad C^{(0)} = \eta\, c^{(0)}/H\,, \qquad V_{s,x}^{(0)} = 1 + C^{(0)}\,. \tag{3.2.7}$$

Since the typical contribution to the surface speed due to internal creep is given by $v_{d,x}^{(0)} = H\sigma_{xz}^{(0)}(-H)/\eta$, it follows from (3.2.7) and (2.3.21) that the new parameter $C^{(0)}$ is equal to the ratio of the mean basal sliding velocity and the mean forward deformational velocity:

$$C^{(0)} = \frac{v_{b,x}^{(0)}}{v_{d,x}^{(0)}}\,. \tag{3.2.8}$$

This quantity is also called the *slip ratio*. Remark that the viscosity η and the mean ice thickness H only enter the transfer function indirectly via the slip ratio.

The steady state response can be found by taking the limit $t \to \infty$ for T_{sb}:

$$T_{sb}|_{t\to\infty} = \tilde{a}/\left(\tilde{d} + \mathrm{i}\tilde{b}\right) . \tag{3.2.9}$$

The transient and steady-state transfer functions are both complex functions with an amplitude and a phase. The amplitude corresponds to the amplitude ratio between the surface and basal topography, whereas the phase describes the shift (in Fourier space) of the surface undulations with respect to the perturbations in the bedrock.

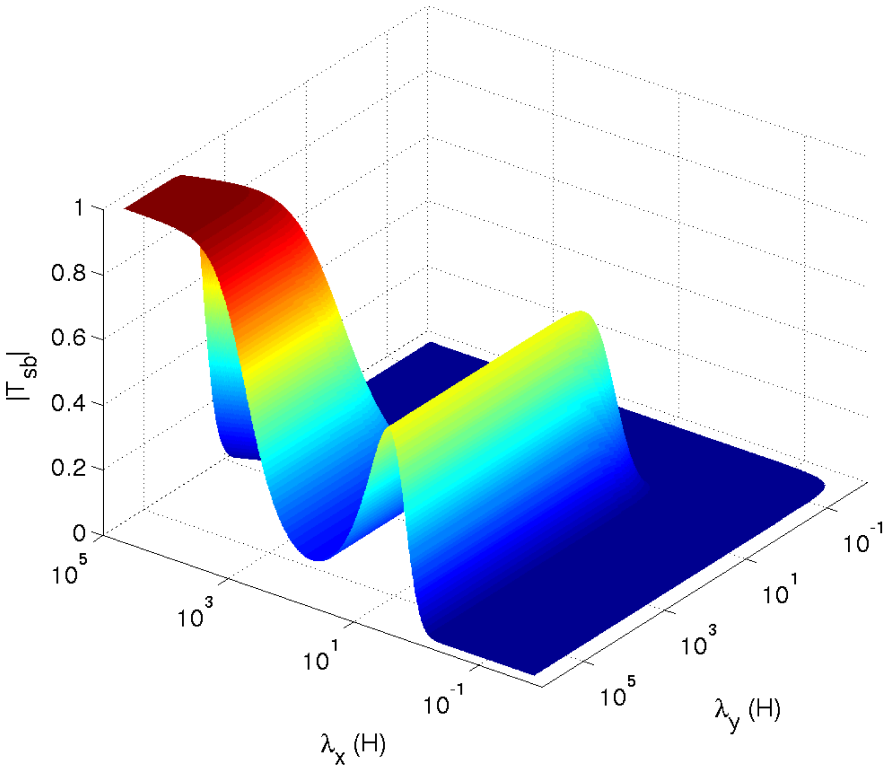

Figure 3.1: Steady-state transfer amplitude $|T_{sb}|$ for $\alpha = 0.003$ and $C^{(0)} = 100$.

In Figure 3.1 we present the steady-state transfer amplitude $\left|T_{sb}(k_x, k_y, C^{(0)}, \alpha)\right|$ for $C^{(0)} = 100$ and $\alpha = 0.003$ (these are typical values for a fast-flowing Antarctic ice stream). The x- and y-axis have a logarithmic scale and represent the wavelengths λ_x and λ_y in units of ice thickness. We can distinguish between different regimes. For short wavelengths $\lambda_y < H$, the transfer is close to zero for all values of λ_x. For intermediate and long wavelengths $\lambda_y > H$, the transfer amplitude develops a non-

trivial behavior as a function of λ_x: for small values of $\lambda_x < H$, the transfer is zero; for long wavelengths $\lambda_x > 10^4 H$ the transfer converges towards 1; and for intermediate wavelengths the transfer functions shows a local peak.

We are particularly interested in the characteristic behavior of $|T_{sb}|$ for long wavelengths λ_y. This is motivated by the fact that the flow of an ice stream in chapter 4 will be treated as a 2-dimensional problem, and basal perturbations transverse to the flow direction (i.e., in the y-direction) will be neglected. This effectively corresponds to taking the limit $k_y \to 0$ in (3.2.9), and we can concentrate on the behavior of the resulting function $\left|T_{sb}(k_x, C^{(0)}, \alpha)\right|$.

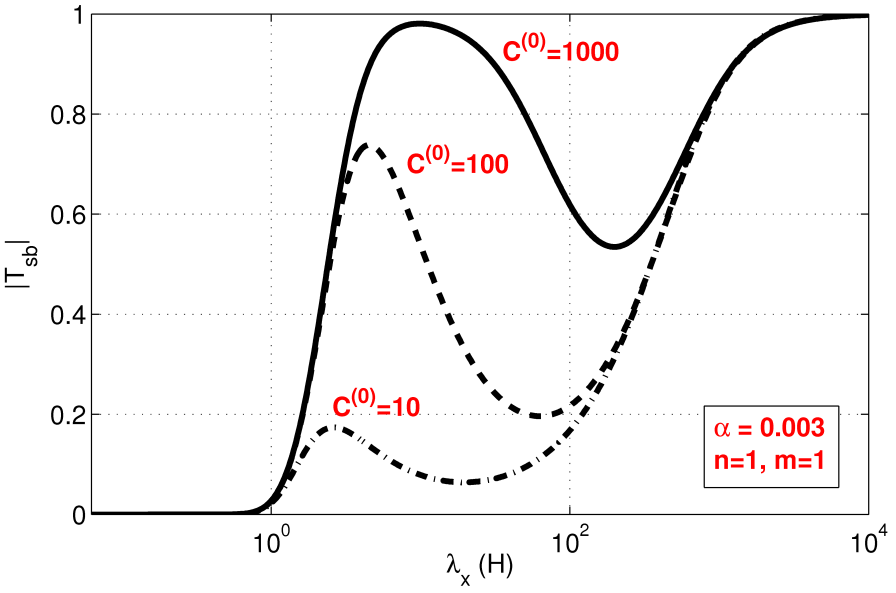

Figure 3.2: 2-dimensional steady-state transfer amplitude $|T_{sb}|$ for $\alpha = 0.003$ and 3 values of the mean slip ratio.

Figure 3.2 shows the 2-dimensional transfer amplitude for $\alpha = 0.003$ and 3 different values of $C^{(0)}$. As we pointed out before, the transfer function has a local maximum for intermediate wavelengths $H < \lambda_x < 10^2 H$. However, we now see that the amplitude of this maximum is strongly dependent on the value of $C^{(0)}$. For low values of the slip ratio, i.e., $C^{(0)} < 10$, the peak is almost absent, whereas it is much more prominent for $C^{(0)} > 100$. In other words, for slippery beds – such as those underneath fast-flowing ice streams – the transfer of information about bedrock undulations to the surface

happens very efficiently for intermediate wavelengths. This feature distinguishes ice streams with a high slip ratio from ice flows that have a low slip ratio, such as the surrounding ice sheet. It is exactly this important distinction that will be the subject of our research in chapter 4, and that will allow us to test the validity of the theoretical model.

However, recall that the solution for T_{sb} in (3.2.5) is only valid for $n = 1$ and $m = 1$. Therefore the question remains whether the predicted peak in the transfer amplitude is related to this specific choice of n and/or m, or whether it is a more general, and therefore present for more realistic values of n and m. Since there does not exist an analytical solution to the full-Stokes transfer problem for arbitrary n and m, an answer to this question relies on numerical analysis of the momentum equations and boundary conditions. In Raymond and Gudmundsson [2005] this numerical problem was addressed, and in the next paragraph we briefly review the results.

3.2.2 Numerical results

We discuss Figures 8b and 11a in Raymond and Gudmundsson [2005], which summarize the dependence of T_{sb} on Glen's exponent n and the sliding exponent m respectively (for convenience we repeat these figures in Figure 3.3a and 3.3b respectively). From Figure 3.3a one can see that for values $n = 3$ and $n = 5$ the local peak in the transfer function is still present, but its amplitude increases and the maximum shifts towards longer wavelengths. Despite these changes, there is little qualitative difference between the solutions for a linear ice rheology and a non-linear medium.

Figure 3.3b in Raymond and Gudmundsson [2005] shows the transfer amplitude for $n = 3$ and $m = 1$, 3 and 20. Again there is no qualitative difference between the different values of m, and a peak is clearly present in all cases. The dependence of T_{sb} on m is weak, with only a minor decrease in the transfer amplitude for $m = 20$ with respect to $m = 1$. It is also expected that $|T_{sb}|$ exhibits a fast convergence towards a limiting curve for increasing values of m. As a consequence, the transfer amplitude for

a plastic bed ($m \to \infty$) is roughly equal to the transfer amplitude for $m = 20$.

We conclude that for high values of the slip ratio, a peak in the transfer function is to be expected, irrespective of the physical values of n and m. This is an important result in the light of our work in chapter 4.

Finally, in order to prepare for the results presented in chapter 5, we conclude this section about transfer functions with a short discussion about the form of the analytical transfer functions in the shallow-ice-stream approximation.

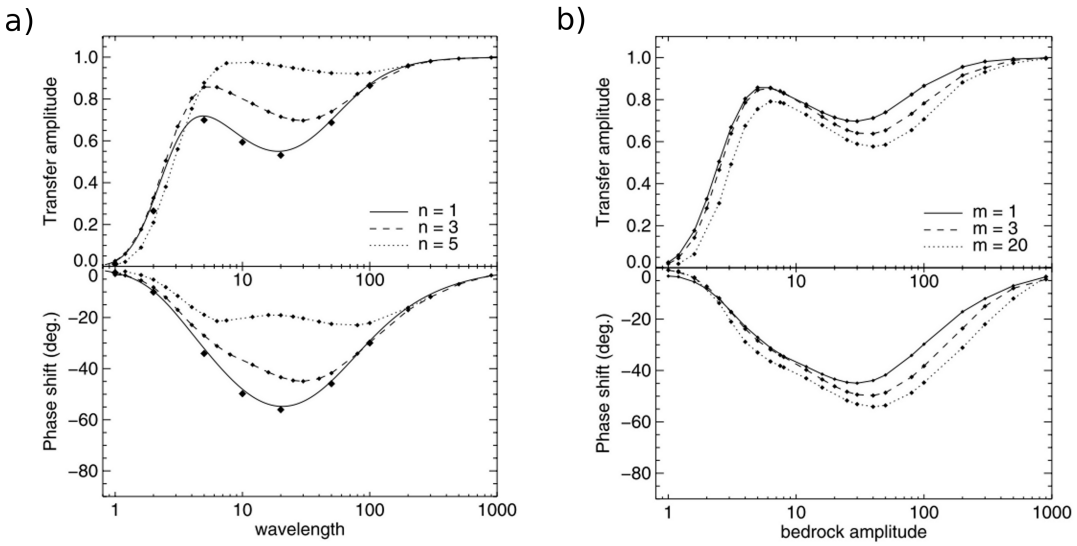

Figure 3.3: **(a)** Steady state amplitude ratios and phase shifts for a perturbation in basal topography for $C^{(0)} = 10$. Diamonds indicate calculated values. The solid line is the analytical solution valid for $n = 1$. The dashed and the dotted lines are linear interpolations of calculated values for $n = 3$ and $n = 5$, respectively. The mean surface slope is $\alpha = 0.05$. **(b)** Same as in (a) but for 3 different basal sliding exponents $m = 1$, 3, and 20 and $n = 3$. These figures are reproduced from Raymond and Gudmundsson [2005].

3.2.3 The shallow-ice-stream solution

The results presented in this paragraph were obtained by Gudmundsson [2008].[1] Recall from section 2.3 that the shallow-ice-stream approximation assumes that the extend of a glacier or ice stream is large compared to its mean ice thickness, and that the vertical shear stresses can be ignored. In terms of the notations used in (2.3.22) and (2.3.23), it means that $\delta \to 0$. In this limit, an analytical solution for the transfer functions can be found for $n = 1$ and arbitrary sliding exponent m. The final expressions, which are now functions of t, k_x, k_y, α, $C_{(0)}$ and m, are quite involved and it is not instructive to show them here. Instead, we plot some of the steady-state results, investigate their dependence on wavelength, m and $C^{(0)}$, and compare them to the full-Stokes solution.

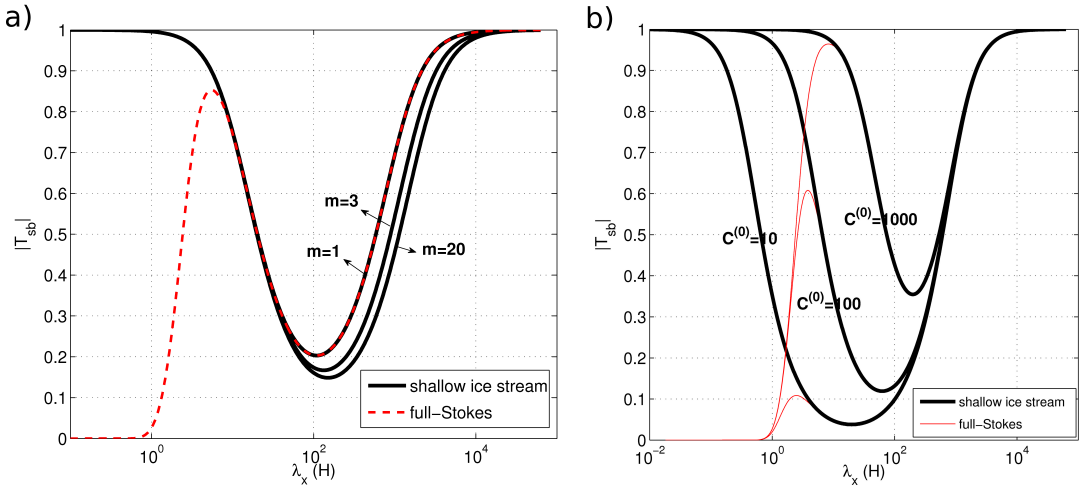

Figure 3.4: **(a)** Transfer amplitude for the shallow-ice-stream approximation with mean slope $\alpha = 0.003$, mean slip ratio $C^{(0)} = 300$ and 3 values of the sliding law exponent $m = 1$, 3, and 20. The full-Stokes solution is plotted for comparison. **(b)** Transfer amplitude for the shallow-ice-stream approximation with mean slope $\alpha = 0.003$, sliding law exponent $m = 1$ and three values of the mean slip ratio $C^{(0)} = 10$, 100, and 1000. Again the corresponding full-Stokes solutions are plotted.

In Figure 3.4a we present the shallow-ice-stream solution for the steady-state am-

[1] It should be noted that momentum equations (1) and (2) in Gudmundsson [2008] – which form the starting point of that paper – contain an error in their third term on the left hand side. However, Gudmundsson [*unpublished*] has obtained the solutions to the correct equations, and the results do not differ significantly from those presented in Gudmundsson [2008]. In this text, we present the corrected solutions.

plitude $|T_{sb}|$ in the limit $k_y \to 0$ and for 3 values of the sliding exponent: $m = 1$, 3 and 20 (black lines). The inclination angle was chosen to be $\alpha = 0.003$ and the slip ratio $C^{(0)} = 300$. For comparison, we also plot the corresponding full-Stokes solution (dashed red line), which is only valid for $m = 1$. For wavelengths $\lambda_x > 10H$ the full-Stokes and shallow-ice-stream solutions coincide exactly. At shorter wavelengths, the shallow-ice-stream approximation converges towards 1, and largely overestimates the bed-to-surface transfer. For values $m > 1$, a small decrease in transfer occurs for $\lambda_x > 50H$. This is in agreement with the numerical results for the full-Stokes problem, presented in Figure 3.3b. In the limit $m \to \infty$, the shallow-ice-stream transfer amplitude converges towards a curve that is well approximated by the curve for $m = 20$.

From the correspondence between the shallow-ice-stream and full-Stokes solutions, and the $C^{(0)}$-dependence of the latter (recall Figure 3.2), we expect to find a decrease in transfer at intermediate wavelengths for low values of the slip ratio. Indeed, Figure 3.4b shows that for low values of the slip ratio, the transfer becomes negligible for a large interval of intermediate wavelengths. For higher values of $C^{(0)}$, this local minimum is less pronounced, and the transfer amplitude remains relatively constant for a large part of the spectrum. The curves in Figure 3.4b are plotted for $\alpha = 0.003$ and $m = 1$, and the corresponding full-Stokes solutions are shown for comparison.

We conclude that the shallow-ice-stream solution is only a good approximation to the full-Stokes solutions for wavelengths $\lambda_x > 10H$. In particular, it does not reproduce the local maximum at intermediate wavelengths that was characteristic for the full-Stokes solution. The benefit of having the shallow-ice-stream solution is its analytical dependence on m. This property will be exploited in chapter 5. In order to make that analysis as accurate as possible, we will be careful not to include short wavelengths where the shallow-ice-stream approximation cannot be trusted.

3.3 Summary

We recall the following important results from this section.

- Transfer functions relate bed topography (b) and basal slipperiness (c) to surface topography (s) and velocity components (v_i). They are functions of the longitudinal and transversal wavelengths and of the parameters that determine the undisturbed (zeroth-order) flow, sliding law and ice rheology.

- An analytical expression for T_{sb} was presented for the 3-dimensional linear full-Stokes model up to first order in the basal and surface perturbations. The main feature of this solution is the presence of a local maximum for the transfer at wavelengths between 1 and 20 ice-thicknesses. The amplitude of this maximum depends critically on the mean slip ratio $C^{(0)}$, with more efficient transfer for slippery beds.

- Numerical solutions for a non-linear full-Stokes model have shown no critical dependence on the values of m and n.

- The shallow-ice-stream approximation overestimates the effects of basal perturbations on the surface topography for wavelengths less than 5 to 10 ice-thicknesses. It correctly reproduces the transfer of the full-Stokes solution for longer wavelengths. An interesting feature of the shallow-ice-stream solution is its analytical dependence on the sliding exponent, which makes it an important tool to analyze the dependence of ice stream dynamics on the sliding exponent.

In the next two chapters, our research results will be presented. In chapter 4 experimental evidence is provided for the form of the theoretical transfer amplitudes presented in this section.

Chapter 4

Observational evidence for the bed-to-surface transfer of Antarctic ice streams

4.1 Introduction

In the previous chapter we described the estimated response of a glacier's surface to bedrock irregularities using the theory of transfer functions. We saw that for high values of the mean slip ratio, theory predicts that information about the bedrock topography is most efficiently transmitted to the surface for two distinct windows of length-scales. (i) For basal undulations with wavelengths longer than 10^3 ice thicknesses, perfect transfer to the surface is expected. (ii) In addition, a local maximum in the theoretical transfer function appears for wavelengths between 1 and 20 ice thicknesses, irrespective of the values of Glen's flow law exponent and the sliding parameter.

On the other hand, Gudmundsson [2003] has pointed out that variations in basal slipperiness are only transmitted efficiently to the surface for *long wavelengths* ($\lambda_x > 10^2 H$, see Figure 4.1). Therefore, we expect that small and medium-scale variations in surface topography of fast-flowing ice streams are primarily determined by the underlying bedrock profile, whereas the effect of basal variations in slipperiness is limited. This observation has been confirmed by a study of radar data along a profile of the

Rutford Ice Stream [Raymond-Pralong and Gudmundsson, 2011]. Apart from a general increase in basal slipperiness toward the grounding line, the authors found no evidence for variations in basal slipperiness, and all short-scale variability ($< 10H$) in surface topography and surface velocities could be explained by variations in basal topography only.

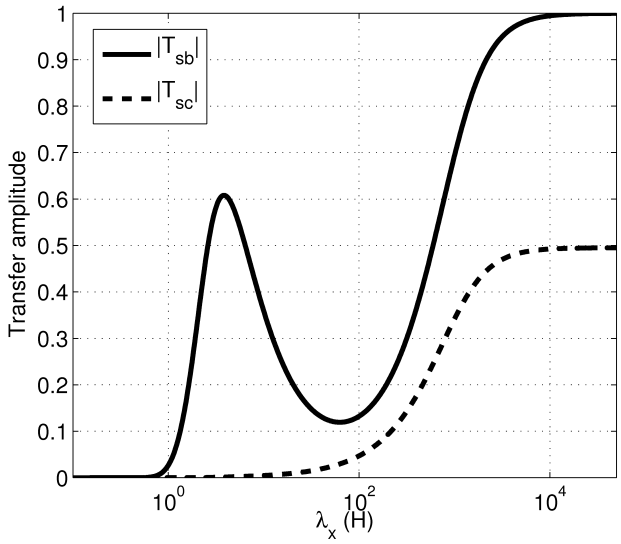

Figure 4.1: Transfer amplitudes that describe the effect of bedrock geometry ($|T_{sb}|$) and basal slipperiness ($|T_{sc}|$) on the surface topography. The surface response to c-variations is only significant for long wavelengths $\lambda_x > 10^2 H$.

The use of observational data to verify the theoretical results of Gudmundsson [2003] and Raymond and Gudmundsson [2005] has been very limited (see e.g. Gudmundsson et al. [2003]), and the effects on ice flow dynamics have mainly been studied using synthetic data. In particular, no direct experimental evidence has been obtained for the form of the transfer amplitude $|T_{sb}|$ that was presented in (3.2.5). In this section we address the issue directly for the first time. We analyze recently acquired radar data for the bed and surface topography of Rutford and Evans Ice Streams, Antarctica, and estimate their bed-to-surface response. We find a clear maximum in the bed-to-surface transfer function for wavelengths between 1 and 20 ice thicknesses, and discuss the dependency of this feature on flow characteristics such as the slip ratio and the value of Glen's flow law exponent. Several interesting discrepancies between the observed

and theoretical estimates are found, and we aim to provide a physical explanation for these disagreements.

4.2 Data and methods

4.2.1 Data description

We used unmigrated bed and surface returns[1] from an extensive radio echo sounding survey (RES) over the southwestern margin of the Filchner-Ronne Ice Shelf and the adjacent West Antarctic Ice Sheet (inset of Figure 4.2). In January 2007, the British Antarctic Survey flew twenty-two RES sorties from two remote field camps (Rutford Ice stream Camp at 78°08'S, 83°54'S and Ski-Blu at 74°51'S, 71°35'W), covering a total distance of about 20.000 km. The radar platform consisted of a Twin-Otter equipped with the ice-sounding radar system PASIN (Polarimetric Airborne Survey INstrument), dual-frequency carrier-wave GPS for navigation and high frequency radar altimeter. The RES system operated at a center frequency of 150 MHz and 12 MHz bandwidth. More details about the radar system and data processing methods can be found in Corr et al. [2007] and Vaughan et al. [2006], Rippin et al. [2011] respectively.

Comparisons of ice thickness recorded at flight-line crossover points for a similar RES survey using the same equipment at Pine Island Glacier, has indicated a root-mean-square error of $\sim 23\,\mathrm{m}$ [Vaughan et al., 2006]. The errors from crossovers in measurements of ice-surface elevation were considerably lower, $\sim 1\,\mathrm{m}$. The uncertainty in bed-elevation measurement is therefore roughly equivalent to that in the ice thickness. The greatest sources of uncertainty for the surface measurements are the false determination of the airplane's position and the local build-up of snowdrift, the errors in the ice thickness result largely from off-nadir reflections and interpretation/digitizing uncertainty. The errors in surface- and bed profile are small and will not be of any concern for our work.

[1] We refer to Rippin et al. [2011] for a remark on the use of unmigrated data.

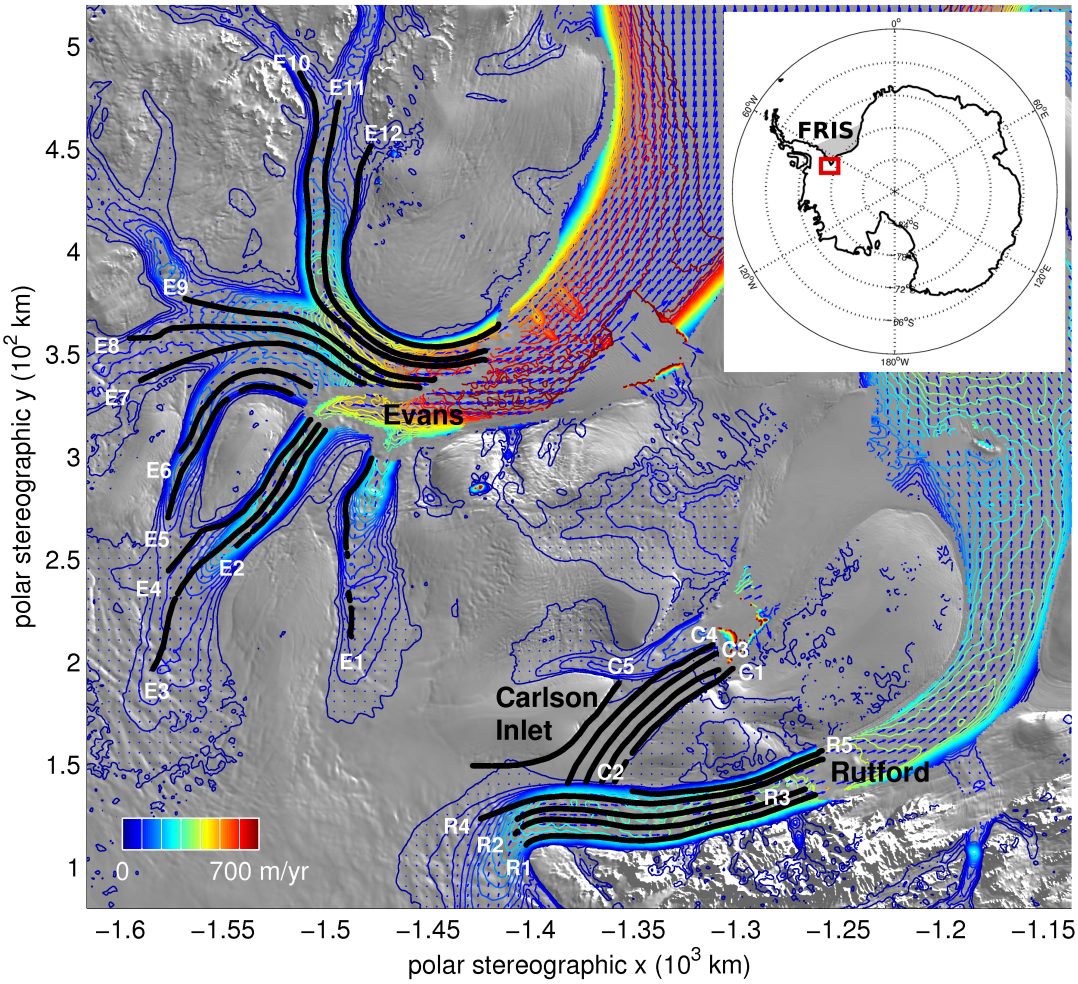

Figure 4.2: Map showing the Rutford Ice Stream, Evans Ice Stream and Carlson Inlet which flow into the Filchner-Ronne Ice Shelf (FRIS), West Antarctica (see inset). The color scale and arrows indicate the InSAR-derived surface velocity field [Joughin et al., 2006] overlaid on a subset of the MODIS mosaic for Antarctica. Only velocities higher than 20 m/yr are shown. Black lines represent the 22 sections of radar profiles that were analyzed in this work.

For our analysis, we selected 17 segments of flightlines along fast-flowing sections of the Ice Sheet. They are represented by the black lines in Figure 4.2, and enumerated R1-R5 for the Rutford Ice Stream and E1-E12 for the Evans Ice Stream. Moreover, 5 profiles selected for the slow-moving Carlson Inlet are indicated by C1-C5 in Figure 4.2. All 22 profiles satisfy the following criteria:

(i) Each profile is approximately parallel to the ice velocity field. This allows us to

treat the bed-to-surface transfer problem in a 2-dimensional plane (1 horizontal and 1 vertical direction), with the ice velocity vector lying in that plane. Of course, transverse effects can never be entirely excluded, an issue that will be discussed at length in section 4.4.

(ii) All profiles were restricted to the grounded part of the ice sheet. Some sections were also cut off at their upstream end to guarantee relatively constant flow conditions, i.e., limited variations in surface and basal velocity. On the other hand, profile lengths need to be sufficiently long, since we are interested in elevation perturbations with wavelengths up to 20 times the ice thickness. For our dataset, track lengths (l) vary from $l = 72\,\mathrm{km}$ for E2 to $l = 207\,\mathrm{km}$ for E10, and the mean ice thickness has values between $H = 1300\,\mathrm{m}$ and $H = 2600\,\mathrm{m}$.

(iii) There are no substantial gaps in the data, although some smaller gaps ($< 5\mathrm{km}$) are present for R2, C1, E2, E3 and E7. Two larger gaps of 18 km and 8 km were included for E1 and E5 respectively, and results for these two profiles should thus be treated with greater caution.

4.2.2 Plane-slab approximation

For each flowline, the bed and surface profiles were separated into a mean value and a deviatoric part, as in (2.3.20). The mean values correspond to the parameters of the zeroth-order plane-slab plug flow – recall (2.3.21). The slope and the mean ice thickness of the inclined slab were determined via a linear interpolation of the bed (denoted by $b^{(0)}$ in Figure 4.3) and the surface (denoted by $s^{(0)}$ in Figure 4.3). The value of α was set equal to the slope of $s^{(0)}$, the mean ice thickness H is the difference between $s^{(0)}$ and $b^{(0)}$ averaged along the profile. The fact that H is now measured vertically, whereas previously it was measured perpendicular to the mean bed profile (see Figure 2.1) is not a major issue. The fact that α is usually on the order of $0.002 - 0.005$ means that both definitions of H are almost equal. The "small" deviations Δs and Δb were defined as in (2.3.20), i.e., the difference between the original and the mean profile.

The third parameter in the plug flow is the mean slipperiness (or slip ratio). Recall from (3.2.8) that the slip ratio is defined as the ratio of the mean basal sliding velocity and the mean forward deformation due to creep. The latter is given by $v_{d,x}^{(0)} = \frac{2}{n+1}\left(\frac{\rho g \sin(\alpha)}{\eta}\right)^n H^{n+1}$ with H and α the values that were determined via the method described above. Furthermore, we used $n = 3$ and the viscosity for ice at $-10°$C, i.e., $\eta = 1.4 \times 10^8 \text{s}^{1/3}\text{Pa}$ [Cuffey and Paterson, 2010].[2] The sliding velocity, on the other hand, is given by the difference between the surface velocity and the forward deformation:

$$v_{b,x}^{(0)} = v_{s,x}^{(0)} - v_{d,x}^{(0)} \,. \tag{4.2.1}$$

The mean surface velocity along the profile ($v_{s,x}^{(0)}$) was estimated using InSAR data [Joughin et al., 2006]. Hence, both $v_{b,x}^{(0)}$ and $v_{d,x}^{(0)}$ can be determined, which allows us to estimate the mean slip ratio $C^{(0)}$ for each profile.

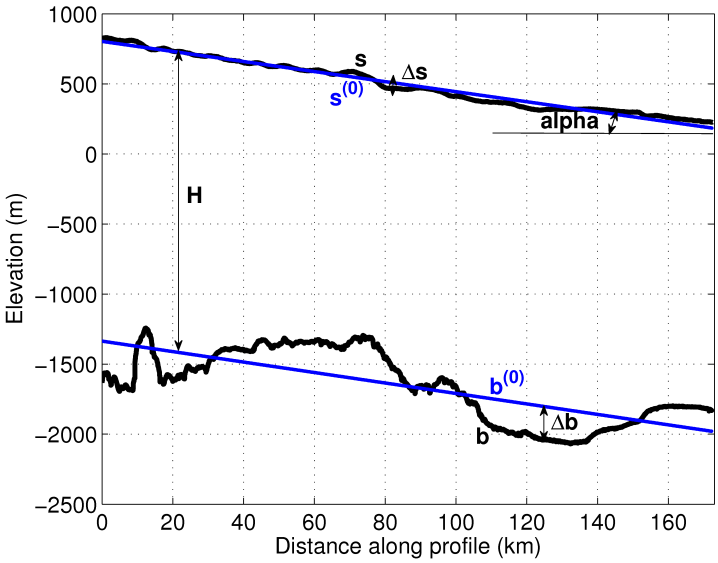

Figure 4.3: Bed (b) and surface (s) returns for flightline R4 along the Rutford Ice Stream (see Figure 4.2). A linear interpolation of b and s determines the mean parameters of the plug flow, i.e., the undisturbed bed ($b^{(0)}$) and surface ($s^{(0)}$) profiles, the mean ice thickness (H) and the mean slope (α). Deviations are defined as the difference between the mean and measured values ($\Delta b = |b - b^{(0)}|$ and $\Delta s = |s - s^{(0)}|$).

[2]Recall that η is expected to vary throughout the ice column, with close-to-temperate ice near the base, and stiffer ice at the surface. A slightly different value for η can have a large impact on the resulting forward deformation. Both issues will be discussed in section 4.4.

4.2.3 Estimated transfer amplitudes

For each flightline we estimate the transfer amplitude between the measured bed profile (Δb) and the surface profile (Δs) as a function of wavelength. The estimated amplitude will be denoted by $T_{sb}^{(\mathrm{m})}(\lambda_x)$ and is defined as the quotient of the Cross Power Spectral Density of Δb and Δs (i.e., the Fourier transform of the cross-correlation between the bed and surface signal), and the Power Spectral Density of Δb (i.e., the Fourier transform of the autocorrelation of the bed signal). The use of this definition has been tested extensively with synthetic data. In Figure 4.4 we present the results for such a test for a bed profile consisting of a single delta-peak with amplitude $0.1H$:

$$\Delta b(x) = 0.1\, H\, \delta(x - x_0)\,, \tag{4.2.2}$$

with x_0 the center of a 1-dimensional grid with 2^{13} grid points and grid scale 25 m (these grid parameters correspond roughly to those encountered in the dataset of measured radar profiles). First, the forward surface response, Δs, is calculated using the 2-dimensional steady-state expression for T_{sb} and (3.2.1) with $\Delta c = 0$. Next, $T_{sb}^{(\mathrm{m})}$ is estimated from Δb and Δs using the definition in terms of power spectral densities. In Figure 4.4 the estimated transfer $|T_{sb}^{(\mathrm{m})}|$ and analytical expression $|T_{sb}|$ are presented. Both curves coincide exactly, except for wavelengths $\lambda_x > 30H$. This is due to particular details of the analysis method that will be discussed in due course. We will point out why this discrepancy cannot be avoided, and why it does not pose any problems for our analysis.

The evaluation of $|T_{sb}^{(\mathrm{m})}|$ requires a Fourier-based analysis of the data. Therefore, each section was re-sampled onto an equally spaced grid of 2^N data points. The value of N was chosen independently for each profile, such that the new sampling interval is close to the mean original sampling interval (between 19.9 m and 23.8 m). The new data points were obtained using a cubic spline interpolation method, which also fills the data gaps discussed in item (iii) above. (It should be noted that our results do not crucially

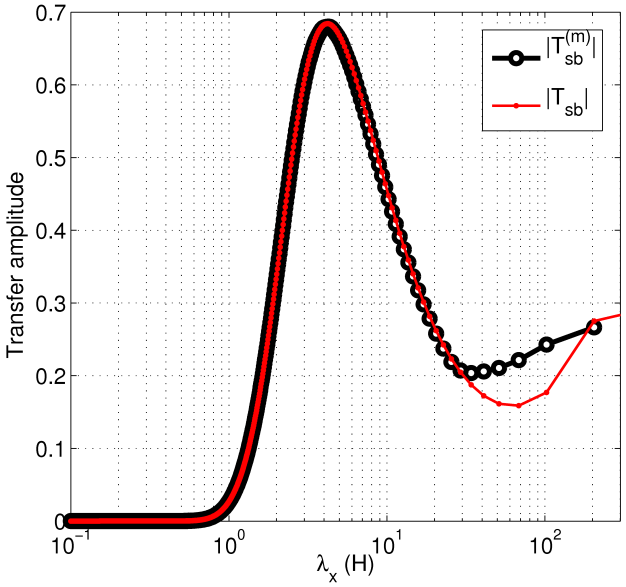

Figure 4.4: Estimated and theoretical transfer amplitudes for a synthetic bed consisting of a single delta-peak.

depend on this interpolation method, and a piecewise linear interpolation could be used instead, although this was found to introduce extra noise at high frequencies.)

The calculation of transfer amplitudes (or equivalently, power spectra) from real data can be surprisingly difficult, and results are often sensitive to various assumptions made in the analysis method. A common issue is the leakage of power between adjacent frequency bands, which results in a large variance for the spectral coefficients. In order to minimize this systematic error, we used Welch's averaged periodogram method [Welch, 1967]. Each elevation profile was divided into K overlapping segments of fixed length $L = 45\,\mathrm{km}$. For each segment, a Hamming window was applied, and the resulting power spectra for all segments were averaged. The value of L was fixed for all profiles, whereas K was allowed to vary depending on the length of each profile, i.e., $K \sim l/L$. Our choice $L = 45\,\mathrm{km}$ guaranteed that $K \geq 2$ for all profiles, given an overlap of 50% between different segments. Since the variance of the power spectral coefficients scales with $11/9K$, longer profiles (and hence larger values of K) generally lead to more reliable results. A smaller value for L would further reduce these errors, but valuable information about wavelengths on the order of 45 km would be lost.

This delicate balance between resolution and variance is one of the main drawbacks of Welch's method, and it highlights the importance of having long flightlines. Since lengths in our dataset are in the range $72\,\mathrm{km} < l < 207\,\mathrm{km}$, a trade-off was made in choosing $L = 45\,\mathrm{km}$, and the transfer amplitudes should only be taken seriously for $\lambda_x < 45\,\mathrm{km}$. Depending on the value of H, this limit of validity lies between $17H$ and $34H$, and only 3 profiles (R1, R2 and E2) have a ratio L/H smaller than 20. This is acceptable since we are only interested in the behavior of $T_{sb}^{(\mathrm{m})}(\lambda_x)$ for $H < \lambda_x < 20H$.

4.3 Results

We have obtained the transfer amplitudes for all 22 profiles along the Evans and Rutford ice streams and the Carlson Inlet. Our aim is to answer the following research questions.

- Do we observe enhanced transfer for intermediate wavelengths and high values of the slip ratio?
- If so, how does the peak amplitude depend on the slip ratio?
- Can we explain any possible discrepancies between theoretical predictions and observation?

In order to answer the first question, we restrict our attention to three examples (C5, R2 and E8) which have a wavelength-dependence that is broadly representative for the other profiles in the sample. The estimated transfer amplitudes for C5, R2 and E8 are shown in Figure 4.5a. Similar curves have been obtained for all flightlines, but it is not instructive to individually present them here. We will provide other examples later, when they are beneficial for the discussion. The estimated plane-slab parameters for C5, R2 and E8 are summarized in Table 4.1 (bold text). We also list the values for all other profiles for completeness and later reference.

Table 4.1: Physical properties of all profiles in Figure 4.2: length (l), mean ice thickness (H), mean surface slope (α), mean surface velocity ($v_{s,x}^{(0)}$), mean forward deformational velocity ($v_{d,x}^{(0)}$) and mean slip ratio ($C^{(0)}$). Selected profiles which are discussed in more detail in the text are indicated in bold.

profile	l (km)	H (m)	α (rad)	$v_{s,x}^{(0)}$ (m/yr)	$v_{d,x}^{(0)}$ (m/yr)	$C^{(0)}$
C1	81.0	1781	0.0062	12.1	9.6	0.3
C2	80.8	1742	0.0057	12.6	7.0	0.8
C3	90.9	1611	0.0056	10.8	4.6	1.3
C4	100.0	1686	0.0056	27.0	5.6	3.8
C5	**88.1**	**2081**	**0.0054**	**16.1**	**11.6**	**0.4**
R1	145.3	2553	0.0033	309.5	6.0	50.3
R2	**146.3**	**2351**	**0.0035**	**330.3**	**5.4**	**60.1**
R3	116.9	2149	0.0041	313.3	5.8	53.4
R4	172.3	2151	0.0036	284.0	4.0	70.5
R5	96.3	2073	0.0029	280.6	1.8	155.4
E1	90.9	2091	0.0061	121.3	17.5	5.9
E2	71.5	2272	0.0060	266.6	23.5	10.3
E3	147.0	2631	0.0041	198.6	13.4	13.8
E4	103.7	2174	0.0058	176.5	17.9	8.9
E5	98.8	2233	0.0045	129.3	9.3	12.8
E6	84.2	2294	0.0028	148.1	2.4	60.6
E7	117.0	2114	0.0019	160.7	0.6	279.9
E8	**150.1**	**1933**	**0.0017**	**243.2**	**0.3**	**854.1**
E9	131.0	1696	0.0017	311.4	0.2	2003.6
E10	206.8	1455	0.0025	320.6	0.3	1206.3
E11	183.0	1399	0.0024	336.8	0.2	1650.4
E12	160.0	1316	0.0025	258.7	0.2	1406.7

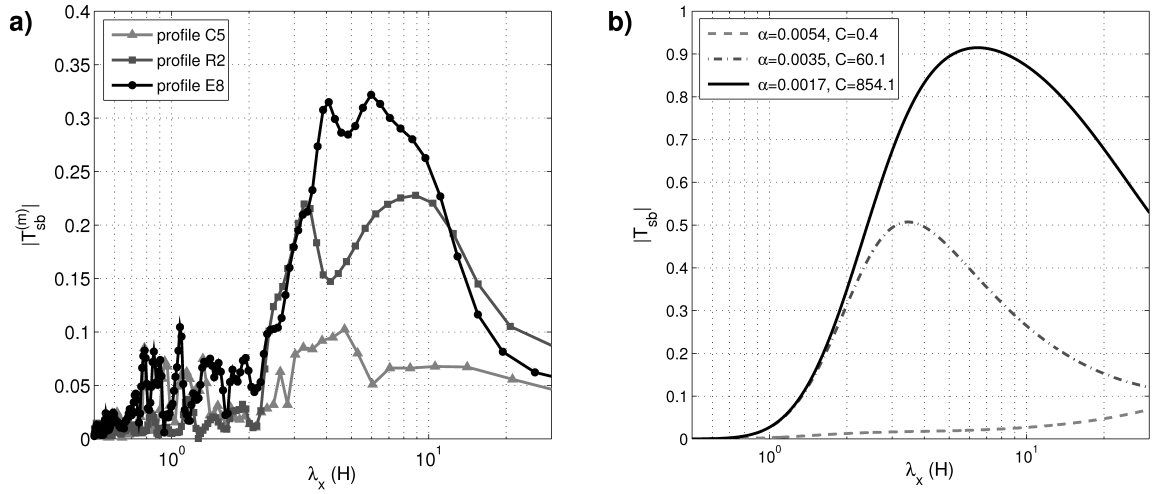

Figure 4.5: **(a)** Estimated transfer amplitudes for C5, R2 and E8. **(b)** Analytical solution for T_{sb} for $n = 1$, $m = 1$, and 3 different combinations of α and $C^{(0)}$, corresponding to the observed values for C5, R2 and E8 (see Table 4.1).

Since we are interested in comparing our results with theoretical predictions, we present in Figure 4.5b the analytical solutions (3.2.5) corresponding to the values α and $C^{(0)}$ for each of the three profiles C5, R2 and E8.

The first profile, C5, runs along a steeper but slow-flowing section of the ice sheet, which results in a small slip ratio ($C^{(0)} = 0.4$). For both the theoretical and observed estimates, we find *small (< 0.1) and relatively constant* values of $T_{sb}(\lambda_x)$. R2 and E8, on the other hand, have mean slip ratios that are several times higher ($C^{(0)} = 60.1$ and $C^{(0)} = 854.1$ respectively), which is reflected in much higher surface speeds. As expected, the observed transfer amplitudes for R2 and E8 show a *distinctive peak at intermediate wavelengths*. This qualitative agreement between theory and observation for low and high values of $C^{(0)}$ is generally true: none of the profiles with $C^{(0)} < 5$ (i.e., C1-C5 – see Table 4.1), shows a noticeable increase of transfer at intermediate wavelengths, whereas all profiles with $C^{(0)} > 50$ (i.e., R1-R5 and E6-E12), have a distinctive maximum at wavelengths between H and $20H$.[3] This answers our first question on page 48: the analyzed radar profiles provide strong evidence for the efficient

[3]For $5 < C^{(0)} < 50$ the tendency is less uniform, with apparent peaks for E4 and E5, and relatively flat curves for E1-E3. However, in the remainder of this work we will be less interested in profiles with a moderate slip ratio.

transfer of medium-scale bedrock undulations to the surface of fast-flowing Antarctic ice streams.

Next, we study the relationship between the peak amplitude and the mean slip ratio. From theoretical considerations (recall section 3.2 and Figure 3.2) we expect to find an increasing peak height with increasing values of $C^{(0)}$. Such a relationship is indeed confirmed by the 3 examples in Figure 4.5a: the profile with the highest slip ratio (E8) has the highest peak. Again, this observation is valid for the entire sample of flightlines. Figure 4.6b shows a scatter plot of slip ratios versus peak amplitudes for all profiles. Despite a substantial amount of scatter, the plot indicates an increasing trend ($\sim +300\%$). This behavior is underlined and better visualized in Figure 4.6a, which shows a box plot for the same data points. The dataset was segmented into 4 equally-sampled groups, corresponding to the ranges $C^{(0)} \in]0.2, 2]$, $C^{(0)} \in]2, 20]$, $C^{(0)} \in]20, 200]$ and $C^{(0)} \in]200, 2000]$. For each group the median, 25th and 75th percentiles and the extreme data points are shown.

We have now obtained a satisfying answer to the first two research questions stated at the beginning of this section. Next, we address the differences between theoretical and observed transfer estimates. A careful comparison between Figures 4.5a and 4.5b reveals several quantitative as well as qualitative discrepancies which will be outlined here. A detailed discussion about their physical (or methodical) origin will be given in section 4.4.

First, it should be noted that, unlike for theoretical estimates, the observed amplitudes do not have one continuous peak, but consist of several local maxima. In the case of R2 and E8, we distinguish two such maxima of comparable height. In our analysis for Figure 4.6, the actual peak value was taken to be the value of the highest maximum. For R2 this results in a maximal value of 0.23, whereas the peak amplitude for E8 is 0.32. A separation into two or more peaks, not necessarily of equal height, is also apparent for most other profiles (R3 being an exception) and some profiles have a strong oscillatory behavior with up to 6 prominent peaks (in particular E6, E7 and E9). This is further illustrated in Figure 4.7 which shows the estimated amplitudes for

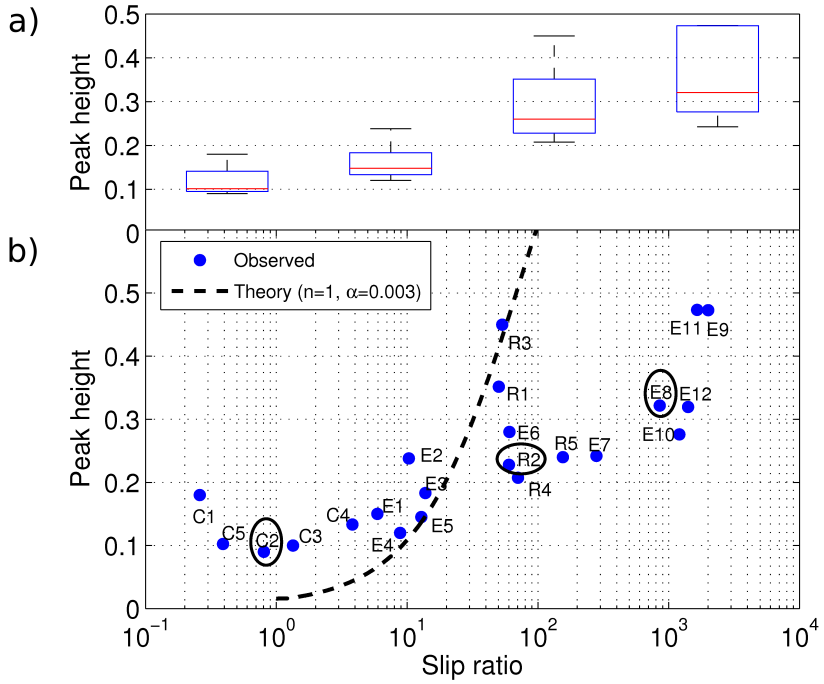

Figure 4.6: Box plot **(a)** and scatter plot **(b)** for the estimated peak height as a function of the mean slip ratio for all 22 profiles shown in Figure 4.2. The categories for the box plot correspond to the ranges $C^{(0)} \in]0.2, 2]$, $C^{(0)} \in]2, 20]$, $C^{(0)} \in]20, 200]$ and $C^{(0)} \in]200, 2000]$ respectively. The profiles highlighted by an ellipse are discussed in more detail in the text (see Figure 4.5a and Table 4.1). The dashed line corresponds to the theoretical prediction, and converges towards 1 for values of the mean slip ratio $C^{(0)} > 10^3$.

R3 and E9.

Another discrepancy between observed and theoretical estimates of the transfer is related to the absolute value of the peak height. Peak amplitudes for R2 and E8 are about 60% lower than expected from theoretical estimates. This observation is generally true for all other profiles with high slip ratios: for R1-R5 and E6-E12 the transfer is significantly dampened, with peak amplitudes at least 60% and up to 70% lower than theoretical estimates. This dampening is also clear from Figure 4.6b, which shows observed peak heights as a function of the slip ratio, and the dashed line represents the theoretical prediction. For $C^{(0)} > 20$, observed peak amplitudes lie consistently below the theoretical curve. In section 4.4 several reasons for this discrepancy will be presented, including 3-dimensional effects and a temperature-dependent viscosity. On

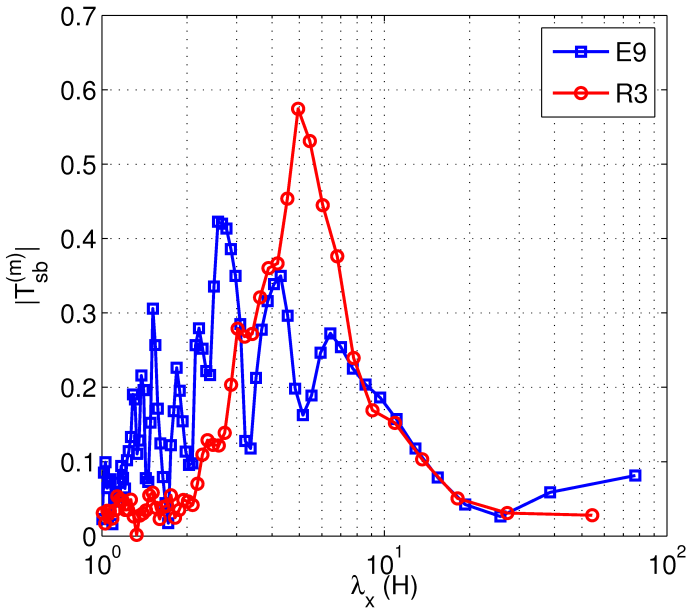

Figure 4.7: Estimated transfer amplitudes for R3 and E9. R3 has one single peak, whereas E9 shows a strong oscillatory behavior.

the other hand, for small values of the slip ratio ($C^{(0)} < 20$), and in particular for all profiles along the Carlson Inlet, a substantial fraction of the observed transfer is due to measurement noise. This leads to observed amplitudes that are larger than theoretical predictions (see Figure 4.6b). Since C1-C5 are also among the shortest profiles, systematic errors in their analysis are also larger than for most other profiles.

Finally, we note that for most profiles the weight of the peak is slightly shifted towards higher (e.g. for R2) or lower (e.g. for E8) wavelengths as compared to the analytical solution. Moreover, the theoretical transfer function for E8 has a shape that is markedly broader than the shape of its corresponding observed curve. Again this feature holds more generally, with lower-than-expected transfer at high wavelengths for the profiles E7-E12.

Summary. The results of our analysis can be summarized as follows. Despite the separation into multiple peaks and a reduced transfer at intermediate and long wavelengths, a *good qualitative agreement* between observed and theoretical transfer char-

acteristics is found. Our results are novel in the sense that no direct evidence for the accuracy of these theoretical predictions has been obtained in the literature before. In particular, the efficient transfer of medium-scale basal undulations to the surface of fast-flowing Antarctic ice streams has not been investigated systematically. Our results are based upon an extensive set of radar measurements with a broad sampling of possible slip ratios, which strengthens the conclusions. Despite these successes, we also found some noticeable differences between theory and observation. A tentative explanation for these phenomena will be provided in the next section.

4.4 Discussion

Despite a good qualitative agreement between estimated transfer amplitudes and their analytical expressions, a closer analysis of Figures 4.5a and 4.6 has revealed quantitative differences that require further discussion. These differences can be summarized as follows.

1. Most noticeably, the transfer amplitudes have several local peaks instead of one overall maximum.

2. Maxima in the amplitude are shifted towards shorter or longer wavelengths, and the width of the peak is smaller in several cases.

3. The transfer is significantly dampened, giving rise to peak amplitudes that are at least 60% lower than expected from theoretical estimates. (Recall that this observation does not apply to the flightlines C1-C5 and E1-E5, which have the lowest slip ratios).

A tentative explanation for each of these observations will be given.

4.4.1 Multiple peaks

The presence of multiple peaks in the observed transfer amplitudes was clearly illustrated in Figures 4.5 and 4.7. It is not immediately obvious how this recurring phenomenon can be explained within the current theoretical framework. Certainly, there is no combination of parameter values (α and $C^{(0)}$) that reproduces such behavior. However, one should recall that $T_{sb}(\lambda_x)$ describes the amplitude ratio between surface undulations (Δs) and bedrock undulations (Δb) for *all* wavelengths. On the other hand, it is likely that certain wavelengths (or intervals of wavelengths) are dampened or totally absent from physical bedrock profiles. Therefore, the overlying ice-flow, and the surface topography in particular, contains little or no information about these wavelengths. This "lack of information" produces gaps in the estimated transfer, and causes the observed splitting into multiple peaks. This explanation will be justified and supported by means of synthetic data, and illustrated for the measured bedrock profile E12.

We construct a synthetic bed on a 1-dimensional grid with 2^{12} points and a grid spacing of 500 m. This allows us to study wavelengths between 10^3 m and 2.048×10^6 m. We choose an ice-thickness $H = 1000$ m such that studied wavelengths are between H and $\sim 10^3 H$ – the interval for which peak transfer is expected. The uniform inclination is $\alpha = 0.004$ and the slip ratio $C^{(0)} = 100$. Next we perform two transfer tests for two different bedrock configurations. The first bedrock profile contains information about all wavelengths, and hence we expect to find a transfer amplitude that perfectly resembles the theoretical curve.[4] In the second case, we deliberately remove information about certain wavelength intervals from the bedrock profile, and study the effect on the retrieved transfer amplitude.

(i) The first synthetic bed consists of several delta-peaks evenly distributed along the profile and each peak has an amplitude of $0.1H$. We note that delta-peaks

[4]This test is very similar to the one described at the end of section 4.2, where we discussed the validity of the power spectral density method as a way to estimate $T_{sb}(\lambda_x)$ from real data.

contain all wavelengths in their spectral profile, and their power spectral density is uniform. For this specific bed we calculate the steady-state surface topography, using the theoretical expression for $T_{sb}(\lambda_x, \alpha, C^{(0)})$ and the relation (3.2.1) with $\Delta c = 0$. Next, the resulting surface profile is used together with the bed profile to estimate the transfer function via the method outlined in section 4.2. The result is presented in Figure 4.8a. As expected, the estimated curve coincides with the theoretical transfer amplitude (except for long wavelengths, which is an effect that has been discussed at length in section 4.2 – recall Figure 4.4).

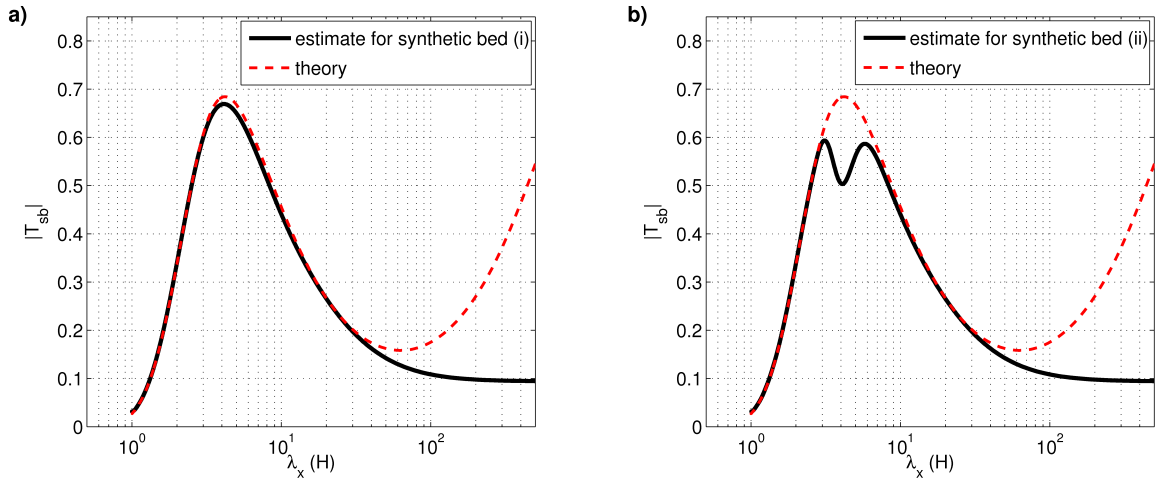

Figure 4.8: **(a)** Red curve: theoretical transfer amplitude, and black curve: estimated transfer amplitude for a synthetic bed described in item (i) in the text. **(b)** Red curve: theoretical transfer amplitude, and black curve: estimated transfer amplitude for a synthetic bed with gaps in the power spectrum, as described in item (ii) in the text. Two separated peaks are distinctly visible.

(ii) In the next step, we set part of the power spectral density of the bedrock profile in (i) to zero. More precisely, all information about wavelengths in the interval $I = [3.73H\,,\, 4.56H]$ is removed. The surface topography is again constructed following the methods described in item (i) above, and the transfer amplitude is estimated. The results are presented in Figure 4.8b (black line). This time, a clear separation into two peaks is visible, with a local minimum around $\lambda_x = 4H$, corresponding to the center of the interval I. The same analysis can be repeated for different intervals I, or a combination of several non-overlapping intervals. In

the latter case, the separation into more than two peaks can be simulated, as has for example been observed for the profile E9 in Figure 4.7.

Our results suggest that the presence of multiple peaks in the transfer amplitude can be explained by the properties of the power spectral density of the bedrock profile only. So far, we have approved this hypothesis using synthetic data. Next, we devise a test that demonstrates how it can be successfully applied to the experimental data in our analysis.

We start from the measured bedrock profile along any of the flightlines and calculate the expected surface topography using the theoretical transfer amplitude $T_{sb}(\lambda_x, \alpha, C^{(0)})$, the values α and $C^{(0)}$ from Table 4.1 and the definition (3.2.1). From the *calculated surface* and the measured bed, the transfer can be estimated and will henceforth be denoted by $T_{sb}^{(\mathrm{sa})}$.[5] This result should be compared to the familiar transfer between the *measured surface* and measured bed (denoted by $T_{sb}^{(\mathrm{m})}$ as usual). Since $T_{sb}^{(\mathrm{sa})}$ and $T_{sb}^{(\mathrm{m})}$ are derived from the same bedrock profile, we expect to see the same oscillatory behavior with corresponding peaks in both profiles. The results of this analysis for the E12-profile are presented in Figure 4.9. Although there is no perfect correspondence, there is a clear resemblance in peak positions between $|T_{sb}^{\mathrm{sa})}|$ (black curve) and $|T_{sb}^{(\mathrm{m})}|$ (blue curve). Very similar results are found for all other profiles R1-R5 and E1-E11, and we conclude that the non-uniform distribution of the bedrock power spectral density is a likely cause for the separation of $|T_{sb}^{(\mathrm{m})}|$ into multiple peaks.

4.4.2 Peak shifting

In section 4.3 we pointed out that for some profiles, the peak positions of the estimated transfer appear to be shifted towards shorter or longer wavelengths as compared to the analytical solution. Such behavior can be demonstrated more clearly when comparing $|T_{sb}^{(\mathrm{m})}|$ to the semi-analytical estimate $|T_{sb}^{(\mathrm{sa})}|$. A distinct example is the profile R3, which is shown in Figure 4.10. The weight of $|T_{sb}^{(\mathrm{m})}|$ is clearly shifted towards longer

[5] "sa" stands for semi-analytical, since the surface profile originates from an analytical calculation, using the measured bedrock profile and estimated values for α and $C^{(0)}$.

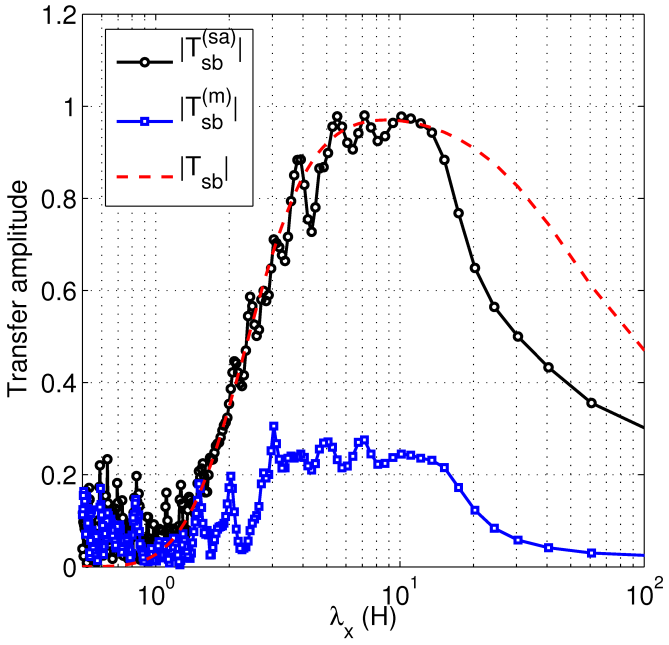

Figure 4.9: Three different forms of the transfer amplitude for E12: (i) the theoretical result $|T_{sb}|$ with values α and $C^{(0)}$ taken from Table 4.1, (ii) the estimated amplitude $|T_{sb}^{(\mathrm{m})}|$, and (iii) the semi-analytical amplitude $|T_{sb}^{(\mathrm{sa})}|$ which has been defined in the text.

wavelengths as compared to the theoretical and semi-analytical estimates for the plane-slab parameters $C^{(0)} = 53.4$ and $\alpha = 0.0041$ (see Table 4.1). Such a shift can have two causes.

(i) The most obvious explanation is an underestimation of the calculated mean slip ratio, $C^{(0)} = 53.4$. Indeed, if we artificially increase $C^{(0)}$ to any value between $C^{(0)} = 150$ and $C^{(0)} = 250$, then $|T_{sb}^{(\mathrm{m})}|$ and $|T_{sb}^{(\mathrm{sa})}|$ coincide much better (see Figure 4.10 for the case $C^{(0)} = 200$). An underestimation of $C^{(0)}$ for R3 could also have been expected from Figure 4.6b, which shows that R3 has a much higher peak value than other profiles with $C^{(0)} \sim 50$ (such as R1, R2, E6).

(ii) The second factor that might affect the peak positions is the ice rheology. The analytical solution we have used so far is only valid for a linear flow law. However, we have seen in section 3 (and Figure 3.3a) that higher values of Glen's exponent generally lead to a shift of the transfer peak to longer wavelengths. Based on our

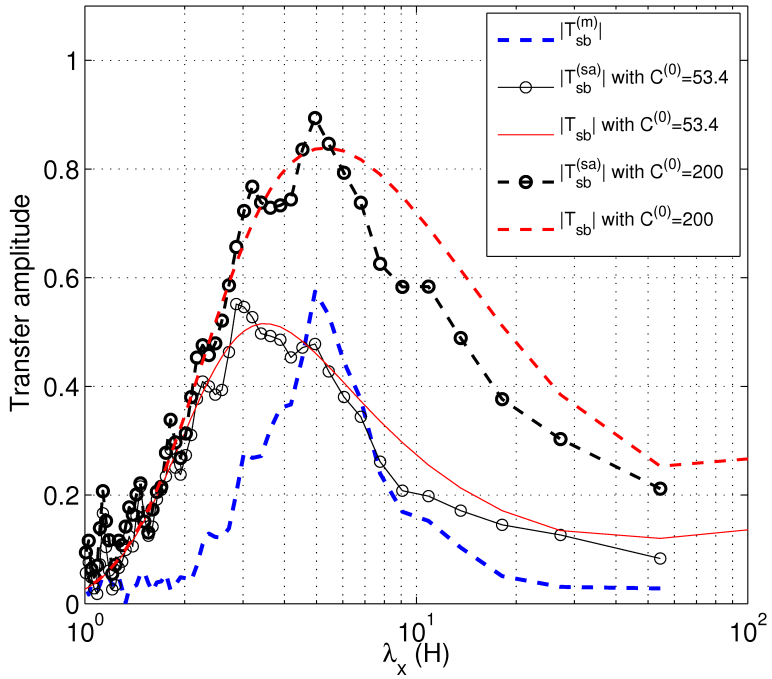

Figure 4.10: Estimated transfer for R3 (blue curve), together with the theoretical and semi-analytical results for two values of the slip ratio: $C^{(0)} = 53.4$ and $C^{(0)} = 200$. The first value corresponds to the original estimate given in Table 4.1, the second value was chosen to obtain a better fit between $|T_{sb}^{(\mathrm{m})}|$ and $|T_{sb}^{(\mathrm{sa})}|$.

analysis it is not possible to discern between this and the previous effect, though, especially because we have little control over the precise value of $C^{(0)}$. Hence we are unable to make a firm statement about the value of n, relying on peak positions alone.

Along the same lines, we point out that a shift of peak positions to shorter wavelengths might be related to an overestimation of $C^{(0)}$; a prime candidate being E10.

4.4.3 Transfer dampening

The last qualitative difference between the observed transfer amplitudes and the corresponding theoretical predictions is a very persistent one. All examples discussed so far (see Figures 4.5, 4.9 and 4.10) show that, for profiles with a slip ratio $C^{(0)} > 10$, the observed transfer amplitudes are generally lower than theory predicts. This damp-

ened response of the ice-flow to bedrock undulations has several (indistinguishable) causes. We first investigate the reasons why the theoretical result might *overestimate* the transfer.

1. 3-dimensional effects. The first and most significant reason is related to the 3-dimensional character of ice flow. Recall that all analyzed radar profiles were measured along the flow of the ice stream. We therefore assumed that, to good approximation, all transverse effects of the ice flow could be neglected. This assumption was implemented in the theoretical transfer amplitude by taking the limit $k_y \to 0$ of the full 3-dimensional solution (3.2.9). However, transverse effects can never be entirely excluded, and one cannot assume that bedrock undulations in the transverse direction have only infinite wavelengths (i.e., $k_y = 0$). The effect of a non-zero ratio between longitudinal and transverse wavelengths has been investigated by Reeh [1987], for example, and he found that 3-dimensional surface amplitudes are reduced significantly as compared to the 2-dimensional case. Using synthetic data, we reproduce the results of Reeh [1987] and show that the presence of wavenumbers $k_y > 0$ leads to dampening of the transfer along the flow.

We study two different situations.

(i) First, a 3-dimensional synthetic bed is constructed on a square $2^{12}\times 2^{12}$-dimensional grid with a grid spacing of 300 m in the x- and y-direction. We choose $H = 1000$ m and $\alpha = 0.004$. The bed consists of a checkerboard pattern of delta-peaks, as illustrated in Figure 4.11a. Clearly, all wavelengths λ_x and λ_y within the interval $[0.6H\,,\,1228.H]$ are represented. For this bed the 3-dimensional surface response is estimated, using the full 3-dimensional solution of the transfer function (see (3.2.9)). Next, a transect of the 3-dimensional bed and surface profiles is taken along the red line in Figure 4.11a – this effectively corresponds to selecting a flightline along a real 3-dimensional ice stream. The transfer characteristics along this flightline are obtained using the familiar techniques. The result is presented in Figure 4.11b (red curves) for 2 values of the slip ratio ($C^{(0)} = 100$ –

solid line, and $C^{(0)} = 1000$ – dashed line).

(ii) Secondly, we pick the bedrock profile along the same flightline, and calculate its surface response in the limit $k_y \to 0$. This corresponds to a situation where the bed does not undulate in the direction transverse to the flow. The resulting transfer is described by the familiar 2-dimensional amplitude $T_{sb}(k_x, \alpha, C^{(0)})$, i.e., the function we have used so far to compare observational results with. The results are represented by the black curves in Figure 4.11b.

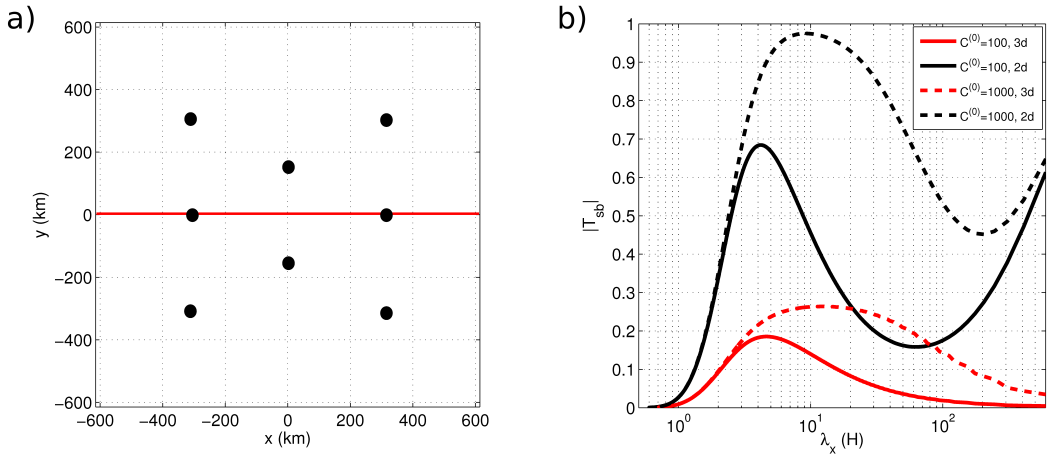

Figure 4.11: **(a)** A 2-dimensional synthetic bed consisting of 8 delta peaks (black dots) distributed over the grid in a checkerboard-like pattern. The red line corresponds to a flightline that is studied in more detail (see text). **(b)** Estimated transfer amplitudes along the red line in (a) taking into account transverse effects (red curves) and discarding transverse effects (black curves).

If we compare red (3d) and black (2d) lines in Figure 4.11b, we find that the 3-dimensional transfer is dampened by a factor of about 60% with respect to the 2-dimensional plane approximation. Comparable values for the dampening-factor have indeed been obtained from real measurements, see e.g. Figures 4.5 and 4.9. We conclude that, in principle, transversal effects are able to account for the total reduction in transfer efficiency. However, it is certainly not the only mechanism that plays a role.

2. Non-isothermal ice. Another possible explanation for the reduced transfer lies in the non-isothermal properties of the ice. Recall that theoretical results in section 3 are

based on a constant ice viscosity. Gudmundsson [*unpublished*] has studied the transfer under the assumption that the viscosity varies exponentially with depth beneath the surface:

$$\eta(z) = \eta_s \mathrm{e}^{\mu z}\,, \tag{4.4.3}$$

with η_s the viscosity at the surface, and μ a factor that scales the vertical variation of η. He found that a gradual increase of the viscosity towards the surface leads to a reduced transfer. The amount of reduction depends on μ, a parameter that can vary along an ice stream and between different ice streams. The reason for the reduced transfer is the presence of stiffer, more viscous ice near the surface, which has a dampening effect. We have partially taken this effect into account by setting η equal to its recommended base value at -10° C. As such, the ice stream is not treated as a temperate feature (~ 0°C) with a value of η that is generally too low, nor is it treated as a cold feature (~ -20°C) with a value of η that is too high and only valid for the uppermost layers. Therefore, we expect that only minor corrections to the theoretical transfer amplitude are needed to incorporate the effects of a temperature-dependent viscosity.

3. Non-uniform power spectral density. Another reason why observed peak amplitudes are generally lower than theoretical results indicate, is related to the non-uniform distribution of the basal power spectral density. We already explained how the absence or suppression of wavelengths clarifies the presence of multiple peaks in the transfer function. In addition, gaps or minima in the spectral density also lead to a decrease of $|T_{sb}^{(m)}|$ at wavelengths were these peaks occur. This can be seen from Figure 4.8b.

4. Errors in the data analysis. So far we have analyzed the question why the theoretical transfer function systematically overestimates the surface response. Here we turn that question around, and present an argument why the observed transfer might actually underestimate the surface response. Such an effect can only be caused by errors in the measurement or analysis method. Indeed, it is important to point out

that the observed values of $|T_{sb}^{(\mathrm{m})}|$ depend on the choice of the window length, L, in Welsh's periodogram method. Smaller values of L generally lead to a lower resolution of the transfer curve, which means that multiple peaks merge and peak values generally become lower. Ideally, one would choose L to be the length (l) of each flightline, but for reasons explained in §4.2.3, this has not been done. Since we chose a constant value $L = 45\,\mathrm{km}$ for the analysis of all flightlines, and $L < l$, a systematic error was introduced that possibly led to the underestimation of the observed transfer. However, it is hard to quantify such an underestimation, because higher values of L increase the variance of the transfer, and the results become less reliable.

4.5 Conclusions

We have analyzed a comprehensive set of radar profiles along fast and slow flowing sections of the West Antarctic Ice Sheet, and determined the response of surface elevations to variations in the bed topography. Our analysis shows that an accurate estimate of the transfer amplitude for wavelengths up to $20H$ requires sufficiently long radar profiles of at least $\sim$ 70km. Since such data has only recently become available, our study provides the first empirical test for theoretical results on transfer amplitudes.

We find that for sufficiently large values of the slip ratio, i.e., for fast-flowing ice streams, the ice is highly transparent to bedrock undulations with wavelengths between 1 and 20 times the ice thickness. The efficiency of the transfer at these wavelengths increases at a rate of $\sim$ 300% with increasing values of the slip ratio. These observations are in good qualitative agreement with the theoretical results obtained by Gudmundsson [2003] and Raymond and Gudmundsson [2005]. It confirms the important qualitative difference between the flow characteristics of ice streams, for which most (95% and often more) of the velocity is due to basal sliding, and Alpine-type glaciers, which attain a considerable fraction of their surface speed by internal creep.

Several differences between theory and observation have been observed and clarified. (i) The separation of the transfer peak into several local maxima has its origin in a non-

uniform power spectral density of the bedrock profile. (ii) The wavelengths for which peak transfer occurs are a good indicator for the value of the mean slip ratio. We found that a straightforward calculation of $C^{(0)}$ using estimated surface velocities, ice thickness and surface slope is often incorrect, and leads to values of the slip ratio that are either too small or too large. (iii) The measured transfer amplitudes for fast-flowing ice are dampened by a factor of 60% or more as compared to theoretical predictions. The main reason for this discrepancy is the 3-dimensional character of an ice stream, whereas theoretical results discard all transverse effects to the flow. Other factors that might have a (minor) impact on the transfer amplitude are the ice viscosity, the ice rheology, and systematic errors in the data analysis.

Despite the uncertainty about the value of the mean slip ratio and parameters such as the flow law exponent, it is still reassuring that data points in Figure 4.6b cluster in groups of profiles along neighboring sections of the ice sheet. Since these sections can be expected to have similar physical conditions, it affirms the consistency of our methods and results. In general, our analysis is an important validation for the use of current theoretical models in ongoing efforts to study ice stream dynamics, and for their use in inverse methods to obtain information about basal perturbations (topography and slipperiness) from surface measurements. Such inversion methods will be discussed at length in the next chapter.

Chapter 5

Bayesian inversion and the form of the basal sliding law

5.1 Introduction

The form of the basal sliding law has an important effect on the results of modeling work for large ice masses [Joughin et al., 2010]. For example, our current understanding of fast-flowing ice streams attributes most of their surface speed to basal sliding, whereas internal creep deformation is negligible. Any accurate prediction about the transient behavior of these ice streams therefore relies on a good understanding of the dynamics at the ice-bed interface.

Over the past decades, numerous attempts have been undertaken to put constraints on the form of the sliding law. For example, borehole experiments have suggested a viscous plastic behavior of sub-glacial till layers [Kamb, 2001], whereas modeling efforts have shown that modulations of ice stream flow in response to ocean tides can only be explained by a non-linear viscous sliding law [Gudmundsson, 2011]. Despite these and numerous other results, important uncertainties still remain. To date, no consensus has been reached on the general applicability of Weertman's sliding law (recall (2.2.12)) in the context of large-scale ice-flow modeling work or on realistic values for the sliding exponent, m. Commonly encountered values in flow modeling range from $m = 1$ (linear

viscous) to $m = \infty$ (plastic).

This fundamental uncertainty about the form of the sliding law is also problematic for inverse modeling techniques, which use surface measurements to infer knowledge about the bed topography and basal slipperiness distribution. Since these methods strongly rely on a theoretical description of how perturbations at the bed propagate to the surface, any inaccuracy in the forward model might lead to wrong estimates about the basal conditions. This lack of robustness of inversion methods with respect to changes in the sliding law is worrying, and undermines their reliability.

In this study we investigate the role of the sliding law in a particular class of inversion methods, the so-called Bayesian statistical inversion methods. Although Bayesian inversion has been used rather successfully to infer information about the bed topography for a flighline along the Rutford Ice Stream, Antarctica [Raymond-Pralong and Gudmundsson, 2011], it's application to determine the basal slipperiness needs greater care. The retrieved values of the slipperiness distribution can strongly depend on the chosen value of the sliding exponent m. The value of m enters the computations at two different points: (i) in the calculation of the a priori knowledge about $c(x, y)$ from ice thickness, surface slopes and surface velocities, and (ii) in the actual inversion procedure itself.

In this work we use synthetic data to show that different values of m lead to the retrieval of different but equally realistic basal conditions, *no matter how accurate surface measurements are*. This result questions the usefulness of the Bayesian inversion method to estimate the basal slipperiness distribution of ice streams without better constraints on the value of m and good (independent) a priori knowledge about the bed.

5.2 Inversion method: the Bayesian approach

Inversion methods provide an estimate for the bed topography and basal slipperiness along a 1-dimensional profile or across a 2-dimensional plane, using the following input:

- *Surface measurement values.* In order to facilitate our discussion, we introduce a compact notation for the measurement vector (or rather its Fourier transform): $\hat{\boldsymbol{y}} = (\hat{s},\, \hat{v}_x,\, \hat{v}_y,\, \hat{v}_z)^H$, where H denotes the Hermitian transpose. In general, the measurement values can be split into true values ($\boldsymbol{y}$) and errors ($\boldsymbol{\epsilon_y}$):

$$\hat{\boldsymbol{y}} = \boldsymbol{y} + \boldsymbol{\epsilon_y}\,. \tag{5.2.1}$$

  This splitting is artificial because only $\hat{\boldsymbol{y}}$ is known to us. However, if all error sources for the measurement and data analysis are identified, then the size of $\boldsymbol{\epsilon_y}$ can be estimated. For example, errors in the surface elevation data presented in chapter 4 are on the order of $\epsilon_s \sim \pm 1\,\mathrm{m}$. For an accurate inversion, measurement errors $\boldsymbol{\epsilon_y}$ have to be as small as possible.

- *A priori knowledge about the bed.* In some cases one has (limited) knowledge about the basal topography or basal slipperiness from independent prior measurements, theoretical consideration (e.g., $\Delta b \ll H$) or reasonable expectations (e.g., $c > 0$). Then the Bayesian inversion approach can be interpreted as a method to *update* prior knowledge about the bed, consistent with new surface data.

  For later convenience we introduce the vector notation $\boldsymbol{x} = (b,\, c)^H$ for the true system state. The a priori estimate is denoted with a tilde, $\tilde{\boldsymbol{x}} = (\tilde{b},\, \tilde{c})^H$.

- *A theoretical forward model.* The relation between basal variables and surface measurements is written as

$$\hat{\boldsymbol{y}} = F(\boldsymbol{x}, p) + \boldsymbol{\epsilon_y}\,, \tag{5.2.2}$$

  where F is the forward model and p are the model parameters as in (3.2.4). We assume that the forward model is *perfect*, such that the true state $\boldsymbol{y}$ is equal to $F(\boldsymbol{x}, p)$.

Recall from section 3 that, to first order in the small perturbations, the relation between bed and surface variations is described by the transfer functions. If we split the true surface and bed into a mean and deviatoric part, $\boldsymbol{y} = \boldsymbol{y_0} + \Delta\boldsymbol{y}$ and $\boldsymbol{x} = \boldsymbol{x}_0 + \Delta\boldsymbol{x}$, then (3.2.1) and (3.2.2) can be written as

$$\Delta\boldsymbol{y} = T\Delta\boldsymbol{x}\,, \qquad \text{with} \qquad T = \begin{pmatrix} T_{sb} & T_{sc} \\ T_{v_ib} & T_{v_ic} \end{pmatrix}\,, \tag{5.2.3}$$

where T is a $4q \times 2r$-dimensional matrix with q the number of datapoints for each variable at the surface, and r the number of locations at which b and c have to be estimated. Using (5.2.3), the relation (5.2.2) can be rewritten as

$$\Delta\hat{\boldsymbol{y}} \equiv \hat{\boldsymbol{y}} - \boldsymbol{y_0} = T\Delta\boldsymbol{x} + \boldsymbol{\epsilon_y}\,. \tag{5.2.4}$$

The result of the inversion method is an a posteriori system state or retrieval ($\Delta\hat{\boldsymbol{x}}$) which is a function of the measurement values, prior knowledge about the bed, and the forward model:

$$\Delta\hat{\boldsymbol{x}} = \Delta\hat{\boldsymbol{x}}(\Delta\hat{\boldsymbol{y}}, \tilde{\boldsymbol{x}}, T)\,. \tag{5.2.5}$$

The conditions that determine the function $\Delta\hat{\boldsymbol{x}}$ are different for different inversion methods.

5.2.1 A posteriori estimates for the bed topography and basal slipperiness

We will introduce the most general expression for $\Delta\hat{\boldsymbol{x}}$ in 3 steps. First, we look at a retrieval problem with no a priori knowledge or measurement errors. In the second step, uncorrelated measurement errors will be included. Finally, we also add the a priori information about the bed.

1. Least-squares inversion without errors. The easiest inversion method assumes the absence of prior knowledge about the bed (i.e., $\tilde{\boldsymbol{x}} = 0$) and uses the well known least-squares approach to solve equation (5.2.4) for $\Delta\boldsymbol{x}$. The solution is set equal to the retrieval $\Delta\hat{\boldsymbol{x}}$. For simplicity we first assume that the measurement errors can be neglected (i.e., $\boldsymbol{\epsilon_y} = 0$) and (5.2.4) reduces to $\Delta\boldsymbol{y} = T\Delta\boldsymbol{x}$. For a matrix T of full column rank, it is easy to see that a solution to this equation is given by

$$\Delta\hat{\boldsymbol{x}} = \Delta\boldsymbol{x} = (T^H T)^{-1} T^H \Delta\boldsymbol{y}\,. \tag{5.2.6}$$

If T has a non-trivial null-space (i.e., a set of non-trivial system states that have no effect on the surface: $T\Delta\boldsymbol{x} = 0$), then $T^H T$ is not necessarily invertible and no unique solution $\Delta\hat{\boldsymbol{x}}$ exists for a given $\Delta\boldsymbol{y}$. Well-known elements of the null-space are longitudinal ridges and stripes. These features are not transfered to the surface, and it is impossible to detect them from surface measurements. Similarly, we discussed in section 3 how the bed-to-surface transfer of *all* basal perturbations with wavelengths $\lambda < 2H$ is highly suppressed. Therefore, these small-scale features do not appear at the surface and cannot be retrieved using the proposed inversion method. Also the more general inversion methods that will be discussed next suffer from these limitations.

2. Least-squares inversion with measurement errors. If we include small measurement errors, the retrieval takes the more complicated form [Menke, 1989]

$$\Delta\hat{\boldsymbol{x}} = (T^H C_{y\hat{y}}^{-1} T)^{-1} T^H C_{y\hat{y}}^{-1} \Delta\hat{\boldsymbol{y}}\,, \tag{5.2.7}$$

with $C_{y\hat{y}}$ the covariance matrix that describes the measurement errors:

$$C_{y\hat{y}} = \begin{pmatrix} < \epsilon_s \epsilon_s^H > & 0 & 0 & 0 \\ 0 & < \epsilon_{v_x} \epsilon_{v_x}^H > & 0 & 0 \\ 0 & 0 & < \epsilon_{v_y} \epsilon_{v_y}^H > & 0 \\ 0 & 0 & 0 & < \epsilon_{v_z} \epsilon_{v_z}^H > \end{pmatrix}. \tag{5.2.8}$$

We assume that these errors are normally distributed and uncorrelated. The solution (5.2.7) minimizes the error-weighted difference between the measured values $\Delta\hat{\boldsymbol{y}}$ and true values $\Delta\boldsymbol{y} = T\Delta\boldsymbol{x}$ in a least-squares sense, i.e.,

$$\frac{\partial}{\partial\Delta\boldsymbol{x}}\left[C_{y\hat{y}}^{-1}\left(\Delta\hat{\boldsymbol{y}} - T\Delta\boldsymbol{x}\right)^{H}\left(\Delta\hat{\boldsymbol{y}} - T\Delta\boldsymbol{x}\right)\right]\Big|_{\Delta\hat{\boldsymbol{x}}} = 0\,. \tag{5.2.9}$$

The expression for $\Delta\hat{\boldsymbol{x}}$ in (5.2.7) was used by Thorsteinsson et al. [2003] in one of the first attempts to obtain simultaneous information about bedrock topography and basal slipperiness from surface measurements. The authors studied the surface topography and variations in the surface velocity field of a part of Ice Stream E, Antarctica, and found evidence for a topographic through with low slipperiness at its base.

3. Bayesian inversion. In a third step, we extend (5.2.7) to include the possibility of a priori knowledge about the basal conditions. This is done using the so-called Bayesian inversion approach. The methodology described below is used frequently in atmospheric sciences and was first implemented for the study of ice flows by Gudmundsson and Raymond [2008] and Raymond and Gudmundsson [2009]. We rely on both papers for our discussion.

The Bayesian method differs from the previously discussed least-squares method because of its inherent statistical nature. The a posteriori estimate should now be thought of as a probability distribution of possible system states, and each state has a certain probability to be realized:

$$P(\boldsymbol{x}|(\hat{\boldsymbol{y}},\tilde{\boldsymbol{x}})) = \frac{P(\hat{\boldsymbol{y}}|\boldsymbol{x})P(\boldsymbol{x}|\tilde{\boldsymbol{x}})}{P(\hat{\boldsymbol{y}})}\,. \tag{5.2.10}$$

The left hand site is the a posteriori distribution and associates a probability to each system state $\boldsymbol{x}$, given the observed data $\hat{\boldsymbol{y}}$ and the a priori knowledge $\tilde{\boldsymbol{x}}$. The equality in (5.2.10) is obtained using Bayes' rule. The right hand side of (5.2.10) contains the likelihood function, $P(\hat{\boldsymbol{y}}|\boldsymbol{x})$, which is a measure for the probability of observing the data $\hat{\boldsymbol{y}}$ given a system state $\boldsymbol{x}$. The denominator $P(\hat{\boldsymbol{y}})$ in (5.2.10) is a formal normalizing

factor and is often not needed.

In the following, we assume that the probability density functions for the likelihood is given by a Gaussian distribution:

$$P(\hat{\boldsymbol{y}}|\boldsymbol{x}) = \exp\left[-\frac{1}{2}\left(\boldsymbol{x}-\hat{\boldsymbol{y}}\right)^T C_{y\hat{y}}^{-1}\left(\boldsymbol{x}-\hat{\boldsymbol{y}}\right)\right]. \tag{5.2.11}$$

Gaussian statistics are usually a good approximation for measurement errors, and they are algebraically convenient. Less realistic, but again convenient, is to assume a Gaussian distribution for the a priori estimate:

$$P(\boldsymbol{x}|\tilde{\boldsymbol{x}}) = \exp\left[-\frac{1}{2}\left(\boldsymbol{x}-\tilde{\boldsymbol{x}}\right)^T C_{x\tilde{x}}^{-1}\left(\boldsymbol{x}-\tilde{\boldsymbol{x}}\right)\right], \tag{5.2.12}$$

where $C_{x\tilde{x}}$ is the covariance matrix describing the error in the prior estimates of the bed topography and basal slipperiness:

$$C_{x\tilde{x}} = \begin{pmatrix} <(b-\tilde{b})(b-\tilde{b})^H> & 0 \\ 0 & <(c-\tilde{c})(c-\tilde{c})^H> \end{pmatrix}. \tag{5.2.13}$$

A reasonable model for the prior basal topography (and slipperiness) is a stationary first-order auto-regressive process [Rodgers, 2000]. For a 1-dimensional grid, such a process assumes that the prior estimate of the basal topography at location i is related to that at location $i-1$ through

$$\tilde{b}_i = \phi_{\tilde{b}}\tilde{b}_{i-1} + \epsilon_{\tilde{b}}\,, \tag{5.2.14}$$

where the regression coefficient $\phi_{\tilde{b}}$ is a constant between zero and unity and $\epsilon_{\tilde{b}}$ is a Gaussian random variable, uncorrelated with $\tilde{b}_i$ and with constant variance $\sigma^2_{\epsilon_{\tilde{b}}}$. For this process it is an easy exercise to show that the entries of the covariance matrix are given by

$$<(b-\tilde{b})(b-\tilde{b})^H>_{ij} = \sigma^2_{\tilde{b}}\mathrm{e}^{-|i-j|/\lambda_{\tilde{b}}}\,, \tag{5.2.15}$$

where the decay length scale $\lambda_{\tilde{b}}$ (measured in units of the grid scale) is related to $\phi_{\tilde{b}}$ via

$$\lambda_{\tilde{b}} = -1/\ln\phi_{\tilde{b}} \tag{5.2.16}$$

and the variance is

$$\sigma_{\tilde{b}}^2 = \sigma_{\epsilon_{\tilde{b}}}^2 / \left(1 - \phi_{\tilde{b}}^2\right) . \tag{5.2.17}$$

The parameter $\sigma_{\tilde{b}}$ will be referred to as the error in the prior basal topography, and is defined in terms of the mean ice thickness H. The effect of the decay length scale on the retrieval is only important on spatial scales where the surface data does not lead to a significant improvement of the prior knowledge [Gudmundsson and Raymond, 2008]. For computational reasons it is sometimes convenient to take the limit $\lambda_{\tilde{b}} \to 0$, such that the covariance matrix becomes diagonal.

For a 2-dimensional grid, a generalization of the auto-regressive process leads to a similar expression for the covariance matrix. However, the computational complexity of the inversion, and the limited computational resources available, force us to restrict our analysis to the case of a diagonal covariance matrix, i.e.,

$$< (b - \tilde{b})(b - \tilde{b})^H >_{ij,kl} = \sigma_{\tilde{b}}^2 \, \delta_{ik}\delta_{jl} \, . \tag{5.2.18}$$

The likelihood distribution (5.2.11) and a priori distribution (5.2.12) can be substituted into the probability distribution for the a posteriori estimate, (5.2.10). The latter is then a well-defined function of the unknown system state $\boldsymbol{x}$, the measurement results $\hat{\boldsymbol{y}}$, the a priori estimate $\tilde{\boldsymbol{x}}$ and the corresponding errors. The value $\boldsymbol{x}$ for which this function reaches its maximum is called the maximum a posteriori estimate (IMAP) of the system state. The IMAP will be denoted by $\hat{\boldsymbol{x}}$, and standard arguments [Rodgers, 2000] show that it is given by

$$\hat{\boldsymbol{x}} = \left(T^H C_{y\hat{y}}^{-1} T + C_{x\tilde{x}}^{-1}\right)^{-1} \left(T^H C_{y\hat{y}}^{-1} \hat{\boldsymbol{y}} + C_{x\tilde{x}}^{-1} \tilde{\boldsymbol{x}}\right) . \tag{5.2.19}$$

This is the generalization of (5.2.7) which incorporates our knowledge about the a

priori system state. It forms the basis for the remainder of our analysis in this chapter. In particular, we will investigate how the retrieval depends on the form of the basal sliding law.

5.2.2 Dependence on the sliding exponent: the forward model

The expression (5.2.19) has been used by Raymond-Pralong and Gudmundsson [2011] to obtain simultaneous information about the bed topography and basal slipperiness of a flightline along the Rutford Ice Stream, Antarctica. The authors used a two-dimensional plane strain forward model with a non-linear ice rheology ($n = 3$) and linear sliding law ($m = 1$). Since no analytical solution exists for the transfer functions in this case, their analysis is done with a numerical finite-element program.

We will *not* apply the described inversion method to obtain information about realistic bedrock properties along specific profiles, though. Instead, we are rather interested in the *general properties and structure* of the inversion procedure. In particular, we will study the dependence of the retrieval $\hat{\boldsymbol{x}}$ on the form of the basal sliding law and more precisely on the value of the sliding exponent, m. The latter is indirectly incorporated in $\hat{\boldsymbol{x}}$ via the transfer functions T.

In general, the dependence of T on m is very complicated and a closed analytical expression for $T(m)$ only exists under strong assumptions about the forward model.[1] However, in order to facilitate our study, and to minimize the computational complexity of the problem, it is appropriate to have such an analytical expression. In particular, due to our interest in the dependence of $\hat{\boldsymbol{x}}$ on m, we require that this analytical solution is known for *all* values of the sliding exponent, i.e., $T = T(m)$.

These requirements are fulfilled by the *shallow-ice-stream approximation with a linear ice rheology*: analytical transfer functions for this approximation have been obtained by Gudmundsson [2008] (recall section 3), and the sliding exponent is a free parameter in the solution. The transfer functions for the shallow-ice-stream approx-

[1] For example, recall from chapter 3 that in the full-Stokes model, an analytical expression for $T(m)$ only exists for $m = 1$.

imation will be used in the remainder of this chapter. The possible consequences of working with this approximation will be briefly discussed in section 5.4.

5.2.3 Research question in a schematic form

With all this information in mind, we are now able to precisely state the research question that will be answered in the remainder of our study. In schematic form:

$$\forall\, \boldsymbol{x},\, \tilde{\boldsymbol{x}},\, m_1 \neq m_2 : \quad T(m_1)\, \hat{\boldsymbol{x}}\Big(T(m_1)\boldsymbol{x},\, \tilde{\boldsymbol{x}},\, T(m_1)\Big) = T(m_2)\, \hat{\boldsymbol{x}}\Big(T(m_1)\boldsymbol{x},\, \tilde{\boldsymbol{x}},\, T(m_2)\Big)\ ? \tag{5.2.20}$$

This question can be interpreted as follows. Assume that $\boldsymbol{x}$ describes the *true* basal conditions and m_1 is the *true* sliding exponent. Then $\boldsymbol{y} = T(m_1)\boldsymbol{x}$ is the true surface, assuming a perfect forward model. The retrieval of $\boldsymbol{y}$ using m_1 as the sliding coefficient and a priori knowledge $\tilde{\boldsymbol{x}}$ is given by $\hat{\boldsymbol{x}}_{\mathbf{1}}$, where we introduced the notation

$$\hat{\boldsymbol{x}}_{\mathbf{1}} = \hat{\boldsymbol{x}}\Big(T(m_1)\boldsymbol{x},\, \tilde{\boldsymbol{x}},\, T(m_1)\Big)\,, \tag{5.2.21}$$

It is expected that $\hat{\boldsymbol{x}}_{\mathbf{1}} \approx \boldsymbol{x}$, and the left hand side of the equality in (5.2.20) is therefore given by $T(m_1)\hat{\boldsymbol{x}}_{\mathbf{1}} \approx T(m_1)\boldsymbol{x} = \boldsymbol{y}$.

Now assume that m_2 is our current *best estimate* of the sliding parameter, and $m_2 \neq m_1$. In any retrieval of physical data we will use the value m_2 (because m_1 is unknown to us), and the result is given by $\hat{\boldsymbol{x}}_{\mathbf{2}}$, with

$$\hat{\boldsymbol{x}}_{\mathbf{2}} = \hat{\boldsymbol{x}}\Big(T(m_1)\boldsymbol{x},\, \tilde{\boldsymbol{x}},\, T(m_2)\Big)\,. \tag{5.2.22}$$

Obviously, $\hat{\boldsymbol{x}}_{\mathbf{2}}$ will in general be different from the true system state $\hat{\boldsymbol{x}}_{\mathbf{1}}$. However, if the equality in (5.2.20) is satisfied, we have *no means* to detect this difference, exactly because the forward of $\hat{\boldsymbol{x}}_{\mathbf{2}}$ using m_2 also reproduces the true surface $\boldsymbol{y}$:

$$\boldsymbol{y} \approx T(m_1)\hat{\boldsymbol{x}}_{\mathbf{1}} \overset{(5.2.20)}{=} T(m_2)\hat{\boldsymbol{x}}_{\mathbf{2}}\,. \tag{5.2.23}$$

Such a result would be problematic for the success of the retrieval method, since our knowledge about the sliding exponent m is indeed very limited. If the equality in (5.2.20) turns out to be valid for at least certain subsets of $\boldsymbol{x}$ and $\tilde{\boldsymbol{x}}$, then there is currently no hope to obtain accurate information about basal properties from the inversion of surface data.

5.2.4 Synthetic data

In order to test (5.2.20), we will make use of synthetic data. We study a perturbed parallel-slab flow with mean ice thickness $H = 1000\,\mathrm{m}$, mean slope $\alpha = 0.003$ and mean slip ratio $C^{(0)} = 300$. The 1-dimensional synthetic flows are constructed on a grid with 2^9 data points and a grid spacing of $2H$. This allows us to study wavelengths between $\lambda_x = 4H$ and $\lambda_x = 1.024 \times 10^3 H$. Note that for this range of intermediate and long wavelengths, the transfer in the shallow-ice-stream approximation corresponds almost perfectly to the full-Stokes transfer (see Figure 3.4a). The 2-dimensional flows are studied on a grid with $2^9 \times 2^9$ grid points and a grid spacing of $2H$.

5.3 Results

A definite answer to the question in (5.2.20) requires testing for an infinite set of parameters (m_1, m_2, $\boldsymbol{x}$, $\tilde{\boldsymbol{x}}$), which is obviously not possible. Therefore, we first try to get some insight into the solution of the problem by restricting our attention to a limited number of realistic combinations of parameter values. The results for some of these tests are presented in §5.3.1 for a 1-dimensional flow, and in §5.3.2 for a 2-dimensional flow. In §5.3.3 we turn to an analytical argumentation, which allows us to make more general statements, irrespective of the particular values for (m_1, m_2, $\boldsymbol{x}$, $\tilde{\boldsymbol{x}}$).

5.3.1 Flowline inversion

We start from a synthetic Gaussian bedrock topography and Gaussian basal slipperiness distribution, represented by the green curves in Figures 5.1a and 5.1b respectively. We apply the forward model on these basal perturbations, using the value $m_1 = 3$ for the sliding exponent. The resulting surface topography (s) and velocity fields (v_x, v_z) are shown in Figure 5.2.

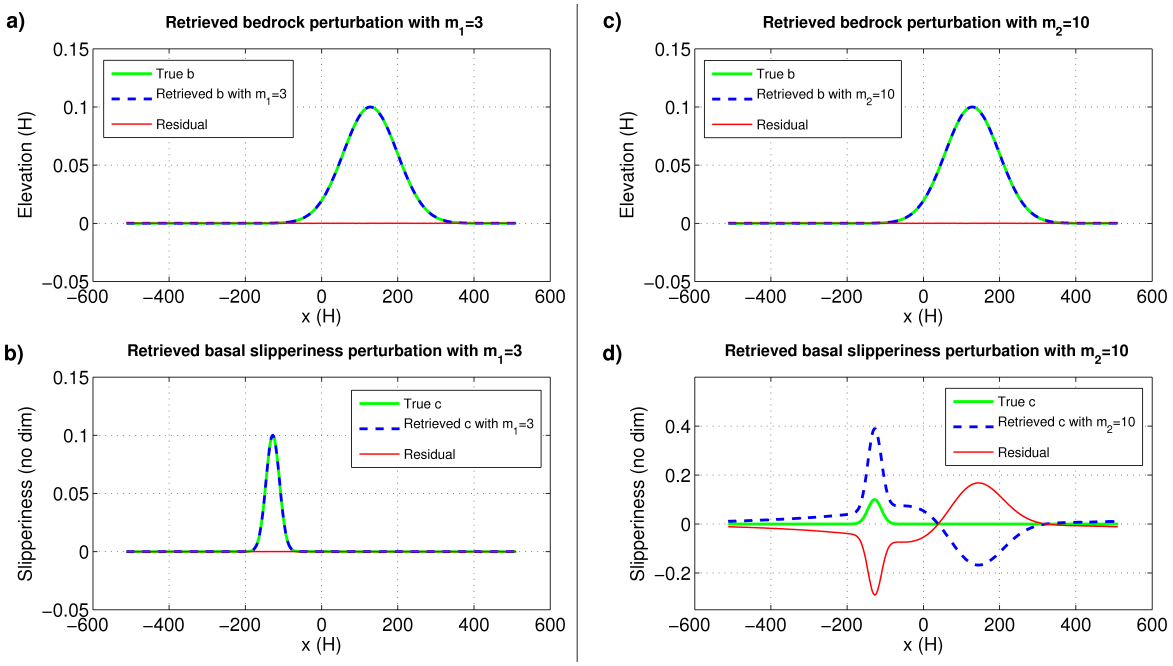

Figure 5.1: **(a)** True and retrieved bedrock topography for $m_1 = 3$. **(b)** True and retrieved basal slipperiness distribution for $m_1 = 3$. **(c)** True and retrieved bedrock topography for $m_2 = 10$. **(d)** True and retrieved basal slipperiness distribution for $m_2 = 10$.

These are the true surface properties. In the second step, we calculate the retrieval $\hat{\boldsymbol{x}}$ from s, v_x and v_z, imposing the following assumptions:

- The surface errors are small, i.e., $\sigma_s = 10^{-8}H$, $\sigma_{v_x} = 10^{-8}v_s^{(0)}$ and $\sigma_{v_y} = 10^{-8}v_s^{(0)}$, with $v_s^{(0)}$ the mean horizontal surface velocity (recall (2.3.21)).
- We have limited a priori knowledge about the basal perturbations. We set $\tilde{b} = 0$ and $\tilde{c} = 0$, and assume large errors for both the bed topography and basal

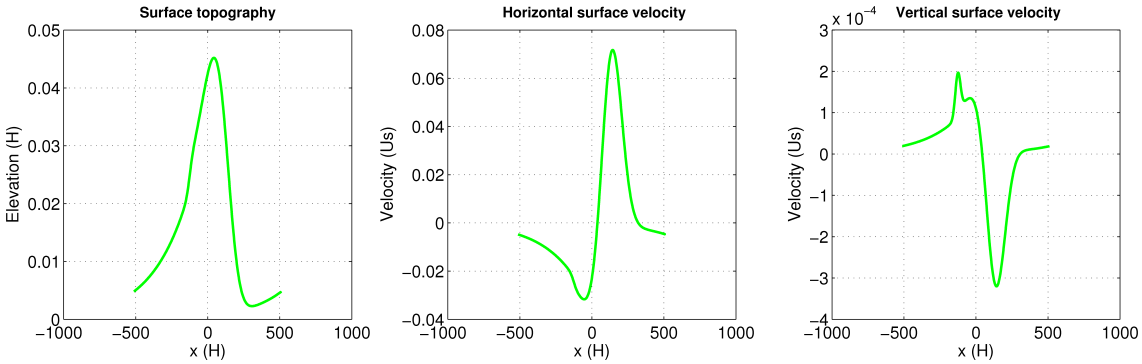

Figure 5.2: Surface perturbations corresponding to the bed topography and basal slipperiness distribution shown in Figures 5.1a and 5.1b and for a sliding exponent $m = 3$.

slipperiness: $\sigma_{\tilde{b}} = H$ and $\sigma_{\tilde{c}} = 1$. The decay lengths scales have little influence on the result and are set equal to the arbitrary values $\lambda_{\tilde{b}} = \lambda_{\tilde{c}} = 50H$.

Under these assumptions, the retrieval $\hat{\boldsymbol{x}}$ is calculated for two different values of the sliding parameter. First, the calculation is done for $m = m_1 = 3$. The results are presented in Figures 5.1a and 5.1b (blue curves). As expected, the true basal perturbations are retrieved up to great accuracy. We have shown that our methods are consistent, and that $\hat{\boldsymbol{x}}_{\mathbf{1}} \approx \boldsymbol{x}$, as we anticipated below equation (5.2.22).

Next, we compute the retrieval for a different (ad hoc) value of the sliding exponent: $m = m_2 = 10$. The results are presented in Figures 5.1c and 5.1d. This time we have retrieved the correct bedrock topography, but the basal slipperiness distribution differs considerably from its true value. This means that $\hat{\boldsymbol{x}}_{\mathbf{1}} \neq \hat{\boldsymbol{x}}_{\mathbf{2}}$.

Finally, we apply the forward model to both $\hat{\boldsymbol{x}}_{\mathbf{1}}$ and $\hat{\boldsymbol{x}}_{\mathbf{2}}$ and find that

$$T(m_1)\hat{\boldsymbol{x}}_{\mathbf{1}} = T(m_2)\hat{\boldsymbol{x}}_{\mathbf{2}}\,, \tag{5.3.24}$$

at least within the limits of the (tiny) measurement errors at the surface.

The same experiment can be repeated for different values m_1 and m_2 and different basal perturbations; the results are always similar to the ones above. Essential to this result, however, is the assumption that we have limited prior knowledge about the bed

topography and basal slipperiness. This translates into large errors $\epsilon_{\tilde{b}}$ and $\epsilon_{\tilde{c}}$. If we assume good a priori knowledge about the bed, (5.3.24) still holds. On the other hand, if we also assume good a priori knowledge about c (which is very unlikely in reality), then the retrieval method for m_2 forces $\hat{\boldsymbol{x}}_{\mathbf{2}}$ to be as close as possible to $\hat{\boldsymbol{x}}_{\mathbf{1}}$, which results in surface perturbations that are not equal to their true values anymore. Hence for $\tilde{c} \approx c$ and $\epsilon_{\tilde{c}}$ small, the equality in (5.3.24) breaks down. We stress again that detailed knowledge about c along real ice stream profiles is very unlikely in the near future, and more independent measurements such as borehole experiments need to be done.

5.3.2 2-dimensional inversion

The same analysis can be done for a 2-dimensional flow over a Gaussian bedrock bump and Gaussian basal slipperiness distribution. The true values for b and c are shown in Figure 5.3. The forward model with $m = m_1 = 3$ leads to the surface perturbations shown in Figure 5.4.

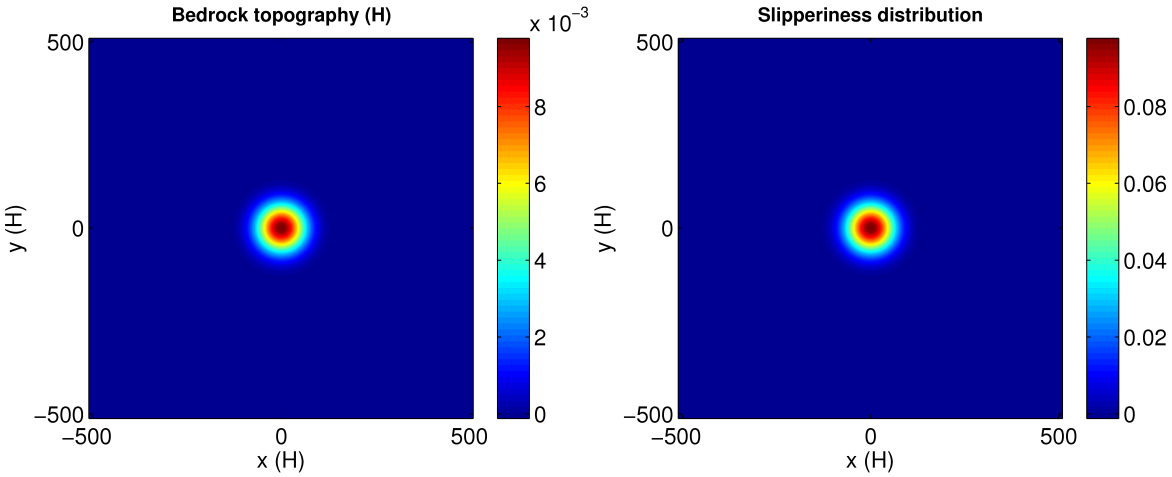

Figure 5.3: True Gaussian bedrock topography and Gaussian basal slipperiness distribution.

Now we follow the same procedure as described for the 1-dimensional inversion in the previous section. We assume limited a priori knowledge about the basal slipperiness distribution ($\tilde{c} = 0$ and $\epsilon_{\tilde{c}} = 1$), but numerical considerations force us to assume almost

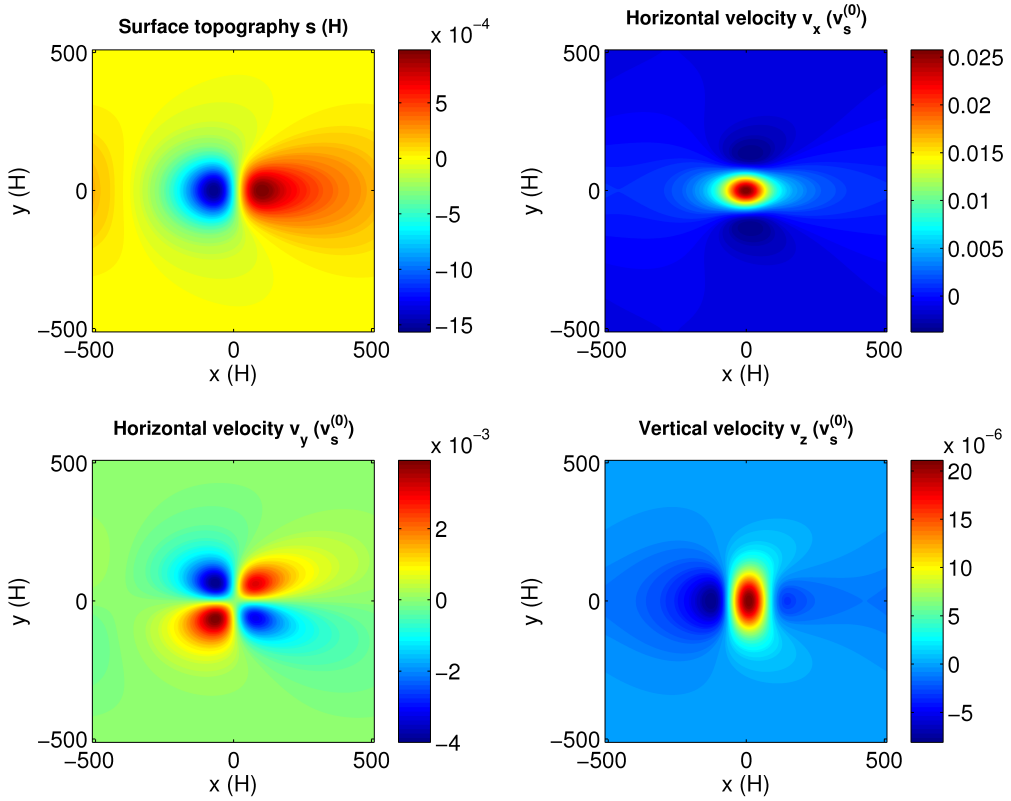

Figure 5.4: True surface perturbations (s, v_x, v_y and v_z) corresponding to the bed topography and basal slipperiness distribution shown in Figure 5.3 and for a sliding exponent $m = 3$.

perfect knowledge about the bed ($\tilde{b} = b$ and $\epsilon_{\tilde{b}} = 10^{-8}H$). Poor knowledge about the bed topography leads to an unwanted oscillatory behavior of the retrieval, with wavelengths at the order of the grid scale and amplitudes that are on the order of the ice thickness.

The retrieval $\hat{\boldsymbol{x}}$ is first calculated for $m = m_1 = 3$, and next for $m = m_2 = 10$. We plot in Figure 5.5 the results for $\hat{\boldsymbol{x}}_{\boldsymbol{2}} - \hat{\boldsymbol{x}}_{\boldsymbol{1}}$; the residues for the bed topography are shown in Figure 5.5a, the residues for the basal slipperiness in Figure 5.5b. We see that $\hat{b}_1$ and $\hat{b}_2$ coincide withing the error limits ($\epsilon_{\tilde{b}} = 10^{-8}H$). However, $\hat{c}_1$ and $\hat{c}_2$ differ significantly, with the retrieval for $m_2 = 10$ having slipperiness values that are up to 2.5 times higher than the true values $\hat{c}_1$. So clearly $\hat{\boldsymbol{x}}_{\boldsymbol{1}} \neq \hat{\boldsymbol{x}}_{\boldsymbol{2}}$. However, also in the

2-dimensional case we find that

$$T(m_1)\hat{\boldsymbol{x}}_{\mathbf{1}} \approx T(m_2)\hat{\boldsymbol{x}}_{\mathbf{2}}\,. \tag{5.3.25}$$

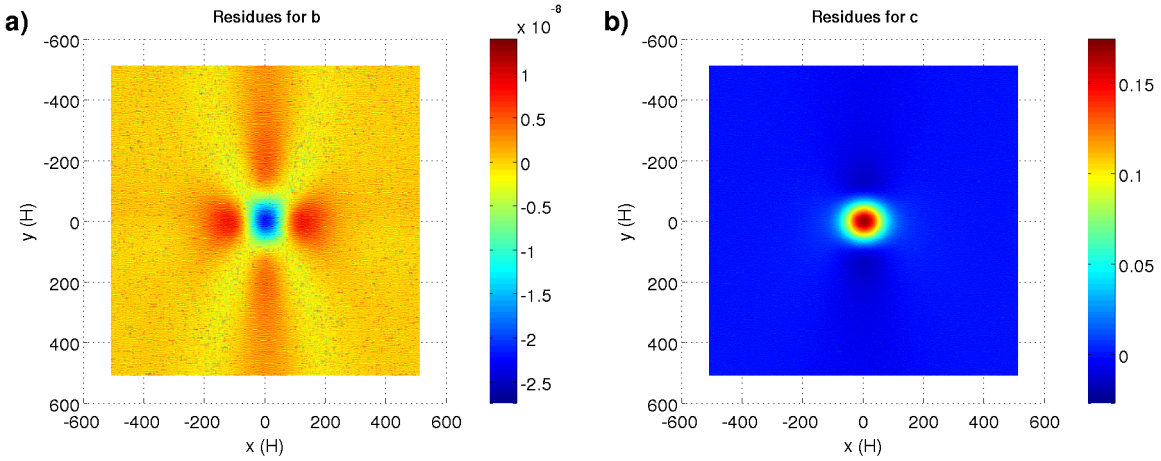

Figure 5.5: **(a)** Residues between the retrieved bedrock topography for $m_1 = 3$ and $m_2 = 10$. The difference lies within the allowed a priori error margins. **(b)** Residues between the retrieved basal slipperiness distribution for $m_1 = 3$ and $m_2 = 10$; $\hat{c}_2$ is up to 2.5 times higher than $\hat{c}_1$.

5.3.3 Analytical arguments

So far, we have presented results from numerical experiments for particular choices of m_1, m_2, the true basal conditions, the a priori knowledge and the error bounds. We found evidence for the validity of the equality sign in (5.2.20) from both 1-dimensional and 2-dimensional inversion experiments. However, it would be nice if we could argue about the validity of (5.2.20) on more general grounds. To a certain extend, this can be done by relying on analytical arguments.

For convenience, let us first repeat the general expression for the retrieval, $\hat{\boldsymbol{x}}$, obtained in (5.3.27):

$$\hat{\boldsymbol{x}} = \left(T^H C_{y\hat{y}}^{-1} T + C_{x\tilde{x}}^{-1}\right)^{-1} \left(T^H C_{y\hat{y}}^{-1} \hat{\boldsymbol{y}} + C_{x\tilde{x}}^{-1} \tilde{\boldsymbol{x}}\right)\,. \tag{5.3.26}$$

It was shown by Rodgers [2000] that $\hat{\boldsymbol{x}}$ can be rewritten in the following equivalent form:

$$\hat{\boldsymbol{x}} = \tilde{\boldsymbol{x}} + C_{x\tilde{x}} T^H \left(T C_{x\tilde{x}} T^H + C_{y\hat{y}} \right)^{-1} (\hat{\boldsymbol{y}} - T\tilde{\boldsymbol{x}}) \; . \tag{5.3.27}$$

The retrieval is nothing but an update of the a priori knowledge with the error-weighted difference between the measurement and the forward of the a priori.

The alternative expression (5.3.27) can be used to obtain more insight into the equality (5.2.20). Indeed, the left hand side and right hand side of (5.2.20) can now be rewritten as

$$T(m_1)\hat{\boldsymbol{x}}_{\mathbf{1}} = \tag{5.3.28}$$
$$T(m_1)\tilde{\boldsymbol{x}} + T(m_1) C_{x\tilde{x}} T^H(m_1) \left[T(m_1) C_{x\tilde{x}} T^H(m_1) + C_{y\hat{y}} \right]^{-1} \left[T(m_1)\boldsymbol{x} - T(m_1)\tilde{\boldsymbol{x}} \right] \; ,$$
$$T(m_2)\hat{\boldsymbol{x}}_{\mathbf{2}} = \tag{5.3.29}$$
$$T(m_2)\tilde{\boldsymbol{x}} + T(m_2) C_{x\tilde{x}} T^H(m_2) \left[T(m_2) C_{x\tilde{x}} T^H(m_2) + C_{y\hat{y}} \right]^{-1} \left[T(m_1)\boldsymbol{x} - T(m_2)\tilde{\boldsymbol{x}} \right] \; .$$

If we define the new matrix

$$I(m) = T(m) C_{x\tilde{x}} T^H(m) \left[T(m) C_{x\tilde{x}} T^H(m) + C_{y\hat{y}} \right]^{-1} \; , \tag{5.3.30}$$

then the question in (5.2.20) can be reformulated as

$$\forall\, \boldsymbol{x},\ \tilde{\boldsymbol{x}},\ m1 \neq m2 :$$
$$T(m_1)\tilde{\boldsymbol{x}} + I(m_1) \left[T(m_1)\boldsymbol{x} - T(m_1)\tilde{\boldsymbol{x}} \right] = T(m_2)\tilde{\boldsymbol{x}} + I(m_2) \left[T(m_1)\boldsymbol{x} - T(m_2)\tilde{\boldsymbol{x}} \right] \; ? \tag{5.3.31}$$

It is immediately clear that the answer to this question is affirmative (i.e., the equality sign is valid) if and only if

$$\forall\, m : \qquad I(m) = \mathbb{1} \, . \tag{5.3.32}$$

Although the detailed form of $I(m)$ is rather complicated, it has the following easy

structure:

$$\begin{aligned} I(m) &= J(m)\left[J(m)+C_{y\hat{y}}\right]^{-1}\,, \\ &= \left[\mathbb{1}+C_{y\hat{y}}J^{-1}(m)\right]^{-1}\,, \qquad \text{with} \qquad J(m)=T(m)C_{x\tilde{x}}T^{H}(m)\,, \end{aligned} \tag{5.3.33}$$

assuming that the inverse of $J(m)$ exists.[2] If we can show that the entries of $C_{y\hat{y}}J^{-1}(m)$ are on the order of $\epsilon \ll 1$, then $I(m)$ can be expanded as

$$I(m) = \mathbb{1} + \mathcal{O}(\epsilon)\,. \tag{5.3.34}$$

This means that $I(m)$ is "to a good approximation" given by the unity matrix. By "good approximation" we understand that the parameter ϵ should be on the order of the surface measurement errors, such that $T(m_1)\hat{\boldsymbol{x}}_{\mathbf{1}}$ and $T(m_2)\hat{\boldsymbol{x}}_{\mathbf{2}}$ only differ up to terms that are on the order of the measurement errors.

An answer to the question whether the entries of $C_{y\hat{y}}J^{-1}(m)$ are small is not easily given, and depends on the form of the transfer functions, the value of m and the covariance matrices $C_{y\hat{y}}$ and $C_{x\tilde{x}}$. We have performed numerical calculations and could show that $||C_{y\hat{y}}J^{-1}(m)|| \sim \mathcal{O}(\epsilon)$ with $\epsilon < \boldsymbol{\epsilon}_y$ for all values of m, as long as the errors in the surface measurements are small compared to the errors in the a priori estimate. This assumption is true for most real profiles. When measurement and a priori errors are comparable, $||C_{y\hat{y}}J^{-1}(m)||$ is not necessarily small and (5.3.34) breaks down. This has indeed been observed from numerical calculations, and was mentioned at the end of §5.3.1: for small $\boldsymbol{\epsilon}_y$ and $\boldsymbol{\epsilon}_{\tilde{\boldsymbol{x}}} \sim \boldsymbol{\epsilon}_y$, different retrievals do not give rise to the same surface response and can therefore be distinguished.

[2] This might not always be true, for example if the forward model (described by the transfer functions T) has a null-space. This interesting possibility will not be considered here.

5.4 Discussion

Both from numerical experiments and analytical arguments it is clear that for a large class of realistic surface profiles and associated errors, the retrieved bedrock topography and basal slipperiness distribution depend on the particular form of the sliding law. We have no means to distinguish between these retrievals, unless very accurate knowledge about the basal conditions is already available. However, various side remarks about our results are in order.

- So far, we have assumed perfect knowledge about the surface topography and surface velocities of an ice stream in a steady state regime. If, however, the ice stream is in a transient state, measurements at different times give rise to different surface conditions. For both surface states the best retrieval can be calculated, using the transient transfer functions. If we assume that the bed conditions have not changed between the two measurement times, then consistency requires that both retrievals are exactly the same. In general, we expect that this requirement is not satisfied for arbitrary values of the sliding exponent. Therefore, for ice flows in a transient state, multiple measurements might provide a way to constrain the value of m.

- All numerical experiments were done using the transfer functions in the shallow-ice-stream approximation, mainly for 2 reasons: (i) numerical simplicity, and (ii) their analytical dependence on the sliding exponent m. However, the shallow-ice-stream approximation is only a valid approximation of the full-Stokes solution for wavelengths $\lambda_x > 10H$. Moreover, it is only valid for a linear ice rheology. Could these assumptions influence our results? First, we point out that in our numerical analysis, we have chosen synthetic data which contains only wavelengths $\lambda_x > 4H$ for which the shallow-ice-stream solution is a very good approximation to the full-Stokes solution. Moreover, we do not expect our results to change if shorter wavelengths are included, because different wavelengths do not mix in

the calculation of the retrieval, at least not if the error covariance matrices are diagonal. Also the ice rheology is not expected to play a major role in our study, since we have seen in §3.2.2 that for values $n = 3$ or $n = 5$, the transfer functions only undergo minor changes, whereas their qualitative behavior remains the same.

- Our final remark relates to the error covariance matrices. For 2-dimensional flows we have assumed diagonal covariance matrices, because it strongly reduces numerical computation times. Non-diagonal covariance matrices are not expected to substantially influence our results. A good indication is given by the 1-dimensional case, for which we studied both diagonal and non-diagonal covariance matrices. The results are identical for both cases.

5.5 Conclusions

Using numerical experiments and analytical arguments, we have shown that Bayes' inversion method for different sliding exponents generally leads to different a posteriori estimates for the bed topography and basal slipperiness distribution (for any given dataset of surface measurements). All retrieved basal configurations are physically feasible, in that they are smooth solutions that reproduce the correct surface response. Therefore, it is not possible to distinguish between different basal conditions, no matter how accurate the measurements of the surface properties. This result is independent on the form of the true basal conditions, and applies to the entire range of sliding exponents from $m = 1$ to $m = \infty$.

Our study shows that without further constraints on the form of the sliding law, or sufficient independent a priori knowledge about the bed, it is very unlikely that Bayes' inversion method can be used to obtain an unambiguous estimate for the basal conditions beneath active ice streams.

Bibliography

R. B. Alley. In search of ice-stream sticky spots. *Journal of Glaciology*, 39(133): 447–454, 1993.

S. Anandakrishnan, D. D. Blankenship, R. B. Alley, and P. L. Stoffa. Influence of subglacial geology on the position of a West Antarctic ice stream from seismic observations. *Nature*, 394:57–59, 1998.

D. B. Bahr, W. T. Pfeffer, C. Sassolas, and M. F. Meier. Response time of glaciers as a function of size and mass balance: 1. Theory. *Journal of Geophysical Research*, 103:9777–9782, 1998.

M. J. Balise. *The relation between surface and basal velocity variations in glaciers, with application to the mini-surges of Variegated Galcier.* PhD thesis, Univ. of Wash., Seattle, 1987.

M. J. Balise and C. F. Raymond. Transer of the basal sliding variations to the surface of a linearly viscous glacier. *Journal of Glaciology*, 31(109):308–318, 1985.

J. L. Bamber, D. G. Vaughan, and I. Joughin. Widespread complex flow in the interior of the Antarctic ice sheet. *Science*, 287(5456):1248–1250, 2000.

D. R. Baral and K. Hutter. *An iterative solution procedure for shallow stokes flows. The shallow ice approximation revisited*, pages 273–284. Springer Berlin, Heidelberg, 1999.

C. R. Bentley, N. Lord, and C. Liu. Radar reflections reveal a wet bed beneath stagnant Ice Stream C and a frozen bed beneath ridge BC, West Antarctica. *Journal of Glaciology*, 44(146):149–156, 1998.

D. D. Blankenship, C. R. Bentley, S. T. Rooney, and R. B. Alley. Seismic measurements reveal a saturated porous layer beneath an active Antarctic ice stream. *Nature*, 322, 1986.

D. D. Blankenship, C. R. Bentley, S. T. Rooney, and R. B. Alley. Till beneath ice steam B 1. properties derived from seismic travel times. *Journal of Geophysical Research*, 92(B9):8903–8911, 1987.

W. F. Budd. Ice flow over bedrock perturbations. *Journal of Glaciology*, 9(55):29–48, 1970.

W. F. Budd. Stress variations with ice flow over undulations. *Journal of Glaciology*, 10(59):177–195, 1971.

G. K. C. Clarke. Subglacial Processes. *Annual Review of Earth and Planetary Sciences*, 33(1):247–276, January 2005.

H. F. J. Corr, F. Ferraccioli, N. Frearson, T. Jordan, C. Robinson, E. Armadillo, G. Caneva, E. Bozzo, and I. Tabacco. Airborne radio-echo sounding of the Wilkes Subglacial Basin, the Transantarctic Mountains, and the Dome C region. *Terra Antartica Reports*, 13:55–63, 2007.

K. M. Cuffey and W. S. B. Paterson. *The Physics of Glaciers*. Butterworth-Heinneman, 4th edition, 2010.

A. C. Fowler and D. A. Larson. On the Flow of Polythermal Glaciers. I. Model and Preliminary Analysis. *Proceedings of the Royal Society A: Mathematical, Physical and Engineering Sciences*, 363(1713):217–242, 1978.

A. M. Gades, C. F. Raymond, H. Conway, and R. W. Jacobel. Bed properties of Siple Dome and adjacent ice streams, West Antarctica, inferred from radio-echo sounding measurements, February 2000. ISSN 00221430.

O. Gagliardini, D. Cohen, P. Raback, and T. Zwinger. Finite-element modeling of subglacial cavities and related friction law. *Journal of Geophysical Research*, 112 (F2):1–11, May 2007.

O. Gagliardini, F. Gillet-Chaulet, and M. Montagnat. A Review of Anisotropic Polar Ice Models: from Crystal to Ice-Sheet Flow Models. *Physics of Ice Core Records*, 2, 2009.

J. W. Glen. The Creep of Polycrystalline Ice. *Proceedings of the Royal Society A: Mathematical, Physical and Engineering Sciences*, 228(1175):519–538, March 1955.

J. W. Glen. The flow law of ice: A discussion of the assumptions made in glacier theory, their experimental foundations and consequences. *IASH*, 47:171–183, 1958.

D. L. Goldsby and D. L. Kohlstedt. Superplastic deformation of ice: Experimental observations. *Journal of Geophysical Research*, 106(B6), 2001.

G. H. Gudmundsson. Transmission of basal variability to a glacier surface. *Journal of Geophysical Research*, 108(B5):1–19, 2003.

G. H. Gudmundsson. *Estimating basal properties of glaciers from surface measurements*. Blackwell Publishing Ltd, 2004.

G. H. Gudmundsson. Analytical solutions for the surface response to small amplitude perturbations in boundary data in the shallow-ice-stream approximation. *The Cryosphere*, 2(2):77–93, July 2008.

G. H. Gudmundsson. Ice-stream response to ocean tides and the form of the basal sliding law. *The Cryosphere*, 5(1):259–270, March 2011.

G. H. Gudmundsson and A. Jenkins. Ice-flow velocities on Rutford Ice Stream, West Antarctica, are stable over decadal timescales. *Journal of Glaciology*, 55(190):339–344, 2009.

G. H. Gudmundsson and M. Raymond. On the limit to resolution and information on basal properties obtainable from surface data on ice streams. *The Cryosphere Discussions*, 2(3):413–445, June 2008.

G. H. Gudmundsson, C. F. Raymond, and R. Bindschadler. The origin and longevity of flow stripes on Antarctic ice streams. *Annals of Glaciology*, (27):145–152, 1998.

G. H. Gudmundsson, G. Adalgeirsdóttir, and H. Björnsson. Observational verification of predicted increase in bedrock-to-surface amplitude transfer during a glacier surge. *Annals of Glaciology*, 36(1):91–96, 2003.

W. K. Hamblin and E. H. Christiansen. *Earth's Dynamic Systems*. Prentice Hall, 10th edition, 2003. URL `http://earthds.info/`.

W. D. Harrison, D. H. Elsberg, K. A. Echelmeyer, and R. M. Krimmel. On the characterization of glacier response by a single time-scale. *Journal of Glaciology*, 47 (159):659–664, 2001.

K. Hutter. Time-dependent surface elevation of an ice slope. *Journal of Glaciology*, 25 (92):247–266, 1980.

K. Hutter. Dynamics of glaciers and large ice masses. *Ann. Rev. Fluid Mech.*, 14: 87–130, 1982.

K. Hutter. *Theoretical Glaciology; Material Science of Ice and the Mechanics of Glaciers and Ice Sheets*. D. Reidel, Norwell, Mass., 1983.

K. Hutter, F. J. Legerer, and U. Spring. First-order stresses and deformations in glaciers and ice sheets. *Journal of Glaciology*, 27(96):227–270, 1981.

A. Iken. The effect of the subglacial water pressure on the sliding velocity of a glacier in an idealized numerical model. *Journal of Glaciology*, 27:407–421, 1981.

T. Johannesson. *Landscape of temperate ice caps*. PhD thesis, University of Washington, Seattle, 1992.

I. Joughin and S. Tulaczyk. Positive mass balance of the Ross Ice Streams, West Antarctica. *Science*, 295(5554):476–480, 2002.

I. Joughin, D. R. MacAyeal, and S. Tulaczyk. Basal shear stress of the Ross ice streams from control method inversions. *Journal of Geophysical Research-Solid Earth*, 109 (B9), 2004.

I. Joughin, R. A. Bindschadler, M. A. King, D. Voigt, R. B. Alley, S. Anandakrishnan, H. Horgan, L. Peters, P. Winberry, S. B. Das, and G. Catania. Continued deceleration of Whillans Ice Stream, West Antarctica. *Geophysical Research Letters*, 32(22):2–5, 2005.

I. Joughin, J. L. Bamber, T. Scambos, S. Tulaczyk, M. Fahnestock, and D. R. MacAyeal. Integrating satellite observations with modelling: basal shear stress of the Filcher-Ronne ice streams, Antarctica. *Philosophical transactions. Series A, Mathematical, physical, and engineering sciences*, 364(1844):1795–814, 2006.

I. Joughin, B. E. Smith, and D. M. Holland. Sensitivity of 21st century sea level to ocean-induced thinning of Pine Island Glacier, Antarctica. *Geophysical Research Letters*, 37, 2010.

B. Kamb. Sliding motion of glaciers: Theory and observation. *Reviews of Geophysics*, 8(4):673, 1970.

B. Kamb. Rheological Nonlinearity and Flow Instability in the Deforming Bed Mechanism of Ice Stream Motion. *Journal of Geophysical Research*, 96(B10):16585–16595, 1991.

B. Kamb. Basal zone of the West Antarctic ice streams and its role in the lubrication of their rapid motion. *The West Antarctic Ice Sheet: Behavior and Environment, Antarct. Res. Ser.*, 77, 2001.

E. C. King. Ice stream or not? Radio-echo sounding of Carlson Inlet, West Antarctica. *The Cryosphere Discussions*, 5(2):1219–1238, April 2011.

E. C. King, R. C. A. Hindmarsh, and C. R. Stokes. Formation of mega-scale glacial lineations observed beneath a West Antarctic ice stream. *Nature Geoscience*, 2(8): 585–588, 2009.

J. Landon and C. F. Raymond. Chislenniy raschet reaktsii poverkhnosti lednika na izmeneniya tolshchiny l'da [Numerical calculation of adjustment of a glacier surface to pertubations of ice thickness]. *Mater. Glyatsiol. Issled. Khron. Obsuzhdeniya*, 32: 123–133 (in Russian); 233–239 (in English), 1978.

G. J. Leysinger Vieli and G. H. Gudmundsson. On estimating length fluctuations of glaciers caused by changes in climatic forcing. *Journal of Geophysical Research*, 109 (F1):1–14, 2004.

W. Lick. The propagation of disturbances on glaciers. *Journal of Geophysical Research*, 75(12), 1970.

L. Lliboutry. Contribution à la théorie du frottement du glacier sur son lit. *C.R. Hebd. Séances Acad. Sci.*, 247(3):318–320, 1958.

L. Lliboutry. Une théorie du frottement du glacier sur son lit. *Ann. Géophys.*, 15(2): 250–265, 1959.

L. Lliboutry. General theory of subglacial cavitation and sliding of temperate glaciers. *Journal of Glaciology*, 7(49):21–58, 1968.

L. Lliboutry. The glacier theory. *Adv. Hydrosci.*, 7:81–167, 1971.

M. P. Lüthi. Transient response of idealized glaciers to climate variations. *Journal of Glaciology*, 55(193):918–930, December 2009.

D. R. MacAyeal. Large-scale ice flow over a viscous basal sediment: theory and applications to ice stream B, Antarctica. *Journal of Geophysical Research*, 94:4071–4087, 1989.

D. R. MacAyeal. The Basal Stress Distribution of Ice Stream E, Antarctica, Inferred by Control Methods. *Journal of Geophysical Research*, 97(B1):595–603, 1992.

D. R. MacAyeal. A tutorial on the use of control methods in ice sheet modeling. *Journal of Glaciology*, 39(131), 1993.

D. R. MacAyeal, R. A. Bindschadler, and T. A. Scambos. Basal friction of Ice Stream E, West Antarctica. *Journal of Glaciology*, 41(138):247–262, 1995.

W. Menke. *Geophysical data analysis: discrete inverse theory.* New York, etc., Academic Press, revised edition, 1989.

J. F. Nye. The flow of glaciers and ice-sheets as a problem in plasticity. *Proceedings of the Royal Society of London. Series A, Mathematical and Physical Sciences*, 207 (1091):554–572, 1951.

J. F. Nye. The motion of ice sheets and glaciers. *Journal Of Glaciology*, 3(26):493–507, 1959.

J. F. Nye. The Response of a Glacier to Changes in the Rate of Nourishment and Wastage. *Proceedings of the Royal Society A: Mathematical, Physical and Engineering Sciences*, 275(1360):87–112, 1963a.

J. F. Nye. On the Theory of the Advance and Retreat of Glaciers. *Geophysical Journal of the Royal Astronomical Society*, 7(4):431–456, 1963b.

J. F. Nye. The frequency reponse of glaciers. *Journal of Glaciology*, 5:567–587, 1965.

J. F. Nye. A Calculation on the Sliding of Ice Over a Wavy Surface Using a Newtonian Viscous Approximation. *Proceedings of the Royal Society A: Mathematical, Physical and Engineering Sciences*, 311(1506):445–467, 1969.

J. F. Nye. Glacier Sliding Without Cavitation in a Linear Viscous Approximation. *Proceedings of the Royal Society A: Mathematical, Physical and Engineering Sciences*, 315(1522):381–403, 1970.

S. Overgaard and N. S. Gundestrup. *Bedrock topography of the Greenland ice sheet in the Dye 3 area*, pages 49–56. American Geophysical Union, Washington, DC, 1985.

F. Pattyn. Transient glacier response with a higher-order numerical ice-flow model. *Journal of Glaciology*, 48(162):467–477, 2002.

W. T. Pfeffer, C. Sassolas, D. B. Bahr, and M. F. Meier. Response time of glaciers as a function of size and mass balance: 2. Numerical experiments. *Journal of Geophysical Research*, 103(B5):9783–9789, 1998.

H. D. Pritchard, R. J. Arthern, D. G. Vaughan, and L. A. Edwards. Extensive dynamic thinning on the margins of the Greenland and Antarctic ice sheets. *Nature*, 461 (7266):971–975, 2009.

C. F. Raymond. Shear margins in glaciers and ice sheets. *Journal of Glaciology*, 42 (140):90–102, 1996.

M. Raymond. *Estimating basal properties of glaciers and ice streams from surface measurements*. PhD thesis, ETH Zurich, 2007.

M. J. Raymond and G. H. Gudmundsson. On the relationship between surface and basal properties on glaciers, ice sheets, and ice streams. *Journal of Geophysical Research*, 110(B8):1–17, 2005.

M. J. Raymond and G. H. Gudmundsson. Estimating basal properties of ice streams

from surface measurements: a non-linear Bayesian inverse approach applied to synthetic data. *The Cryosphere*, 3(2):265–278, 2009.

M. Raymond-Pralong and G. H. Gudmundsson. Bayesian estimation of basal conditions on Rutford Ice Stream, West Antarctica, from surface data. *Journal of Glaciology*, 57(202):315–324, 2011.

N. Reeh. Steady-state three-dimensional ice flow over an undulating base: first-order theory with linear ice rheology. *Journal of Glaciology*, 33(114):177–185, 1987.

R. Retzlaff and C. R. Bentley. Timing of stagnation of Ice Stream C, West Antarctica, from short-pulse radar studies of buried surface crevasses. *Journal of Glaciology*, 39 (133):553–561, 1993.

E. Rignot, J. L. Bamber, M. R. Van den Broeke, C. Davis, Y. H. Li, W. J. Van De Berg, and E. Van Meijgaard. Recent Antarctic ice mass loss from radar interferometry and regional climate modelling. *Nature Geoscience*, 1(2):106–110, 2008.

G. P. Rigsby. Effect of hydrostatic pressure on velocity of shear deformation on single ice crystals. *Journal of Glaciology*, 3(24):271–278, 1958.

D. M. Rippin, J. L. Bamber, M. J. Siegert, D. G. Vaughan, and H. F. J. Corr. Basal conditions beneath enhanced-flow tributaries of Slessor Glacier, East Antarctica. *Journal of Glaciology*, 52(179):481–490, 2006.

D. M. Rippin, D. G. Vaughan, and H. F. J. Corr. The basal roughness of Pine Island Glacier , West Antarctica. *Journal of Glaciology*, 57(201):67–76, 2011.

E. S. Robinson. On the relationship of ice-surface topography to bed topography on the south polar plateau. *Journal of Glaciology*, 6(43):43–54, 1966.

C. D. Rodgers. *Inverse methods for atmospheric sounding - theory and practice*. World Scientific, Singapore etc., 2000.

C. Schoof. The effect of cavitation on glacier sliding. *Proceedings of the Royal Society A: Mathematical, Physical and Engineering Sciences*, 461(2055):609–627, 2005.

C. Schoof. A variational approach to ice stream flow. *Journal of Fluid Mechanics*, 556: 227, 2006.

A. M. Smith and T. Murray. Bedform topography and basal conditions beneath a fast-flowing West Antarctic ice stream. *Quaternary Science Reviews*, 28(7-8):584–596, 2009.

A. M. Smith, T. Murray, K. W. Nicholls, K. Makinson, G. Adalgeirsdóttir, A. E. Behar, and D. G. Vaughan. Rapid erosion, drumlin formation, and changing hydrology beneath an Antarctic ice stream. *Geology*, 35(2):127, 2007.

S. Steinemann. Results of preliminary experiments on the plasticity of ice crystals. *Journal of Glaciology*, 2:404–413, 1954.

S. Steinemann. Experimentelle Untersuchungen zur Plastizität von Eis. *Geotechnische Serie Nr 10, Beiträge ur Geologie der Schweiz*, 1958a.

S. Steinemann. Résultats expérimentaux sur la dynamique de la glace et leurs correlations avec le mouvement et la pétrographie des glaciers. *International Association of Scientific Hydrology*, 47:184–198, 1958b.

R. Thomas, E. Frederick, J. Li, W. Krabill, S. Manizade, J. Paden, J. Sonntag, R. Swift, and J. Yungel. Accelerating ice loss from the fastest Greenland and Antarctic glaciers. *Geophysical Research Letters*, 38(10):1–6, 2011.

D. E. Thompson. Stability of glaciers and ice sheets against flow perturbations. *Journal of Glaciology*, 24(90):427–441, 1979.

T. Thorsteinsson, C. F. Raymond, G. H. Gudmundsson, R. A. Bindschadler, P. Vornberger, and I. Joughin. Bed topography and lubrication inferred from surface measurements on fast-flowing ice streams. *Journal of Glaciology*, 49(167):481–490, 2003.

S. Tulaczyk, W. B. Kamb, and H. F. Engelhardt. Basal mechanics of Ice Stream B, West Antarctica 1. Till mechanics. *Journal of Geophysical Research-Solid Earth*, 105 (B1):463–481, 2000.

S. Tulaczyk, B. Kamb, and H. F. Engelhardt. Estimates of effective stress beneath a modern West Antarctic ice stream from till preconsolidation and void ratio. *Boreas*, 30(2):101–114, 2001.

R. S. W. van de Wal and J Oerlemans. Response of valley glaciers to climate change and kinematic waves: a study with a numerical ice-flow model. *Journal of Glaciology*, 41(137), 1995.

D. G. Vaughan, H. F. J. Corr, F. Ferraccioli, N. Frearson, A. O'Hare, D. Mach, J. W. Holt, D. D. Blankenship, D. L. Morse, and D. A. Young. New boundary conditions for the West Antarctic ice sheet: Subglacial topography beneath Pine Island Glacier. *Geophysical Research Letters*, 33(9):2–5, 2006.

A. Vieli and A. J. Payne. Application of control methods for modelling the flow of Pine Island Glacier, West Antarctica. *Annals of Glaciology*, 36(1):197–204, 2003.

J. Weertman. On the sliding of glaciers. *Journal of Glaciology*, 3:33–38, 1957.

J. Weertman. The theory of glacier sliding. *Journal of Glaciology*, 5:965–978, 1964.

J. Weertman. The unsolved general glacier sliding problem. *Journal of Glaciology*, 23: 97–115, 1979.

P. Welch. The use of fast Fourier transform for the estimation of power spectra: A method based on time averaging over short, modified periodograms. *IEEE Transactions on Audio and Electroacoustics*, 15(2):70–73, 1967.

I. M. Whillans, K. C. Jezek, A. R. Drew, and N. S. Gundestrup. Ice flow leading to the deep core hole at Dye 3, Greenland. *Annals of Glaciology*, 5:185–190, 1984.

Z. Yosida. Internal stress and viscous flow of snow covers on sloping ground surfaces: I. Snow cover on wavy ground of mean inclination alpha. *Low Temp. Sci., Ser. A*, 22:83–100, 1964.

H. J. Zwally, R. L. Brooks, H. R. Stanley, and W. J. Campbell. Ice-sheet surface elevation and changes observable by satellite radar altimetry. *Journal of Glaciology*, 24(90):491–493, 1979.

H. J. Zwally, R. A. Bindschadler, A. C. Brenner, T. V. Martin, and R. H. Thomas. Surface elevation contours of Greenland and Antarctic Ice Sheets. *Journal of Geophysical Research*, 88(C3):1589–1596, 1983.